The Simulation and Study of Conditions Leading to Axial Offset Anomaly in Pressurized Water Reactors

A Thesis
Presented to
The Academic Faculty

By

Joshua Mahlon Hawkes

In Partial Fulfillment
Of the Requirements for the Degree
Master of Science in Nuclear Engineering
School of Mechanical Engineering

Georgia Institute of Technology
December, 2004

The Simulation and Study of Conditions Leading to Axial Offset Anomaly in Pressurized Water Reactors

Approved By:

Dr. Said I. Abdel-Khalik, Advisor

Dr. E. Kent Barefield

Dr. Nolan E. Hertel

November 12, 2004

ACKNOWLEDGEMENTS

I would like to thank the consistent and timely contributions to this project of Dr. E. K. Barefield, Dennis Sadowski, Dr. L. Detter-Hoskin, and of course my advisor Dr. S. Abdel-Khalik. Without the contributions of these individuals, this project and this writing would have not been successful.

TABLE OF CONTENTS

Acknowledgements iii

List of Tables vi

List of Figures viii

Glossary (symbols or abbreviations) xi

Summary xii

Chapter 1 Introduction 1
1.1 Motivation and Objectives 5

Chapter 2 Literature Review 10
2.1 Introduction 10
2.1.1 Industry Perspective and Review 10
2.2 AOA Science 14
2.2.1 Thermodynamic Perspective 14
2.2.2 Corrosion and Crud Characterization 21
2.2.3 Useful Models 31
2.3 Mitigation Strategies 37

Chapter 3 Methodology 41
3.1 Description of Apparatus 41
3.1.1 Test Loop 41
3.1.2 Coolant Preparation Systems 50
3.1.3 Data Acquisition and Safety 51
3.2 Experimental Procedures 53
3.2.1 Preparation of the Facility 53
3.2.2 Typical Experiment 57
3.2.3 Post Experiment Analysis and Facility Maintenance 63

Chapter 4 Results 65
4.1 Preliminary Results 69
4.2 Thesis Project Results 76

Chapter 5 Conclusions and Recommendations 94

Appendix A: Raw Data 98
A.1 Facility Optimization 98
A.1.1 Experiment Number 10 98
A.1.2 Experiment Number 11 99

A.1.3 Experiment Number 12 100
A.2 Coolant Composition Analysis 101
A.2.1 Experiment Number 23 101
A.2.2 Experiment Number 24 102
A.2.3 Experiment Number 26 102
A.2.4 Experiment Number 27 103
A.2.5 Experiment Number 31 104
A.2.6 Experiment Number 32 105
A.2.7 Experiment Number 33 105
A.2.8 Experiment Number 34 106
A.2.9 Experiment Number 35 107
A.2.10 Experiment Number 36 108
A.2.11 Experiment Number 37 109
A.2.12 Experiment Number 38 110
A.2.13 Experiment Number 39 113
A.2.14 Experiment Number 40 113
A.2.15 Experiment Number 41 116
A.3 Unconventional Experiments 120
A.3.1 Experiment Number 28 120
A.3.2 Experiment Number 29 123
A.3.3 Experiment Number 30 123

Appendix B: Determination of pH 127

Appendix C: Surface Analysis Techniques 131

References 133

LIST OF TABLES

Table 2.1	Composition of Steam Generator Alloys.	26
Table 3.1	Starting conditions of all experiments.	61
Table 4.1	Result Summary of All Experiments.	66
Table 4.2	Comparison of Boron Concentration and Weight Gain of Experiments 10, 11, and 12.	70
Table A.1	Compositional Information for Experiment Number 10.	99
Table A.2	Compositional Information for Experiment Number 11.	100
Table A.3	Compositional Information for Experiment Number 12.	101
Table A.4	Compositional Information for Experiment Number 23.	102
Table A.5	Compositional Information for Experiment Number 24.	102
Table A.6	Compositional Information for Experiment Number 26.	103
Table A.7	Compositional Information for Experiment Number 27.	104
Table A.8	Compositional Information for Experiment Number 31.	105
Table A.9	Compositional Information for Experiment Number 32.	105
Table A.10	Compositional Information for Experiment Number 33.	106
Table A.11	Compositional Information for Experiment Number 34.	107
Table A.12	Compositional Information for Experiment Number 35.	108
Table A.13	Compositional Information for Experiment Number 36.	109
Table A.14	Compositional Information for Experiment Number 37.	110
Table A.15	Compositional Information for Experiment Number 38.	110
Table A.16	Compositional Information for Experiment Number 39.	113
Table A.17	Compositional Information for Experiment Number 40.	116
Table A.18	Compositional Information for Experiment Number 41.	117

Table A.19	Compositional Information for Experiment Number 28.	120
Table A.20	Compositional Information for Experiment Number 29.	123
Table A.21	Compositional Information for Experiment Number 30.	123
Table B.1	pH as a function of B and Li (in ppm) at 310 °C (590 °F).	125
Table B.2	Weight Fraction of Iron Nitrate Constituent Elements.	127

LIST OF FIGURES

Figure 1.1	Venn Diagram of Suspected AOA Causes.	3
Figure 1.2	Example of Li Behavior During Power Transient [3].	3
Figure 1.3	Measured Axial Offset from Callaway Cycle 5 PWR [7].	4
Figure 2.1	Burn-Up Trends in Westinghouse Fuel [9].	14
Figure 2.2	SNB Principles.	16
Figure 2.3	High Magnification of Crud From PWR [12].	18
Figure 2.4	High Magnification of AOA Crud [3].	18
Figure 2.5	Historical Capacity Loss Due to Corrosion in PWRs.	21
Figure 2.6	pH Control Strategy Used in PWRs.	24
Figure 2.7	Solubility of Different Borate Species.	30
Figure 2.8	Close up of the Solubility of Different Borate Species.	31
Figure 2.9	Schematic of EPRI Ultrasonic Fuel Cleaning System [34].	40
Figure 2.10	Picture Comparing Callaway Fuel Rods Before and After Cleaning [34].	40
Figure 3.1	Schematic of AOA Test Facility.	42
Figure 3.2	Evolution of the Wire Configuration as Experiment Progressed.	44
Figure 3.3	Schematic of Mixing System.	47
Figure 3.4	Baffle Configuration in Vessel.	48
Figure 4.1	SEM Image of Crud on Experiment Number 10 at 100x Magnification.	71
Figure 4.2	SEM Image of Crud on Experiment Number 11 at 100x Magnification.	72
Figure 4.3	SEM Image of Crud on Experiment Number 12 at 500x Magnification.	73

Figure 4.4	SEM Image of Crud on Experiment Number 26 at 250x Magnification.	74
Figure 4.5	SEM Image of Crud on Experiment Number 27 at 500x Magnification.	75
Figure 4.6	Contaminants in Experimental Crud by Experiment Number.	76
Figure 4.7	Nickel and Iron in Experimental Crud by Experiment Number.	78
Figure 4.8	Porous Structure in Experiment Number 39 at 4000x Magnification.	79
Figure 4.9	Porous Structure in Experiment Number 36 at 500x. Magnification	80
Figure 4.10	Chart of Crud Composition.	81
Figure 4.11	SEM Image of Crud on Experiment Number 35 at 40x Magnification.	83
Figure 4.12	XRD Graph of Crud from Experiment Number 35.	84
Figure 4.13	SEM Image of Crystal from Experiment Number 35 at 500x Magnification.	85
Figure 4.14	SEM Image of Crystal from Experiment Number 35 at 500x Magnification.	86
Figure 4.15	SEM Image of Crud on Experiment Number 27 at 40x Magnification. Notice the two distinct regions of porous and non-porous	93
Figure A.1	SEM Image of Crud on Experiment Number 37 at 40x Magnification.	111
Figure A.2	XRD Graph of Crud from Experiment Number 37.	112
Figure A.3	SEM Image of Crud on Experiment Number 39 at 40x Magnification.	114
Figure A.4	XRD Graph of Compounds in the Crud of Experiment Number 39.	115
Figure A.5	SEM Image of Crud on Experiment Number 40 at 50x Magnification.	118

Figure A.6 SEM Image of Crud on Experiment Number 41 at 40x Magnification. 119

Figure A.7 SEM Image of Crud on Experiment Number 28 at 40x Magnification. 121

Figure A.8 XRD Graph of Compounds in the Crud of Experiment Number 28. 122

Figure A.9 XRD Graph of Compounds in the Crud of Experiment Number 29. 124

Figure A.10 SEM Image of Crud on Experiment Number 30 at 40x Magnification. 126

GLOSSARY

Abbreviations:

AES:	Auger Electron Spectroscopy
AOA:	Axial Offset Anomaly
BWR:	Boiling Water Reactor
CHF:	Critical Heat Flux
DNB:	Departure from Nucleate Boiling
EBA:	Enriched Boric Acid
EDX:	Energy Dispersive X-Ray
EPRI:	Electric Power Research Institute
ICP-MS:	Inductively Coupled Plasma Mass Spectrometry
ONB:	Onset of Nucleate Boiling
PID:	Proportional Integral Derivative
RCS:	Reactor Coolant System
SEM:	Scanning Electron Microscope
SIMS:	Secondary Ion Mass Spectrometry
SNB:	Sub-cooled Nucleate Boiling
TH:	Thermal Hydraulic
UFC:	Ultrasonic Fuel Cleaning
XRD:	Power X-Ray Diffraction Analysis

Symbols:

[M]	Molar Concentration of M
ppm	parts per million
MWd/MtU	MegaWatt Days of Power / Metric Ton of Uranium
GWd/MtU	GigaWatt Days of Power / Metric Ton of Uranium

SUMMARY

Axial Offset Anomaly (AOA) refers to a neutron flux depression in the top of a Pressurized Water Reactor (PWR) core, which leads to operational difficulty for the plant. The problem is also known as Crud Induced Power Shift (CIPS), and has grown in severity and occurrence frequency in recent years. In the most severe and well known case of AOA thus far, the Callaway plant had to reduce power to 70 percent for roughly one third of the cycle due to reduction of shutdown margin caused by AOA. AOA is the culmination of three related events within the upper regions of the core: subcooled boiling, corrosion product deposition, and boron deposition within the porous crud layer. Both subcooled nucleate boiling and corrosion product deposition are known to occur in the affected regions of an AOA afflicted core. Examination of fuel assemblies removed from an AOA core has shown a thick porous crud layer on the upper spans which had been tenacious enough to withstand traditional shutdown chemistry techniques meant to remove crud deposits from the cladding. However, direct evidence of boron deposition and specifically the mechanism by which boron deposits in the crud has never been observed by the industry. The two boron deposition schemes that remain under consideration are precipitation of a boron-bearing species and adsorption of boron compounds. Precipitation of a borate species with retrograde solubility is supported by observed lithium hideout and return behavior in plants that have experienced AOA.

This project replicates the conditions that exist inside an operating reactor including pressure (2000 PSIG), temperature (590 °F), water chemistry, coolant velocity, and heat flux (480 kBtu/hr-ft^2) applied to the Zircaloy-4 test element. Under these

conditions, prototypical crud was formed in situ on the heated test element. The facility designed and built for this project is equipped with the ability to end each experiment in such a way as to isolate any soluble species within the experimentally created crud without causing burn-out to the test element; a procedure referred to as the rapid blow-down technique.

With the use of this procedure the exact boron deposition mechanism believed to cause AOA has been determined. Data has been collected from over 40 experiments lasting two to five weeks followed by crud composition analyses using various techniques such as EDX, SEM, ICP-MS, and XRD. Comparative experiments were run to test the effect of the following factors on crud growth and boron deposition: pH of the coolant, particulate and soluble corrosion product inventory, duration of experiment, and coolant velocity. Ideal conditions for crud growth have been shown to consist of particulate and soluble nickel and iron additives combined with a target pH of 7.1. The boron-bearing species deposited in prototypical crud grown under standard reactor operating conditions has been identified to be lithium tetraborate ($Li_2B_4O_7$ – mineral name diomignite). This conclusion is supported by EDX, SEM, and XRD data taken from the crud that had deposited on the test element. The techniques developed in this investigation will allow the data necessary to validate mechanistic models to be systematically collected. Such models can potentially be used to identify the operational regimes to prevent or mitigate AOA without degrading core performance.

CHAPTER 1

INTRODUCTION

Axial offset anomaly (AOA) is defined as an actual axial power distribution in the core that varies significantly from predictions, usually by more than three percent. The bottom and periphery of the core are observed to have larger-than-expected operating power, while the top region of the core exhibits lower-than-expected power. This problem occurs in Pressurized Water Reactor (PWR) plants, and to date, over 40 cycles in at least 16 PWRs have experienced AOA in the United States. AOA can lead to a variety of problems such as economic penalties, safety considerations, loss of shutdown margin and as in the worst case so far, a power reduction [1,2,3]. The cause of AOA is not exactly determined, but experience and expert opinion suggests three things are believed to contribute to this anomaly.

First, impurities in the coolant form deposits on the surface of the cladding at certain preferential locations. These impurities can come from numerous sources, but usually they are from the corrosion of plant systems such as the steam generator piping. Second, sub-cooled nucleate boiling (SNB) occurs at the cladding surface in central areas of the core, aiding the formation of AOA in two ways. The SNB is believed to better enable the deposition of impurities on the surface of the cladding. Also, because this process occurs while the vapor bubbles are trying to escape the nucleation sites, small chimneys are formed in these deposits. This porous layer of deposits on the cladding is

termed crud [4]. SNB is more likely to take place in a high duty core where increased coolant temperatures and higher surface heat fluxes make it more likely for localized boiling to occur at the top of the core. SNB may be one of the most significant contributing factors to AOA, without it the crud may not be able to accumulate in the form of a porous layer with chimneys as observed on AOA fuel assemblies.

Lastly, boron used in the core as a soluble poison is suspected of being concentrated (due to boiling) and depositing within the small chimneys in the porous crud layer creating an uneven distribution of this high neutron absorber. The result is a depression in power at the top of the core as the boron deposited within the crud reduces the local neutron population. A typical four-loop plant has approximately 60,000 square feet of cladding surface area, five percent of which has SNB taking place. According to this theory, in order to observe a negative three percent power shift, approximately eight pounds of crud must from on the surface of the cladding, and about 0.6 pounds of boron must deposit in that crud [3]. The three interrelated causes can be represented in graphical form as seen in Figure 1.1.

Some general properties of AOA behavior that have been observed in affected plants should be mentioned. Consistently during an AOA cycle that undergoes a power transient, there will be an increase of lithium concentration in the coolant. Two such plants, Palo Verde Unit 2 and Callaway, have had this lithium return and hideout studied and documented. Lithium is intentionally added to the coolant (as lithium hydroxide) for reasons that will be explained later. This lithium is suspected of being trapped in the crud along with the boron because of the observed behavior during a power transient. It might also be assumed that the lithium is some how facilitating the deposits of boron in the crud

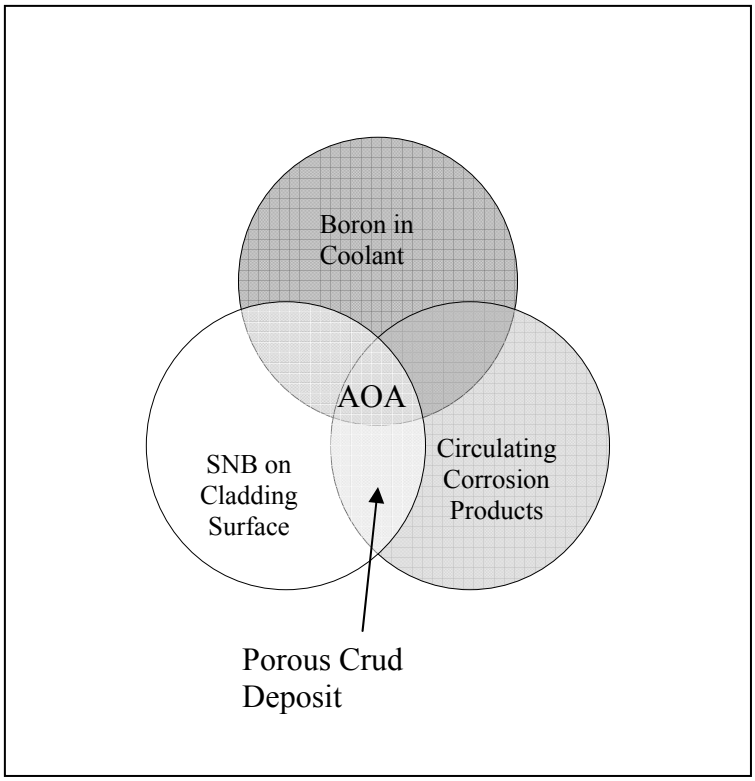

Figure 1.1: Venn Diagram of Suspected AOA Causes.

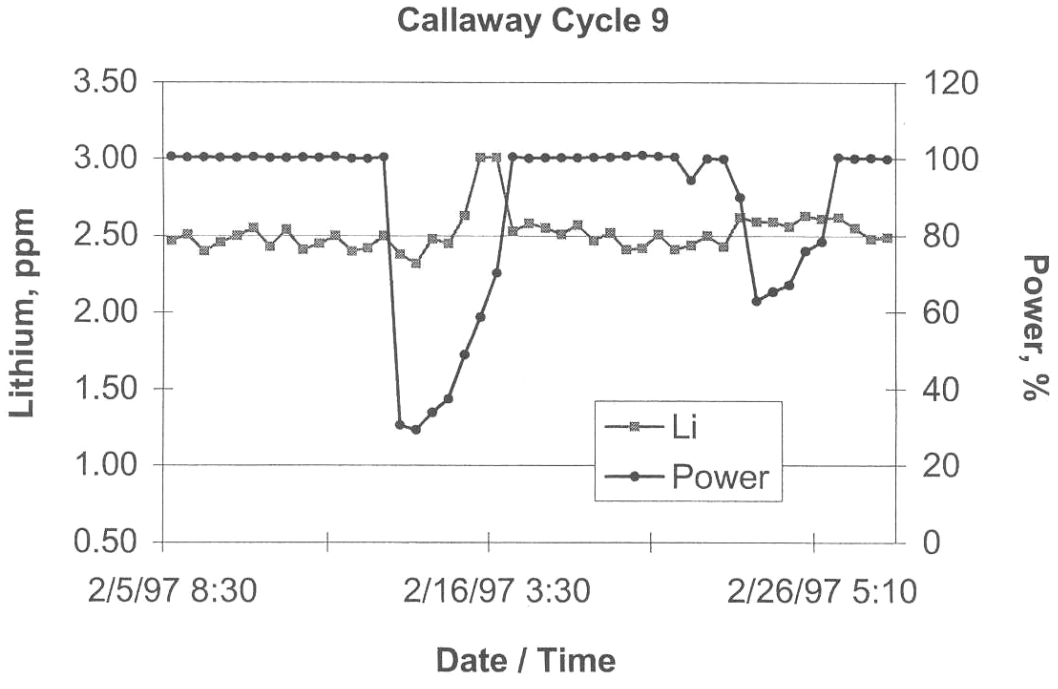

Figure 1.2: Example of Li Behavior During Power Transient [3].

in which case a likely compound for such behavior would be lithium metaborate ($LiBO_2$) [3-5]. An example of what this lithium return/hideout behavior looks like is shown in Figure 1.2.

AOA tends to peak slightly past the middle of an affected cycle as shown in Figure 1.3 below. Here axial offset is defined as the percentage difference between the power generated in the upper and the lower halves of the core:

$$\text{Axial Offset} = (P_t - P_b) / (P_t + P_b) \times 100,$$

where P_t and P_b are the integrated powers in the top and bottom halves of the core, respectively. The trend shown in Figure 1.3 coincides reasonably with the proposed

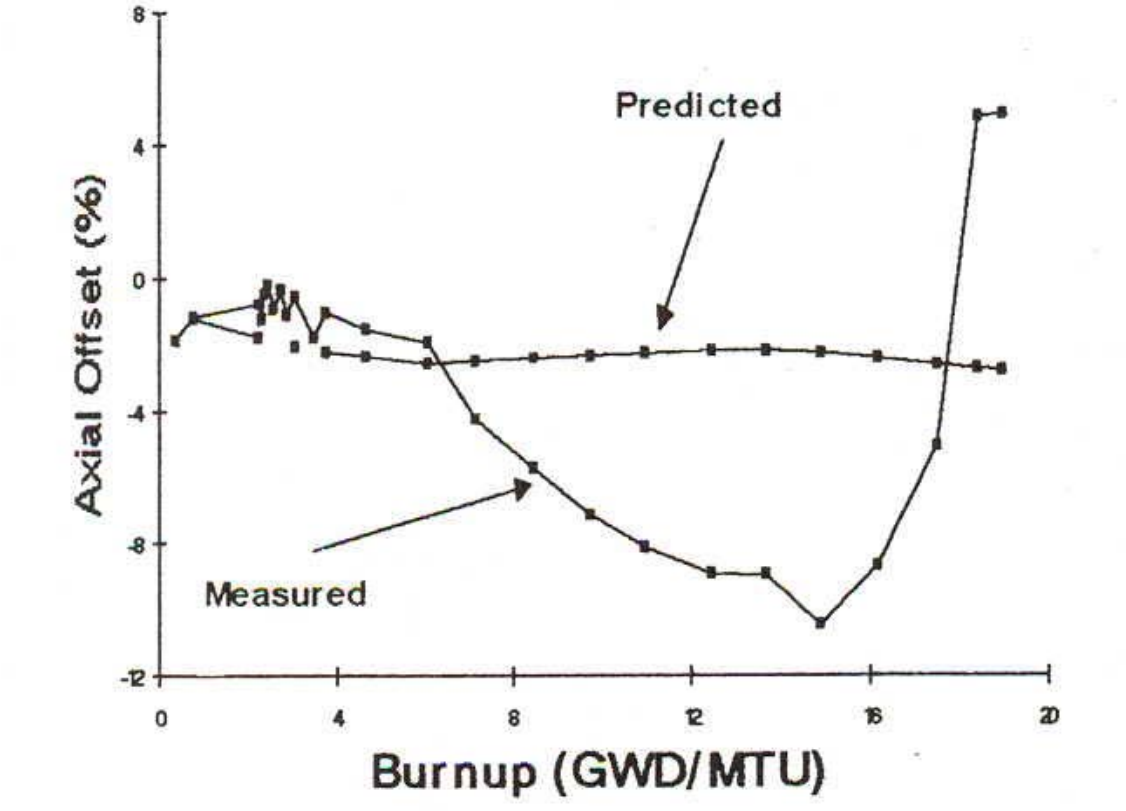

Figure 1.3: Measured Axial Offset from Callaway Cycle 5 PWR [7].

causes, because there has been both a sufficient amount of time for crud to build up and there still remains enough boron in the coolant to cause the observed deviations. Finally, higher duty cores are more susceptible to AOA because of the increased SNB in these cores. An example would be an older PWR that has recently been up-rated to operate at a higher thermal power than previously allowed. This plant is significantly more at risk than a low-duty plant operating under less demanding conditions. Higher duty plants, especially those that have recently increased the demand on the core, have consequently higher temperatures and higher surface heat fluxes. These are both believed to enhance corrosion product deposits on the clad through SNB.

1.1 Motivation and Objectives

Fundamentally, AOA affects plant operations in an unpredictable manner, hence there is sufficient motivation to study and resolve this problem. The most severe effect from AOA is when it influences the shutdown margin. As the anomaly persists, shutdown margin will decrease because the bottom of the core burns up at a faster rate than the top. If AOA becomes severe, the decrease in shutdown margin can force a costly reduction in operating power to maintain conditions within regulation limits. This has already happened to one plant. Callaway has experienced AOA in several cycles, but it was especially severe in Cycle 9 [5]. By the time the cycle was about two-thirds of the way through, plant managers had to reduce power by 30 percent for the remainder of the cycle. The cost for this reduction is estimated at tens of millions of dollars in lost electricity revenue.

Another effect of the abnormal fuel burn-up experienced by AOA plants are the

changes in reactivity throughout the life of the cycle. For the majority of the cycle, AOA will cause a negative axial offset at the top of the core, but at the end of the cycle, the axial offset will shift and become more positive. This behavior is shown in Figure 1.3. The shift is partially due to the soluble boron being removed from the coolant, and also because of the greater abundance of unfissioned fuel toward the top of the core. However, the higher duty temperatures will place an excessive heating load on the cladding because the crud that is still attached adds to the thermal resistance. If this behavior goes unnoticed or is allowed to occur without any intervention, the cladding temperature could rise above material limits and cladding failure may result.

During power transients AOA can affect the reactivity at the top of the core because the boron leaves the crud as power is reduced, increasing reactivity. As power is returned, the boron can deposit again decreasing the reactivity. This response makes it difficult to predict core behavior. Another possibility after such a transient is that the axial offset worsens when the plant returns to power because more ^{10}B is reabsorbed into the crud than was present right before the transient [5]. This is more probable if the fuel remains hot during the transient because the crud will not be displaced.

AOA can also affect the worth of control rods, especially at the top of the core. At high power, the worth of the control rod goes down because there is a smaller neutron population than anticipated. At zero power, the worth of the control rod goes up because there is more fissionable fuel than expected for a core that has experienced AOA for a lengthy amount of time. This will affect criticality predictions, because the reactor may go critical sooner than expected on an approach to criticality procedure. If these AOA symptoms occur in a plant it would result in reduced operational flexibility.

Two other problems that occur in conjunction with AOA are an increased dose rate and a possibility of fuel failure [3]. There has been an observed increase in dose rates at utilities experiencing AOA. An example of this is seen in the increase in the amount of ^{58}Co in the coolant toward the end of the cycle. Higher dose rates in the plant necessitate the use of more workers during refueling outages in order to minimize individual exposure. Additionally, fuel failure at three plants has been attributed to AOA crud: Palo Verde Unit 2, Seabrook, and Three Mile Island Unit 1. The crud on the fuel assemblies of these plants was determined to cause overheating of the fuel because of its high thermal resistance. Not only is the cost to repair or replace these assemblies significant, the damaged fuel assemblies could contaminate the coolant and cause higher exposure.

Operationally, the disturbance from AOA is significant, but it also affects plant economics in more ways than just lost electricity. Although a reduction in power is the most significant cost to date, AOA is expensive to prevent and treat in other ways. A plant that has experienced AOA may decide to clean the fuel assemblies to prevent it from occurring in the next cycle. However, the crud on the fuel assemblies which causes AOA cannot be cleaned by conventional chemical means, requiring a costly and more complicated ultrasonic method to rid the assembly of AOA crud. Another strategy used to reduce AOA used by some higher duty plants is to purchase additional fuel assemblies in order to spread the power load in the core over more surface area. The dollar figure for this strategy is $1.2 million for one fuel assembly at current prices [6]. Finally, manpower costs can go up as the phenomenon requires investigation and additional

measures of safety. Not only does the overhead increase, but efforts made by plant managers to resolve or mitigate AOA can distract from other personnel goals of the utility [3].

AOA is indeed a significant problem for PWRs, and the ability to accurately predict its occurrence is not available. The problem is that crud formation is difficult to prevent, and boron deposition within the crud has never physically been observed in the required amounts to cause the neutron flux depressions that exist in afflicted cores. Whatever boron species that may be depositing in the crud, are also suspected of having a retrograde solubility when the core is shutdown and the coolant temperature decreases. By the time the fuel assemblies are examined only the insoluble porous crud layer is left. This research aims to create prototypical crud that is similar in appearance and structure to that found on the fuel assemblies of a PWR. Once the crud is created it can be examined to figure out the detailed chemical composition of the deposited boron species. A unique method of isolating the test element from the coolant will be employed so as to trap any soluble species that deposited during the experiment including boron-bearing compounds with retrograde solubility. This method separates the coolant and test element very rapidly (<70ms) while simultaneously cutting off heating power to the test element.

Therefore, having created the correct crud under controlled conditions it will be possible to see if and how boron deposits in this crud and in what amounts. Several mitigating strategies have already been proposed to treat AOA. Among them are adding zinc to the coolant, operating the plant at an elevated pH, using enriched boric acid, and cleaning fuel assemblies that are to be inserted for second and third cycles before they are

used again. While all of these attempts have been tried and some have met with varying degrees of success, there may be alternate methods that are more cost effective, or one of these may be far better then the rest. The only definitive way to know is to better understand the potential causes of AOA.

CHAPTER 2

LITERATURE REVIEW

2.1 Introduction

AOA is a complicated problem covering many different scientific disciplines. The nuclear engineering aspect of it is actually the simplest; thermodynamic and chemical issues are far more challenging. This literature review will cover the industry standpoint with a historical perspective and an introduction to some of the related jargon. It will then discuss the essentials of AOA science and possible mitigation strategies that have been proposed. This project's focus is on the crud portion of AOA because it remains the single most effective way to combat this problem. Other issues such as the amount of boron in the core and SNB that occurs are most likely not going to change, or if they do change they will in such a way as to foster more potential for AOA (i.e. increases in both).

2.1.1 Industry Perspective and Review

Axial offset anomaly is an industry term for a problem that occurs entirely in one specific segment of the nuclear industry: electricity generating pressurized water reactors. The problem becomes even more specific when the fact that it is mostly located in large, four-loop, PWRs is considered. To further understand AOA, it is first useful to look briefly at this segment of the nuclear industry for an historical perspective.

AOA became a recognized problem sometime in the early 1990s. The first plant to publicly report on it was Callaway which involved a January 1992 condition the plant had experienced [7]. Operators there had observed an abnormal power distribution starting in the fourth cycle and again in the fifth cycle. They observed the power shifting to the bottom of the core in the middle of each cycle, corresponding to a burn-up of roughly 6000 MWd/MtU. Each cycle continued with a negative offset until the bottom of the core was depleted enough for the power to shift back. This occurred rapidly ending the cycle with a large positive axial offset each time.

Although this was the first time serious attention had been garnered by the AOA problem, it is not the first time it has occurred. Other plants had also undergone isolated instants of AOA, only it was not reported as such. Investigators at Callaway were able to find two previous cases of AOA before their own. The first was at Calvert Cliffs I in October 1979. The power in that plant had shifted in the now typical AOA manner to the bottom and periphery of the core. Because the plant was not in danger of violating any safety constraints, operation continued, and the power slowly redistributed back to within design predictions. However, there remained a large and unexpected pressure differential in the core prompting corrective actions. During a scheduled shutdown, the core was treated with hydrogen peroxide, which caused a large crud release – or crud burst. When the core returned to full power, both the abnormal power distribution and pressure differential were gone. The cause of the problem was not completely identified, but blamed on an oxygen ingress into the coolant. The oxygen in turn, enabled a thick crud deposit on the top of the core. This may have been the case, because the hydrogen peroxide did fix the problem and it did not reoccur in later cycles. However, no evidence

of a higher than normal reactor coolant system (RCS) oxygen concentration was obtained.

The next plant to experience an isolated case of AOA was a Belgian plant called DOEL-2 during the spring of 1986. The axial offset reached a negative four percent deviation from predictions. Thermocouple measurements were taken that indicated fuel bundles undergoing their third cycle of irradiation were experiencing subcooled boiling, causing voids in the coolant. Two other measurements that supported this theory were pressure differentials and neutron noise. In addition, when the assemblies were removed a thick crud layer was seen on the upper portions. It was this crud layer that was suspected of causing the surface temperature increase that led to the high boiling.

Callaway was different than these two plants because it experienced similar AOA conditions in two consecutive cycles. In fact, the offset worsened in cycle five from the previous cycle. The investigators pointed to increased boiling as the likely cause. To make their case, they ran simulations that were based on 5 percent voiding in the upper part of the core. To account for the void, new cross sections were used, the result of which was a decrease by 3.5 percent in the offset. Another simulation used a void multiplier to account for voiding in the core. This multiplier was changed from 1.0 to 20.0 resulting in a decrease of 5 percent in the axial offset. If these conditions were true, than increased voiding may well play a role in AOA. So the conclusion put forth by Callaway investigators was that boiling cased the neutron flux depression in the top half of the core, and this was enhanced by a crud deposition that enabled more vigorous boiling [6].

At the time of the release of Callaway's first report on AOA, there were other plants with similar problems. This begs the question of why all of a sudden are nuclear reactors experiencing this problem when they have operated without it for so long? The answer to this question is because plants began to operate at higher duties than they had been before. Callaway itself was initially licensed to operate at 3411 MWt, but was up-rated to 3565 MWt during its third cycle in 1988, with problems beginning in the very next cycle. These changes are rather common due to the deregulation of the energy market. Deregulation forces nuclear plants to take cost efficiency steps, one of which is up-rating the core in this manner. Two others are obtaining higher burn-ups from the fuel and operating the core at longer cycles.

A typical burn-up value for a traditional PWR 15-20 years ago is 33 GWd/MtU. This has been increased to 40-50 GWd/MtU depending on plant design. Higher burn-ups allow fewer reload fuel assemblies (at higher enrichment) to be used for an equal amount of power generated. Less fresh fuel assemblies in the core reload obviously saves on cost because each one averages about $1.2 million [7]. The trend toward higher burn-up fuels during the 1980s can be seen in Figure 2.1. The most recent burn-up increase in Figure 2.1 from 40 to 44 GWd/MtU correlates almost exactly to the onset of widespread AOA problems. Burn-ups are related to how long the cycle burns for as well. If the cycle is longer, then the fuel will burn more completely, which will give a larger burn-up value [8]. The typical cycle length for the original PWR design is 12 months, but this has been extended to 18 months in most cases and even as much as 24 months in some trials. Larger fuel cycles require a higher boron concentration at the beginning of the cycle to counter the increased core reactivity. The main incentive for a longer cycle length is to

prolong the amount of time before an expensive outage and refueling must be performed. An increase in cycle length actually increases fuel costs, but the operational and maintenance cost savings more than offset the smaller fuel cost increase [9]. These two factors combined with higher operating power are indirectly the main causes for the introduction of AOA.

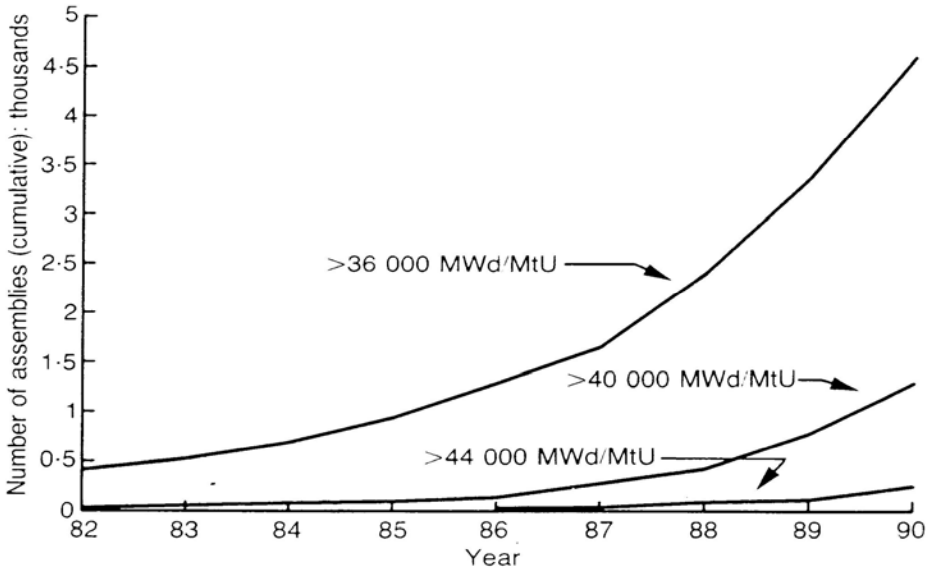

Figure 2.1: Burn-Up Trends in Westinghouse Fuel [9].

2.2: AOA Science

2.2.1 Thermodynamic Assessment

PWRs operate with an intentional amount of subcooled nucleate boiling (SNB) occurring in the upper spans of the core. The coolant enters the bottom of the core with a large amount of subcooling and in single phase. As the coolant passes up through the core it is heated, but the bulk coolant temperature is still below the saturation temperature

when it exits. However, near the walls of the flow channel where heat transfer is taking place, the coolant temperature exceeds that of saturation and bubbles form. A schematic of what a typical developing two phase flow regime would look like is presented in Figure 2.2(A). There are many different regimes of two-phase flow and heat transfer, but the discussion here will focus on the part up to and including subcooled nucleate boiling.

Nucleate boiling actually begins when the bulk coolant is still well below the saturation temperature. This occurs because of nucleation sites; slight imperfections in the cladding surface that expose portions of coolant to more surface area then others. As can be seen in Figure 2.2(B), this nucleation site allows more heat to be transferred to the coolant around it because of the increase in exposure area. Bubbles will form at these sites preferentially, but will remain on the surface of the cladding and condense there until the coolant approaches the saturation temperature. When the coolant is heated more, these bubbles may actually depart from the cladding and travel into the coolant some distance before condensing, as indicated in the figure. Flow with SNB taking place allows for more efficient heat transfer than forced convection which would be the heat transfer regime under single phase flow. Therefore, SNB is preferred from a thermodynamic point of view, and this is why it intentionally occurs in PWRs. The point at which bubbles will begin to form is called onset of nucleate boiling (ONB), and correlations exist for predicting the temperature of the bulk coolant at which ONB will occur. If the coolant continued to be heated, the bubbles will grow larger to the point where they connect with other bubbles and form a vapor film over the entire heat transfer surface. This is called the critical heat flux (CHF) or departure from nucleate boiling (DNB) point. The reactor is operated so that this will not occur because it would result in

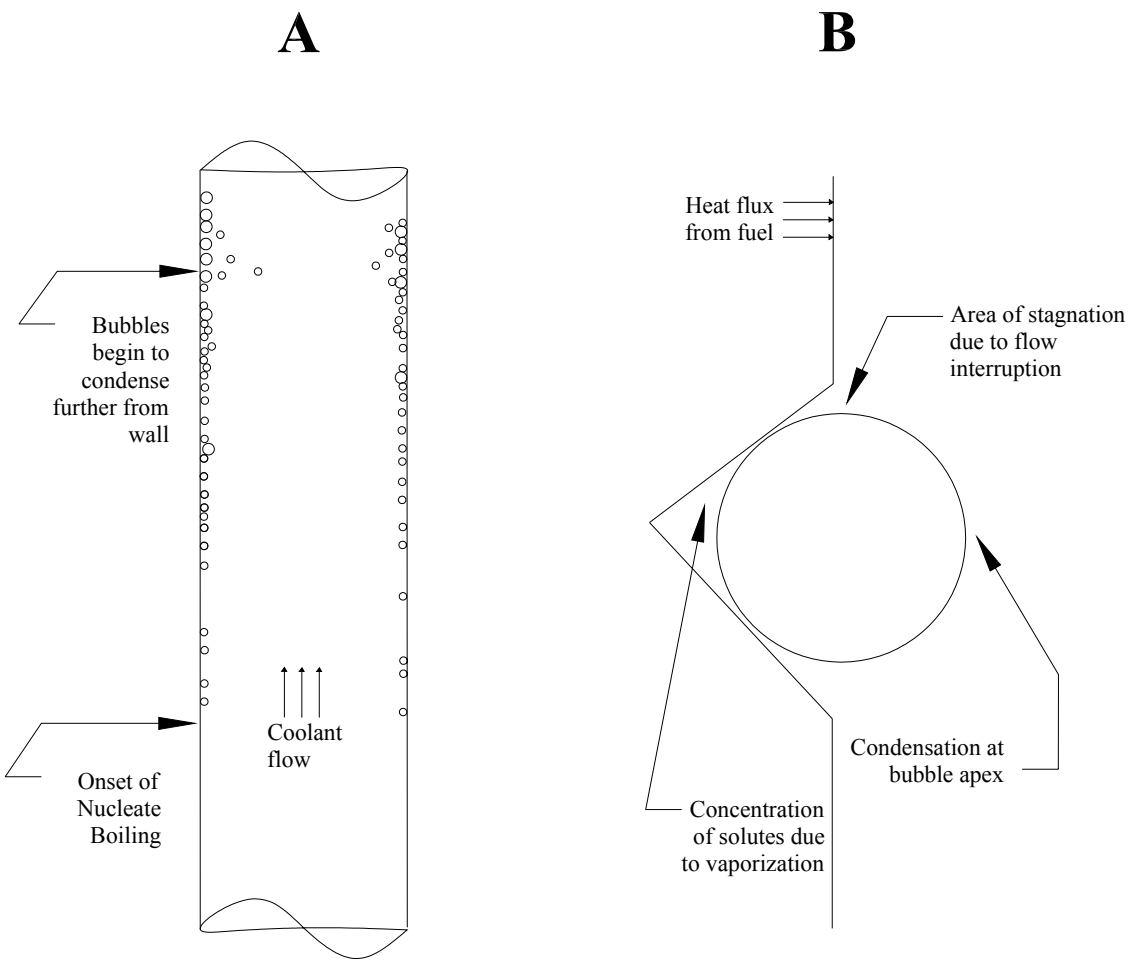

Figure 2.2: SNB Principles.

severe cladding damage. Therefore, power limits (i.e. heat flux limits) are instituted to prevent CHF from occurring using models to predict when CHF will occur [10].

An increase in SNB is obviously due to an increase in thermal duty. As plants up-rate to higher thermal powers, the portion of the core undergoing SNB and the severity of SNB will both increase. The increase is most likely resulting in AOA either directly or indirectly. Therefore, it is useful to look at the effects that SNB has on crud deposition or on AOA itself. The Callaway study is the only one available that directly relates voids to a neutron flux depression. This may be some contributing factor, but is probably not the underlying cause of AOA. Even if all the assumptions used in those calculations were true, there is still not enough voiding to cause the negative reactivity insertions corresponding to flux depressions seen since that time [6]. The voids in that study were given credit for a -5 percent offset in flux under the most extreme conditions. However, that same plant has experienced as much as -15 percent axial offset in subsequent cycles. The next consideration therefore, is how SNB effects crud deposition and therefore indirectly causes AOA.

It is generally assumed that crud deposition and SNB are complimentary processes, at least initially [2]. Boiling serves to concentrate soluble species in the coolant onto the surface of the clad through a process known as wick boiling. This first layer of crud deposition actually creates more nucleation sites, increasing the amount of boiling that occurs. In this way, a coated surface is actually better than a smooth surface in terms of heat transfer [11]. Eventually as the crud layer thickens, the nucleation sites turn into chimneys in the crud. An example [12] of a porous crud layer with chimneys can be seen in Figures 2.3 and 2.4. Both wick boiling and chimneys have been studied to

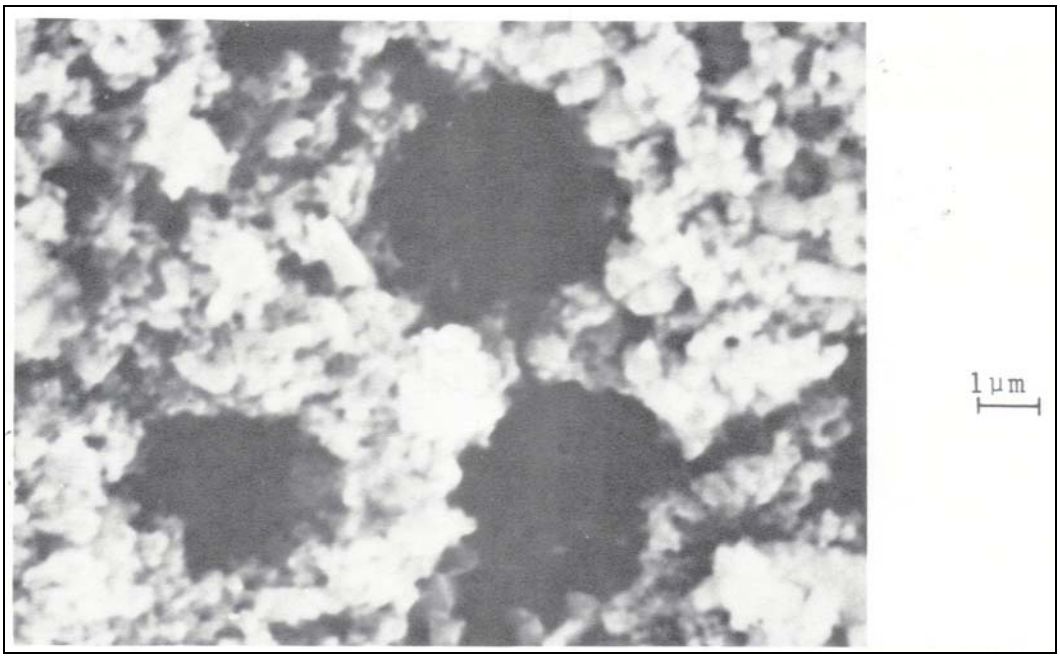

Figure 2.3: High Magnification of Crud From PWR.

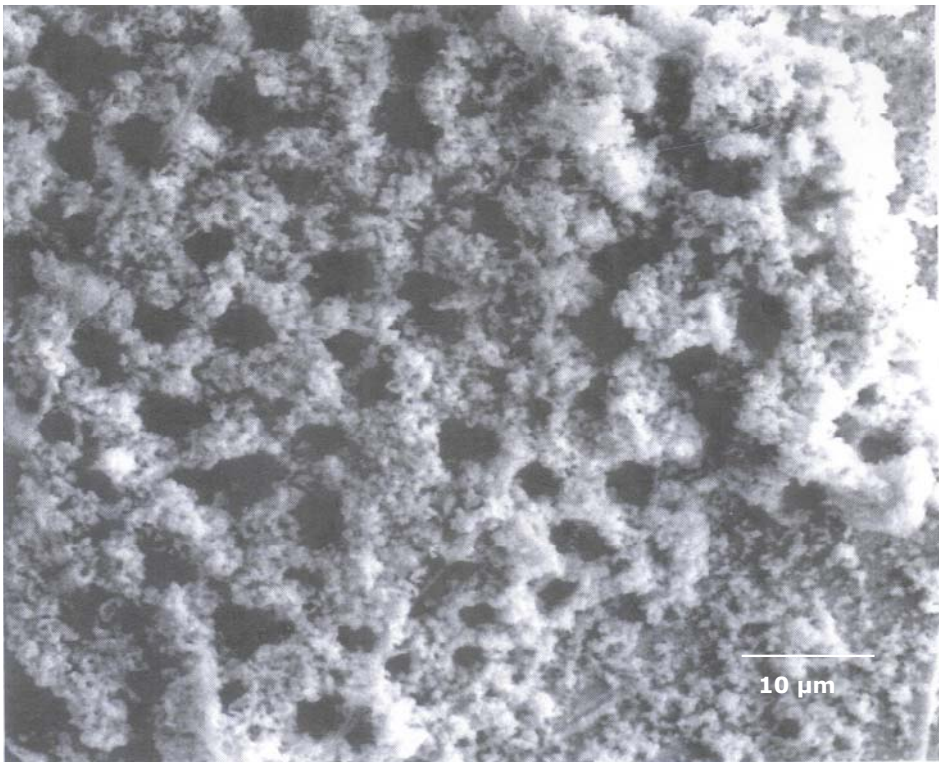

Figure 2.4: High Magnification of AOA Crud [3].

determine how each effects crud deposition, and the two are interrelated in terms of how they affect each other. Boiling is much different on a porous coated surface than it is over a clean surface. The amount of surface area where vaporization takes place is much larger on the coated surface. This is the main reason for more efficient heat transfer on the coated surface, but the process also contributes to the concentration of soluble corrosion products.

The bubbles created by the vaporization process are known to affect the coolant around it. The bubble creates an area of stagnation in the coolant both upstream and downstream. To understand how a bubble serves to concentrate solutes in the liquid, the dynamics of the bubble's formation should be considered. While the bubble is growing, it vaporizes coolant at the interface between the bubble and the cladding, and this pure water vapor then condenses at the bubble's apex. This causes the concentration of solutes when the water is vaporized at the cladding/coolant interface [13]. These solutes may then deposit and form crud. One study [14] experimentally verified the concentration of solutes by bubbles, and measured 50 percent increase of soluble species near the bubble. The experiment was done with only boric acid in the coolant at 3000 ppm, but the important concentration result is demonstrated effectively. Another experiment [15] verified that LiOH concentrates as well near the vapor/liquid interface, although quantitative results were not reported. The stagnant area in the coolant within the boundary layer may also allow particulate matter in the coolant time to settle onto the cladding surface and form crud. Both of these processes are illustrated in Figure 2.2(B).

The other thermodynamic process that is always considered with deposition of corrosion products is the solubility factor. The solubility of all substances varies

significantly with the temperature of the solution as well as the concentrations of other soluble species. Experiments have been run to determine the solubility of specific reactor coolant impurities such as nickel ferrite and magnetite for the entire coolant temperature range of an operating reactor. The results from one study [16] show that nickel and iron solubility varies with temperature, reaching its maximum at 4.1 ppm for iron and 1.0 ppm for nickel at roughly 75 °C. The solubility at typical operating temperatures for iron and nickel are 0.2 ppm and 0.1 ppm respectively, and they continue to decrease past that point. This is important for operating reactors because this temperature range exists during shutdown evolutions where corrosion product transport must be monitored carefully due to the presence of radioactive cobalt (^{58}Co). A later study [17] also reported solubility decreasing as temperature exceeded 300 °C for both nickel ferrite and magnetite, but in addition it reported the effect of pH on the solubility. In order to keep the environment of the coolant non-precipitating, the pH should be kept at or slightly above 7 for 300 °C. The solubility of these corrosion products affects the formation of AOA conditions because as the temperature rises, the corrosion products may come out of solution and are free to deposit as crud on the cladding surface.

The effect of increased heat flux on particulate or insoluble matter should also be mentioned. To study the effect of deposition of particulate matter on Zircaloy surfaces an experiment to imitate Boiling Water Reactor (BWR) conditions was conducted [18]. Some of the results are general enough to apply to PWR reactor conditions. They found that deposition rates actually depended on particulate matter size, but more importantly the researchers found that increased heating will increase the rate of deposition of particulate matter. This agrees well with the observed result that the higher heat flux in

upper portions of reactors has resulted in more crud deposition. This crud deposition in turn is very likely resulting in AOA.

2.2.2 Corrosion and Crud Characterization

The nuclear industry in the United States has dealt with corrosion since its beginning, and it has historically been a high cost problem. Corrosion leads to production capacity losses, maintenance and repair costs, and leads to a major portion of radiation exposure that plant personnel receive. These problems have led to efforts to curb the effects of corrosion and to understand its initiation, and there has been some success as can be seen in Figure 2.5 [19,20]. This figure shows the reduction of capacity losses due to corrosion. The peak was eight percent in 1982, and it has steadily decreased since that time. However, the severity of corrosion in an operating PWR core should not

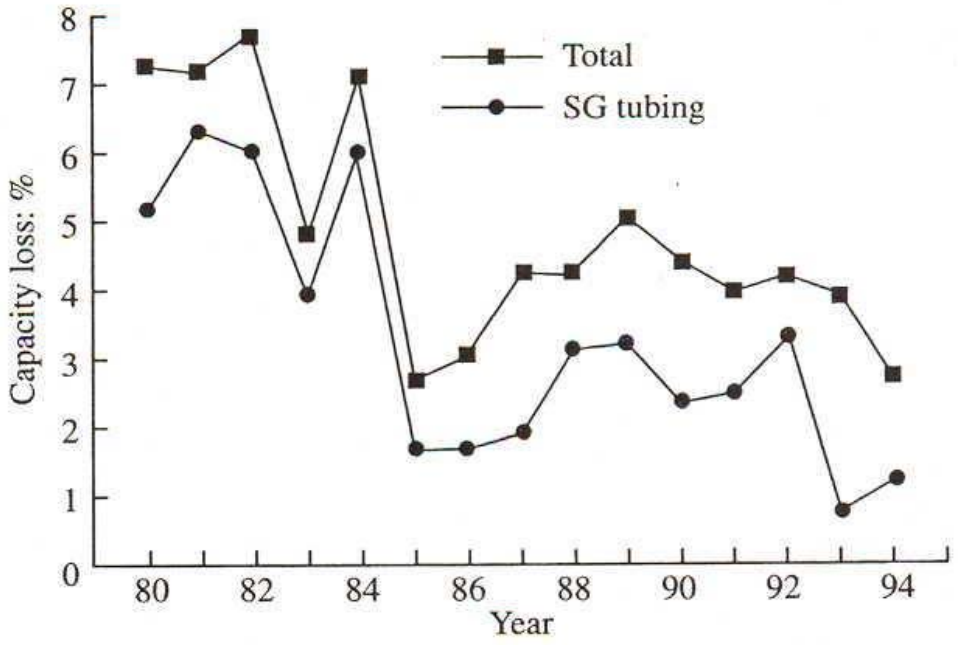

Figure 2.5: Historical Capacity Loss Due to Corrosion in PWRs.

be underestimated, as all of the major classes which make up the structural material to the core are susceptible to one or more forms of corrosion. Considering the fact that many of the plants that comprise the U.S. nuclear fleet are nearing the end of their designed deployment life, and corrosion indeed becomes a serious cause for concern.

From an AOA perspective, corrosion becomes a problem when the products of the corrosion process deposit on the fuel cladding surface. The deposition process is made possible by the thermodynamic effects at the cladding/coolant interface mentioned earlier. To counteract this effect, the major tactic available to plant operators is pH optimization, because the deposition rate is also dependent on this factor of the coolant as well as local temperature. For a long time, PWRs operated with a coordinated pH of 6.9, which was based on the assumption that the bulk of the deposit consisted of magnetite (Fe_3O_4). The pH was calculated at the bulk coolant temperature. More recently, the pH has been calculated at a temperature of 300 °C. The magnetite assumption was in turn used in models to determine an optimum pH for the coolant to minimize corrosion product deposition. This was revised upward when data showed that the bulk of deposits on the cladding actually consisted of a compound with a nickel component such as nickel ferrite ($Ni_xFe_{3-x}O_4$). With the assumption that nickel ferrite is the major corrosion product form, the pH recommendation was increased to 7.4, a difficult pH to achieve because of plant operating conditions.

At the same time as the new pH recommendation was being put into practice, the energy marketplace was deregulating, leading to many major changes in the way the core was operated in order for nuclear plants to remain competitive in the electricity market. The major change that affects pH optimization was the increase in cycle length. A longer

fuel cycle allows a more efficient use of the uranium fuel and a more consistent supply of the plants' product. Typically cycles were 12 months long, which required an initial boric acid concentration of roughly 1200 wppm (boron) to control the excess reactivity. However, in order to improve fuel economics the cycle length was increased to 18 months, which can require up to 2100 wppm of boron depending on the core design. Lithium hydroxide (LiOH) is used to counter the acidic effects of the boron additive, but the recommended maximum of lithium insertion is 2.2 ppm. An exposure to too high of lithium concentration for extended periods of time could lead to stress corrosion cracking of core elements and fuel cladding failures. A 2.2 ppm lithium level is not enough to bring the pH to the desired levels for longer cycle cores, so a modified program is used as shown in Figure 2.6. The core starts the cycle at a pH of 6.9 without exceeding a 3.5 ppm lithium concentration. This pH is maintained until the lithium concentration is at 2.2 ppm. Then the lithium concentration is held constant at 2.2 ppm, and the pH rises to 7.4 as the boron concentration is further reduced with burn-up. Once a pH of 7.4 is achieved, it is maintained for the remainder of the cycle. This type of pH strategy is known as a modified chemistry regime to plant operators. A longer cycle increases the amount of time that a plant must operate at the lower pH. An increase in cycle length from 12 months to 18 months will drop the average pH over the whole cycle by about 0.11 pH units. Whatever implications this lower pH has for crud deposition, one consequence of this lower pH is known, and that is an increase of dose rates by up to six percent, depending on plant specific conditions [21].

The corrosion processes of individual reactor elements such as the cladding and steam generator materials have important repercussions for the development of AOA.

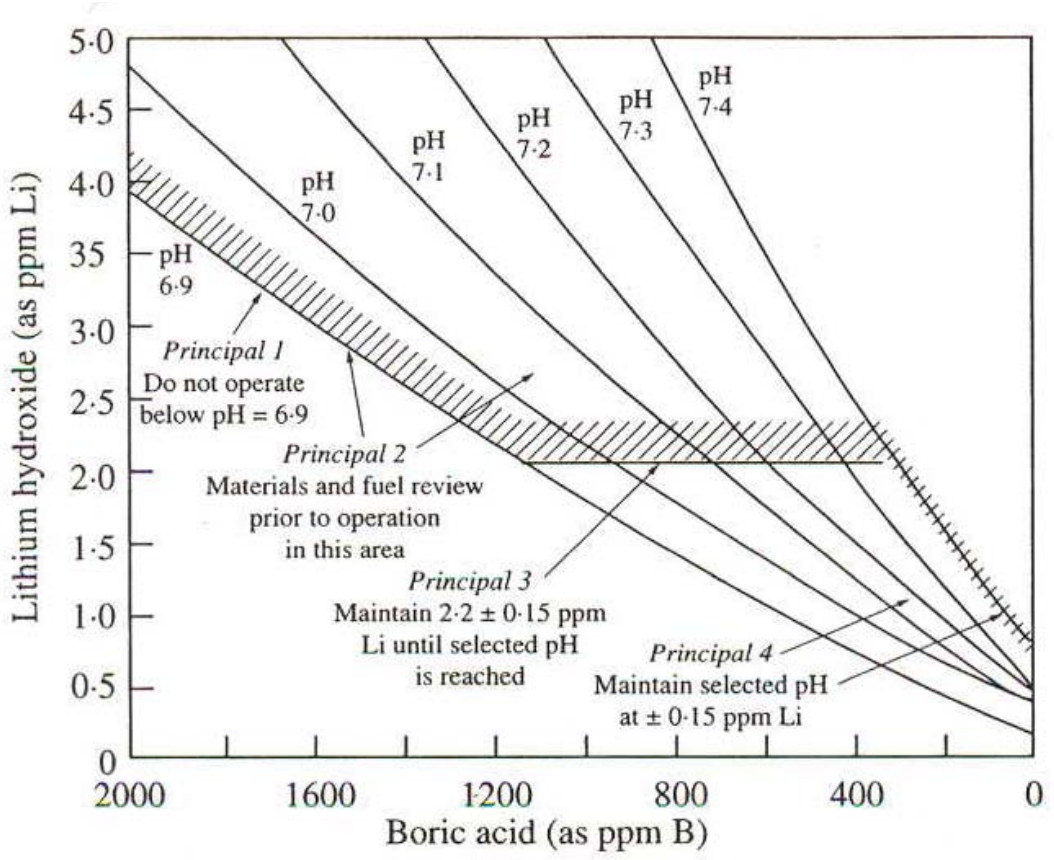

Figure 2.6: pH Control Strategy Used in PWRs.

The materials that corrode off from the steam generators and Zircaloy cladding form the inventory of material able to deposit or redeposit on the cladding surface. First, the corrosion of Zircaloy will be discussed through an experiment that studied the oxide created on such a surface after a standard water corrosion test [22]. This oxide layer has been studied by other projects, and similar results were obtained for a variety of mediums, but these results would change under an aqueous solution containing lithium hydroxide (LiOH). The experiment created oxide layers by submerging 10 cm Zircaloy-4 elements in 1.0 M LiOH water for five days at 360 °C and 2710 PSIA. These extreme conditions are useful for making generalizations about the corrosion behavior of Zircaloy.

Data was then obtained for a basic morphology and compositional analysis with scanning electron microscope-energy dispersive x-ray (SEM-EDX). Auger electron spectroscopy (AES) and EDX were also used to find the microchemistry of the external oxide layer.

One interesting result from this analysis is that the oxide layer created through this process is 120 microns thick, which is just as thick as the severe Callaway AOA core deposit. The severity of this oxide layer shows the extent to which the Zircaloy can corrode under severe conditions. The study also found that a solution containing LiOH greatly enhances the corrosion of the Zircaloy, and the results agreed with other work that the oxidation occurs in two phases. The first stage is a dense oxide consisting of zirconia crystallites. There is then a transition where the oxidation rate increases and a porous upper-layer is formed. The oxide thickness would probably be less if the concentration of LiOH was at a more reasonable level. This is part of the reason the amount of LiOH used in reactors was limited to 2.2 ppm.

Another important result of recent research is that Zircaloy exhibits accelerated corrosion behavior during high burn-up operation. A study pinned the transition point at 30 GWd/MtU as the point at which the acceleration takes place, and attributed the change in behavior to increased hydrogen concentration within the material [23]. By examining test elements that were exposed to varying amounts of initial hydrogen content, it was observed that the acceleration in corrosion was twice as great in samples that were in solution with hydrogen content of 200 to 400 ppm. In order to decrease the corrosion rate, the hydrogen pickup property must be improved.

Steam generators are the primary concern for corrosion product inventory. They are the major contributor of the nickel component seen in modern PWR crud that has led

to the development of AOA. The primary constituents of the three major steam generator alloys are listed in Table 2.1. As can be seen, they all have a large nickel component, and it is this nickel that is finding its way into AOA crud as will be explained in the next

Table 2.1: Composition of Steam Generator Alloys.

	Atomic Percent		
Material	Ni	Fe	Cr
Alloy 600	74	9	16
Alloy 690	60	9	30
Alloy 800	32	47	21

section. In terms of corrosion, it may help to know more about the steam generators themselves. One study sought to determine the oxidation behavior for relatively short exposure times for each of these alloys [24]. The tests were run at conditions similar to PWR operating conditions, and for exposure times up to 400 hours. The oxide structure was determined to have an outer layer of mostly iron, and an inner layer of mostly chromium. The researchers concluded that this result was due to the dissolution of iron and nickel, and at a later time the iron precipitated back on to the chromium oxide layer. This illustrates one potential source of nickel in PWR coolant. These results were similar for each alloy. The only difference was that the oxide thickness varied with Alloy 800 having the thickest oxide layer and Alloy 600 the thinnest by an order of magnitude difference. The overall expected corrosion of Alloy 600 over a 30 to 40 year design lifetime is only 1 mil in the surface thickness [25]. This is negligible from a system integrity point of view, but quite significant from a corrosion product source term point of view.

Although there has been some success controlling the deposition of corrosion products with a pH program, there is still the need for more information on the corrosion products and their deposition. After AOA became a recognized problem, an intensive effort was undertaken to study both the corrosion products in the coolant and the crud depositions of both afflicted AOA cores and similar plants that operate without AOA. The data found suggests that AOA cores have much higher proportion of nickel in their crud than nickel ferrite can account for. The study [1] compared the crud scraped from a core with severe AOA with a core under similar operating conditions yet with no AOA symptoms. First, the non-AOA core had crud that was no greater than 20 microns in thickness. The nickel to iron ratio in the crud was a typical 0.57, which is inline with historic data of ratios in the range of 0.4 to 0.6. The severe AOA core was quite different. The crud was much thicker, up to 125 microns, and the nickel to iron ratio was also much larger from 1.5 to 2.5. To give more of an idea of the nickel behavior as AOA symptoms worsen, cruds were also studied from plants that exhibited moderate cases of AOA. These showed that the nickel was slightly higher than a non-AOA plant, with nickel to iron ratios of 0.7 to 0.9. Two other findings of note from the severe AOA core, was that there was a zirconium deposition approximately 25 microns out of from the surface of the cladding. This suggests that the zirconium had deposited on the crud layer from the coolant instead of being scraped off with the sample. Also, there was a boron bearing species with mineral name bonaccordite (Ni_2FeBO_5), which was located on the surface. This deposit was needle like in shape and very tenacious; meaning that it was resistant to traditional shutdown chemistry techniques used to clean the cladding surface. To put this mineral in context, the only other place that it has been recorded outside of the

U.S. nuclear industry was at a meteor site in South Africa. With the boron constituent, this mineral may contribute to AOA later in the cycle, but because of its location on the crud scrape, it probably does not account for the onset of AOA. There has only been one documented case of this mineral in AOA cores, and another may have had the same compound, but rigorous testing was not done.

The same study that examined the crud deposited on cores, also examined the corrosion products that were circulating in the coolant. In order to ensure that they did not change chemical form, samples were taken from the coolant at temperature on a continuous flow. Corrosion products were taken for approximately a week to get a representative sample of the circulating coolant. In the coolant, the major circulating corrosion products were metallic nickel, iron oxide, chromium, and zirconium oxide. The zirconium oxide had a higher concentration at the beginning of the cycle. These are all in the particulate from; data on soluble species was not available in this study.

More detailed information is available from an English plant, Sizewell B, which published results of corrosion product analysis from the first three cycles [26]. Data was collected in similar manner, with an emphasis on collecting the corrosion products as they are in the coolant. This meant that the sampling was done at temperature, without exposing the sampled coolant to air. Sizewell B is a Westinghouse designed PWR, so it is similar to many U.S. plants that experience AOA, although other designs have experienced AOA as well. The tests show that in general, there is more particulate species in the coolant at the start of a cycle, and then as the cycle progresses the soluble species become more numerous. During normal operation, iron is found to be the most abundant metal ion in the coolant. Also reported, was that particulate matter in the

coolant is relatively insensitive to chemistry changes, but will change from thermodynamic events such as a power loss. This is especially evident at the start of a shutdown, when oxides are released from the cladding surface as the control rods are lowered into the core. Soluble species were found to deposit little during the start of the cycle, leading the researchers to suppose that they do not increase the likelihood of AOA by themselves.

During a lengthy power reduction, it is also observed that crud can be broken up by fluid shear forces. This will only occur if the cladding cools off, because there will be no thermodynamic incentive for the crud to remain attached to the cladding. The fluid turbulence and mixing does indeed seem to have an effect on the amount of crud that is deposited. For example, there are spacer grids in the core that keep the fuel rods properly aligned. The coolant rushes through these grids, and less crud is observed right after these grids where there is expected to be more turbulence. Further downstream from a spacer grid the crud thickness gets larger until the coolant passes through the next grid.

One key component of the crud that has been discussed very little so far is boron and its possible deposition methods. Two possible boron deposition methods are considered as causing AOA: adsorption of boric acid and precipitation of a soluble boron species. Precipitation was the first to be considered because of the lithium hideout and return behavior mentioned earlier. The precipitation of lithium metaborate for example will proceed as the solubility decreases such as the case with increasing temperature. The compounds of concern are those that have both lithium and boron in them, which will generally be referred to as lithium borates. Figures 2.7 and 2.8 below plot the solubility of three lithium borate species lithium monoborate ($Li_2{\cdot}B_2O_3$ − can also be considered

$LiBO_2$), lithium diborate ($Li_2B_4O_7$) and lithium pentaborate ($Li_2{\cdot}5B_2O_3$) [27]. In the first and last compound borate refers to the species B_2O_3, but the middle one refers to just the boron species as is the case in lithium metaborate. This is for consistency within those species suspected of causing AOA. The solubility of lithium diborate is not reported beyond 100 °C, but interestingly similar species all show the decreasing solubility at high temperatures that would be required for precipitation within the crud. Originally lithium metaborate was suggested to have been the precipitating species causing AOA [28]. Another project similar to (but started after) this current work has reported finding several lithium borate compounds, but not lithium metaborate [29]. The project had a limited scope with only four experiments being presented, but the two lithium borate species reported were $Li_3(B_7O_{12})$ and $Li_4B_{10}O_7$.

The other deposition mechanism is adsorption. This process is concerned with

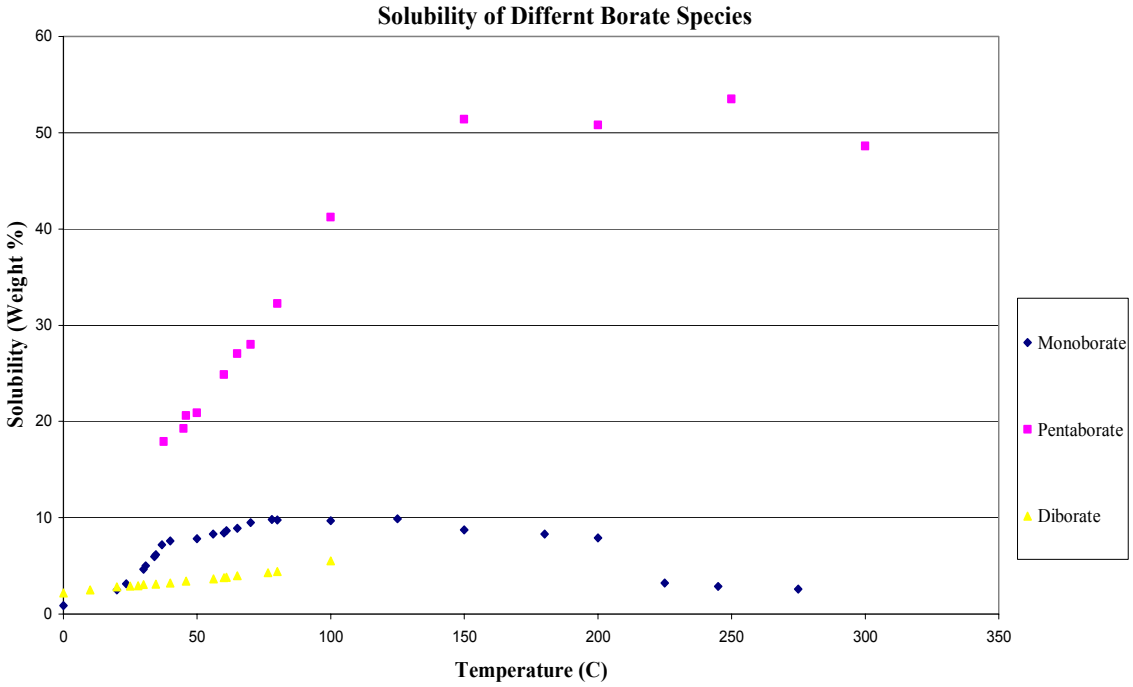

Figure 2.7: Solubility of Different Borate Species.

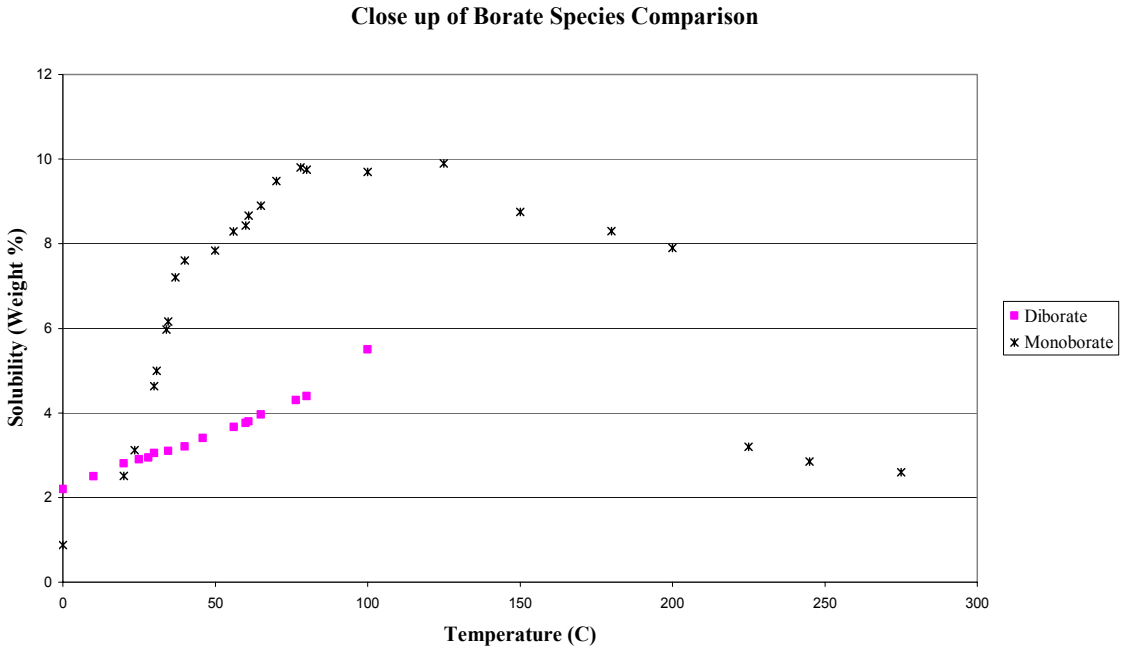

Figure 2.8: Close up of the Solubility of Different Borate Species.

the physical attachment of boron or boric acid to the lattice structure of crud. Experiments have determined that the highest possible adsorption rate for the potential crud species of NiO, $NiFe_2O_4$, ZrO_2, and Fe_3O_4 is 3.8 mg/g [30]. That amount alone is not enough to cause AOA when the calculation presented in Chapter 1 (0.6 pounds of boron depositing in 8 pounds of crud) is considered. However, the amount determined to adsorb on the surface actually decreases with temperature, and at PWR operating temperature ranges it is only 0.2 mg/g. Therefore, the adsorption process is most likely not the primary deposition mechanism for boron within the crud layer.

2.2.3 Useful Models Related to AOA

Many models have been developed in order to understand the complex behavior

of AOA. These models deal with many facets of the problem, and ones that attempt to model crud formation will be discussed here. Each model will be presented and the basics of its methodology will be reviewed. Then, the results will be discussed qualitatively, with reminders of any assumptions made when appropriate.

The first subject to be dealt with through models will be SNB, by an approach introduced by Wu and Jones [13]. This model studied the effects of a bubble on crud formation through simulation. The model assumed a spherical bubble and calculated various parameters of the bubble's dynamic behavior such as the growth rate and the size of a bubble before it departs. The model also assumes that bubbles are the same size, and that each chimney is created at a bubble site. Using these assumptions and a typical chimney density of 3000 to 6000 chimneys per mm^2, the bubble size is determined. The model also assumes that the flow regime within the porous deposit where the bubble forms is laminar, and that therefore the velocity can be approximated as zero. Using these assumptions and calculations, the results of the model show the flow effects around the bubble. The results showed that there is a stagnant region before and after the bubble, and that the local Reynolds number is between 0 and 40. This stagnant region is consistent with how the formation of a chimney might occur. If the bubble has a pumping effect, then it will create a concentration of solutes at the bottom of the bubble.

The next model also studies the effects of boiling in porous media, but places more emphasis on the heat transfer aspect. The model is more robust than the previous one as it calculates with numerical analysis and parametric variation numerous parameters for different scenarios in both one and two dimensions. The model was constructed by using the steady state conservation equations of mass, energy, and linear

momentum. An empirical equation was used to solve for the evaporation rate, which gave enough equations to solve the problem. Once the results were obtained, the effect of heat flux, system pressure, porosity, particle diameter, chimney radius, and crud thickness were obtained. Many trends can be obtained from this research. The wall superheat can be lowered with an optimum configuration of chimney density and porosity. The more porous a layer is, the higher the critical heat flux (CHF) for the coated cladding surface, but the CHF is actually higher for an optimally coated surface than for a clean surface. However, as the coating becomes thicker, the CHF lowers, and for a layer that is too thick, the CHF will be lower for the coated surface than for the clean surface. The model found that these trends are in good agreement with available experimental data.

The third model is on the subject of crud formation. Presented by Joe and Jones [31], this model uses diffusion calculations to study the effect water chemistry and solute concentration has on crud formation. Assuming that mass transfer of the corrosion products from the coolant to the crud deposit occurs in one of two mechanisms of diffusion and/or convection, then the model determines which of these two is dominant. Diffusion is the process whereby molecules move from places of higher concentration to lower concentration, and can occur in stagnant layers. On the other hand, convection can transfer mass when a fluid is mixed, such as the case in turbulent flow. Assuming that the porous layer exists, the mass flow rate is calculated for each mechanism, and the model found that diffusion dominates within the crud layer. This makes sense because the coolant within this layer will be relatively stagnant. With this known, the mass flow rates can be adjusted with different chemical conditions, and the model studied the effects

of radiolysis and boric acid (H_3BO_3). Radiolysis is the chemical recombination produced by radiation within the core such as fast neutrons, gamma rays, and alpha particles. The effect of radiolysis that is of concern to corrosion is that it increases the amounts of free radicals (such as H, OH, HO_2) present in the coolant, which will accelerate corrosion. The purpose of boron in the coolant is to absorb neutrons; however, this has the effect of creating more alpha particles due to the $^{10}B(n,\alpha)^{7}Li$ reaction. This reaction increases water decomposition by radiolysis, and therefore increases the concentration of free radicals in the coolant. The model calculated the mass flow rate of the molecules of interest, and they increased with increasing boric acid concentration and radiolysis.

The next model looked at the process of initial crud formation, using another model of a buddle. Rao and Jones [32] used numerical methods to evaluate a surface tension gradient due to temperature differences in the area around a simulated hemispherical static bubble. The parameters analyzed once the model was complete were the lithium hydroxide concentration around the bubble, the effects of heat flux, and the effects of bubble size. Some important assumptions to note in this model are that the bubble shape is not affected by surface tensions or gravity, the shape and volume of the bubble are constant, and the shape is also symmetric making the problem two dimensional. The results showed that an increasing heat flux caused more liquid to evaporate and condense at the bubble/wall interface, and therefore, more solute concentration. Also reported was that increasing the bubble size will allow more liquid to concentrate, although in a more non-uniform manner. The typical bubble size found in a PWR and used in this model is 10 μm in diameter.

The fifth model to be discussed, deals with boron concentration within a porous layer, and was introduced by Zhou and Jones [33]. The model assumes a uniform chimney distribution and defines a lattice with a chimney in the center surrounded by porous crud medium. Numerical analysis was used to find the boron concentration within this lattice by solving a set of conservation equations. The model showed that boron holdup varies exponentially with crud thickness and porosity, and compared data to the well known Callaway Cycle 9. Results from the model matched well to the plant data, with AOA first appearing at 4000 to 5000 MWd/MtU. The model predicted that 0.895 kg of boron had been deposited into the crud at 8000 MWd/MtU, and plant data suggests that 0.6 to 0.7 kg of boron is necessary to cause the observed power shifts. Boron was assumed to precipitate as boron oxide (B_2O_3), as well as to redissolve into the coolant when the reactor was shut down.

The next model to be discussed was reported by Lukic and Schmidt [34], employed by Arizona Public Service. After discovering a thick and tenacious crud deposit on some high duty fuel assemblies during a 1999 refueling, the plant managers decided they needed the ability to predict crud thickness. This model was developed using thermal-hydraulic (TH) variables to accomplish that goal. The model was to be used as a way to assist in the loading pattern designs in order to optimize plant operation. The objective of redesigning the fuel lattice structure is to more evenly distribute crud deposits over an entire fuel assembly. Previously, crud had been more focused on the periphery of the pin where the flow is lower and temperatures higher. The TH variables used were the fuel cycle length, average crud composition in coolant, and steaming rate. These were weighted and corrected for the particular axial location, and the contribution

from each location was summed for the entire core. The authors noted the difference between crud and oxide layers, and produced a similar model for the oxide layer. The redesign included moving higher enrichment fuel pins to the interior of the fuel assembly and an overall lowering of power for these pins.

The last model to be discussed here started with significant inconsistencies with preceding models [35]. Up to that point, it had been assumed that solubility of corrosion products in the coolant was the main driving force behind crud deposition. Yet crud deposits had been relatively constant over the entire core, although this was at a time before widespread AOA occurrence. The author therefore presented a two-stage sticking model as the means for crud deposition represented by the following equation (P is defined as sticking coefficient):

$$P = P_1 P_2,$$

where the sticking coefficient is the product of two probabilities. The first is the probability that ions on the surface become dehydrated, and the second is the probability that those dehydrated particles overcome the surface barrier and deposit. This sticking coefficient is then used in the deposition and release rate equations to find how much crud is deposited per unit time. The first probability depends on temperature and increases with increasing temperature. This model may serve as a good description for initial crud formation, since it adequately describes uniform core deposition. However, this does not take into account the change in these probabilities as more crud is deposited, or the effects of SNB.

2.3 Mitigation Strategies for AOA

Attempts have been made to reduce the effect of AOA in cores, and several other strategies have been proposed. Efforts that have been implemented in plants include zinc addition and pH optimization. The pH control strategies and theory behind it has already been discussed, and now zinc addition will be mentioned here.

The idea behind zinc addition to the coolant is that it can help form a protective oxide layer on system surfaces that will prevent corrosion product release and stress corrosion cracking (SCC) [36]. The main push for testing zinc in the coolant came more from SCC as it limits the life of steam generator tubing. SCC is not as much as a concern for fuel assemblies because they are replaced relatively often compared to the steam generators. In any case, the ability for zinc to limit the amount of corrosion product release helps reduce AOA by limiting the crud source term. An experiment was conducted to test the effectiveness of zinc additives in simulated PWR environments. Different amounts of zinc were added to an aqueous solution at 330 °C up to 20 ppb. Major materials that are used in PWRs such as Alloy 600, Alloy 690, and Stainless Steel 304 were all tested. The results of the experiment showed that zinc limited the corrosion product release rate by as much as a factor of five as compared to the same coolant without the added zinc.

Other methods that have been suggested to reduce AOA in PWRs are the use of enriched boric acid (EBA) and ultrasonic fuel cleaning. EBA consists of boric acid that is more abundant in the ^{10}B isotope, which is the main neutron absorber with a much higher neutron absorption cross section then the other isotope ^{11}B. Natural boric acid that is currently used in PWR coolant is 19.8 percent abundant in ^{10}B. There are two

advantages to using EBA. The first is that it may actually reduce the amount of boric acid deposited in crud, and the second is that it allows for better chemistry control. One study has shown that less EBA is deposited in crud using an adsorption model. This is true as long as the enrichment is above a threshold value that is determined by the concentration of other components in the coolant such as iron, nickel, and zinc [37]. It also stands to reason that if by using EBA the overall boric acid concentration is lower, then it may fall below the solubility limit of the hideout compound. Suppose for instance, that boron hideout in the crud was due to the precipitation of a compound such as lithium metaborate ($LiBO_2$), which has a low solubility limit. EBA may reduce the amount of $LiBO_2$ to a level below the solubility limit and eliminate boron deposition in the crud. However, if it were still above the solubility limit, than the $LiBO_2$ that did deposit would have a greater abundance of ^{10}B, which could result in a worse axial offset. The other advantage to EBA is that it can allow for more efficient control of the pH of the RCS. The amount of boric acid required would go down, so the reactor may possibly be able to run at a pH of 7.4 for the entire cycle, depending on the boron enrichment. This would be possible because the same lithium concentration would have a greater effect on pH in a core that used EBA as the soluble poison [4]. The operation of a reactor at a higher pH would minimize corrosion product deposition processes and therefore not present a medium for boron to deposit in.

Ultrasonic fuel cleaning is a program developed by the Electric Power Research Institute (EPRI), and is aimed at reducing the overall corrosion product inventory in the reactor. The fuel assemblies that are reinserted for subsequent cycles during an outage are completely rid of the crud deposit by a special proprietary process called ultrasonic

fuel cleaning (UFC). This new process is deemed necessary because AOA crud deposits are tenacious, and resistant to traditional shutdown chemistry techniques meant to clean crud off of the fuel assemblies. The UFC process is to remove the crudded fuel assembly from the reactor, place it in the UFC bath, clean it, and then place it back in the core for the next cycle [38]. It has even been suggested to clean certain fuel assemblies experiencing severe AOA in the middle of a cycle. However, this would be a last resort only used to avoid a mandatory power reduction [4]. A schematic of the process can be seen in Figure 2.9. This method has been tested and showed favorable results. The illustration in Figure 2.10 shows the effectiveness of this method by comparing a before and after cleaning picture of a crudded fuel assembly. The problems with UFC is that it is time consuming during an outage when plants try to get the core back online as soon as possible, and it is also expensive. The alternative method for cleaning the fuel is to create more sophisticated decontaminating agents that rely on a chemical cleaning process. One study has attempted to produce simulated crud in order to test methods of dissolving the crud [39]. However, if UFC proves to be the most viable way to eliminate the crud problem it may be necessary despite the drawbacks.

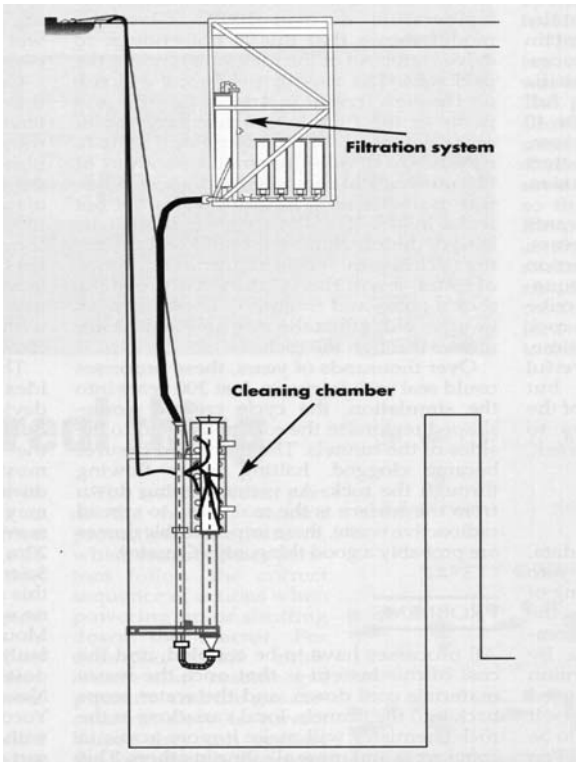

Figure 2.9: Schematic of EPRI Ultrasonic Fuel Cleaning System [34].

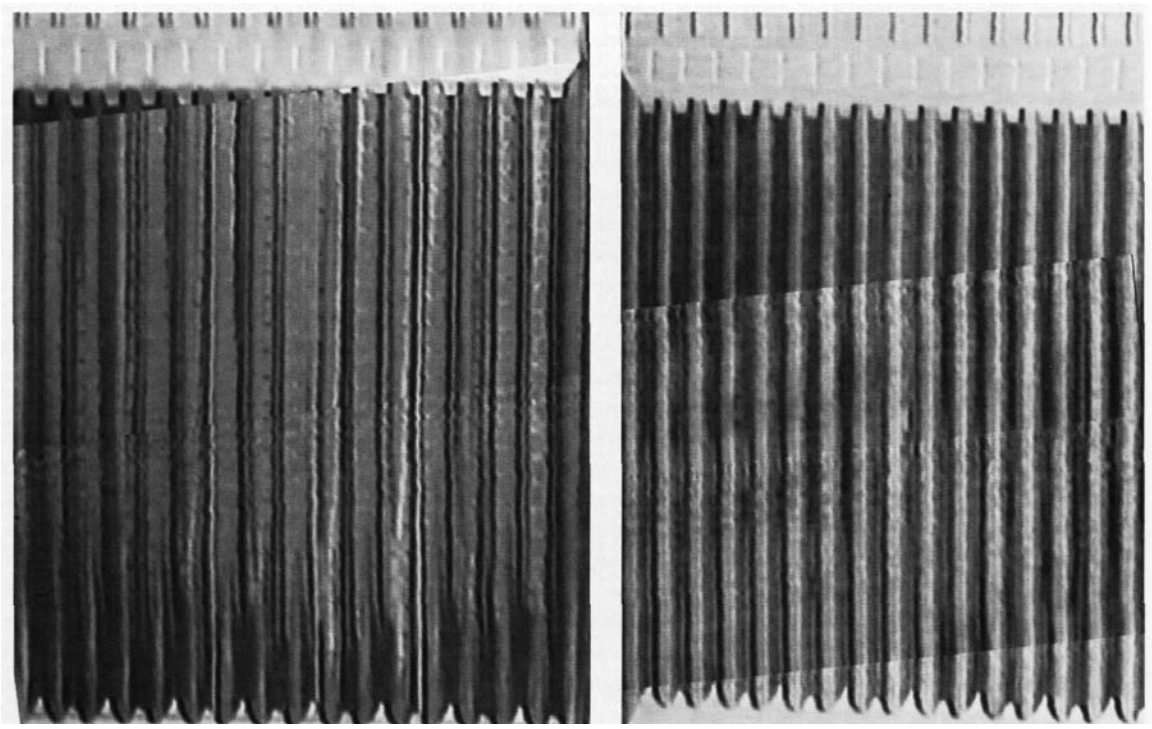

Figure 2.10: Picture Comparing Callaway Fuel Rods Before and After Cleaning [34].

CHAPTER 3

METHODOLOGY

3.1 Description of Apparatus

The test facility that was built to monitor AOA activities is designed to replicate the conditions in the primary coolant of a PWR, and the typical heat flux of the cladding. There are several parameters such as the surface heat flux of the test element, concentration of impurities (used to represent corrosion products in the primary coolant), and other operating conditions that can be adjusted for different experiments. There are three main systems of the facility, which are the test loop, the coolant preparation system, and the data acquisition and safety systems. A schematic of the entire facility is shown in Figure 3.1.

3.1.1 Test Loop

The test loop consists of six major subsystems: the pressure vessel, the electrodes, the mixer, the pressurizer, the blow-down system, and the let down assembly. The pressure vessel is the central component to the experiment. It is rated to a maximum pressure of 2500 PSIG, at a maximum temperature of 650 °F, and made of 316-stainless steel. Compared to these maximum values, the experiment typically operates at a temperature of 590 °F and a pressure of 1930 PSIG. The temperature of the vessel is controlled by a Watlow PID controller and can be maintained indefinitely within 1 °F.

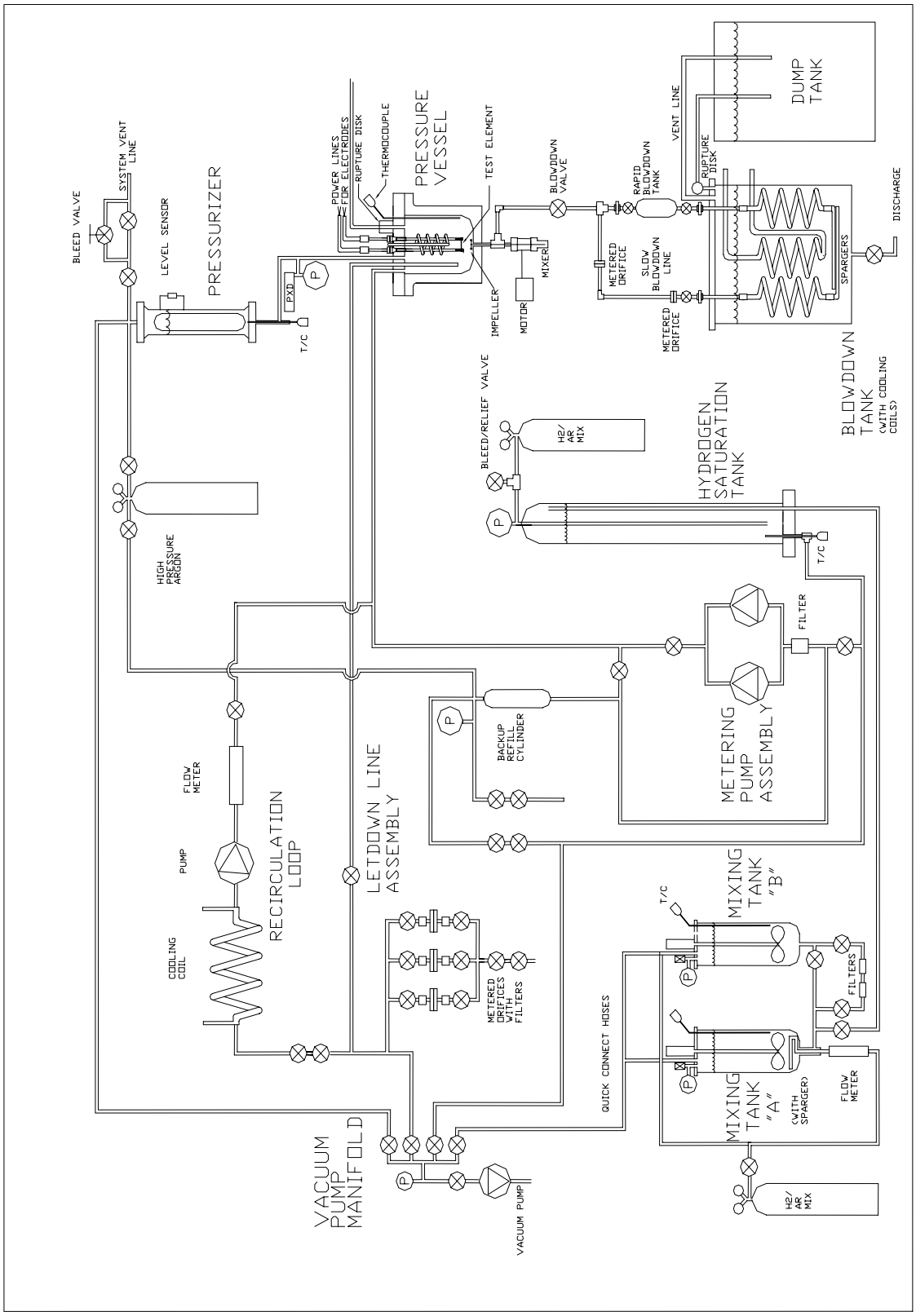

Figure 3.1: Schematic of AOA Test Facility.

There is a 4000 watt heating blanket around the vessel that the temperature controller operates for heating, and cooling coils with a tap water feed in the interior for cooling. The high pressure is achieved by an argon gas cylinder, which will be described in more detail later. The inner volume of the vessel is enough to hold about one gallon of coolant. The vessel has 11 threaded ports on the bolted removable top and one threaded opening through the bottom. The top is sealed with a graphite spiral-wound gasket seal. The top threaded ports accommodate a feed line, let-down line, the electrodes, lines for the cooling coils, a thermocouple, a rupture disk, a pressure transducer port, pressurizer port, and one spare port. The bottom of the vessel has one opening, through which the drain line and the stirrer shaft pass. The vessel is mounted on pneumatic pistons so it can be lowered and the inside prepared for experiments.

A component of the vessel that was added for six experiments (out of a total of forty) was a nickel screen inside to balance out the composition of surfaces exposed to the heated coolant. In a typical PWR the wetted interior components are comprised of 9.6 percent stainless steel, 65.1 percent Inconel 600, and 25.2 percent Zircaloy-4 [40]. That would give an elemental composition of 67 percent nickel, 17 percent iron and 15 percent chromium if the Zircaloy cladding is excluded from the calculation. For this experiment without the nickel screen the approximate composition is 12 percent nickel, 66 percent iron, and 17 percent chromium, which changes to 68, 25 and 7 percent respectively if the nickel screen is added. However, the nickel screen was later removed because the large amounts of soluble iron and nickel added to the coolant would negate the source term from the vessel. The screen also represented a practical problem for cleaning and carrying additives from one experiment to the next.

Test Elements and Elctrodes:

The next component in the test loop are the electrodes that hold the Zircaloy wire test element and deliver a high current to maintain the desired surface heat flux on the heated portion of the wire. This heat flux ranges from 450,000 to 500,000 $^{Btu}/_{(hr\text{-}ft2)}$, which typically requires a current in the range of 90 Amps. The surface heat flux also depends on the heated length of the wire, which can vary slightly with each experiment. The test wire sits approximately two-thirds of the way down in the vessel. The wire shape itself has undergone some evolution as the experiment has progressed. The problem of wires breaking before the scheduled end of an experiment led to a wire design that increases the overall heated length and increases the contact between the wire and the electrodes. As seen in Figure 3.2, the curved wires of configurations four and five yield a much larger heated length between the electrodes. The configurations start with number

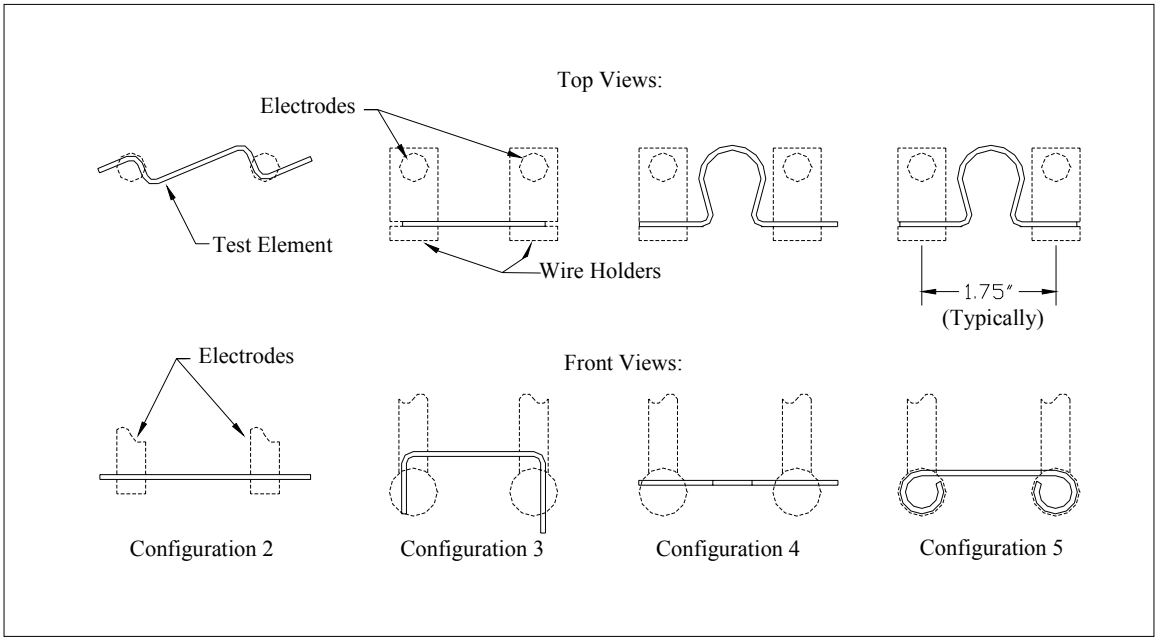

Figure 3.2: Evolution of the Wire Configuration as Experiment Progressed.

two, because the first configuration was simply a straight wire.

The wire holders shown in the figure are simply an interface between the electrodes and the wire. The wire holders are custom-made for this experiment out of 316-stainless steel. The electrodes are made of stainless steel and are sealed with custom-made hybrid Teflon/Lava seals with a maximum rated temperature of 500 °F. This is obviously below the system operating temperature, so the seals are located above the main body of the vessel so as to remain cooler, and a cooling fan is used to keep them below the rated temperature. The typical operating temperature for the seals during an experiment is approximately 350 °F.

Coolant In-Vessel Mixer:

The mixer was added to the test facility in its fourth year of operation. The mixer enhances the experiment by adding two features to the facility that are present in PWR primary coolant. It keeps the coolant turbulent with a similar effective Reynolds's number, and it gives the coolant a comparable volumetric turnover rate. The mixer's brand name is MagneDrive manufactured by Autoclave Engineers (Erie, PA). It uses an external motor to drive an internal shaft coupled with permanent magnets. The internal shaft is $^{5}/_{16}$ of an inch in diameter and passes through piping and into the vessel. On the tip of the shaft a 2 inch diameter Rushton style impeller is mounted that provides the agitation for the coolant. This particular MagneDrive unit is rated to 50,000 PSIG at 450 °F. The temperature is lower than that of the vessel, which is acceptable because the mixer is external to the vessel like the Teflon/Lava electrode seals. The motor that is used to drive the mixer is a Reliance Duty Master (manufactured by Reliance Electric

Company, Cleveland, OH), is rated to 3450 RPM at 1.5 hp, and is connected to the mixer via a belt system. The motor is controlled through a ParaJust AC motor speed controller (manufactured by Parametrics, Orange, CT), which varies the power from zero percent to full power. The maximum operating speed of the MagneDrive is 2000 RPM, but a typical speed for an experiment is less than half of that, around 800 RPM. A schematic of the mixing system is shown in Figure 3.3.

In order for this sort of mixing system to provide adequate agitation of the coolant, baffles in the interior of the vessel are necessary to prevent the coolant from simply swirling in a constant and "rigid body" fashion. A schematic of how the baffles are placed inside the vessel is shown in Figure 3.4. The baffles have the added affect of forcing the liquid to flow vertically upwards past the wire, just as coolant flows vertically upwards past the fuel rods in a PWR. The sort of swirling that occurs without baffles would not provide sufficient agitation in the area around the wire because it is located in the center of the vessel radially, where the coolant would be most stagnant in a swirling regime. The baffles used in this experiment are stainless steel fins located 90^{o} apart from each other in the vessel. They are a half inch wide and mounted on a heavy stainless steel ring. The baffle assembly is removable so it can be cleaned between experiments, and is placed at an orientation as shown in Figure 3.4, which maximizes the distance from the baffles to the test wire. If the baffles are placed too close to the test wire, the current could arc because the vessel is electrically grounded. This occurred in one of the experiments and forced an early shutdown in order to figure out the problem. This also caused some minor damage to the baffle and the electrode holder.

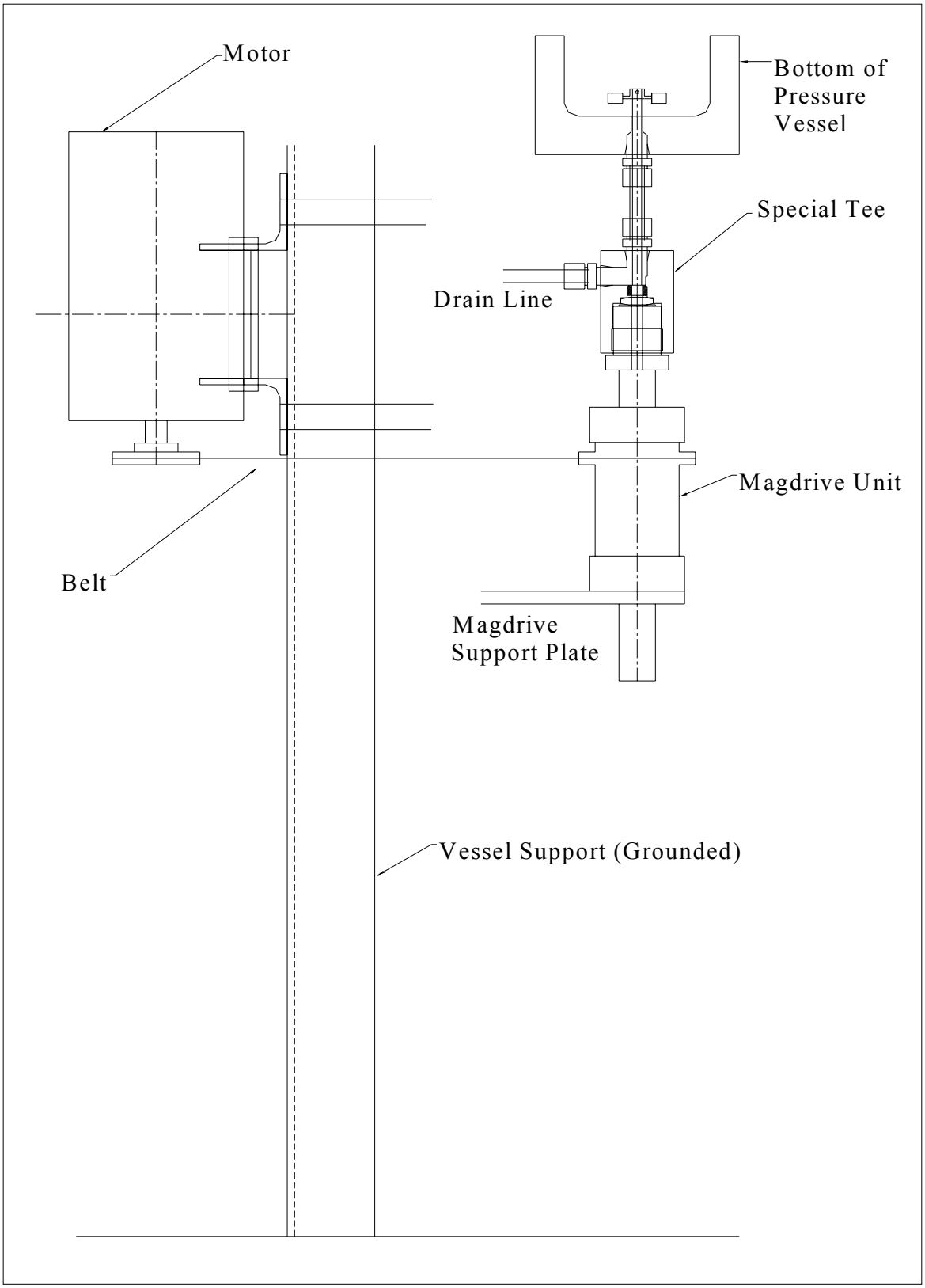

Figure 3.3: Schematic of Mixing System.

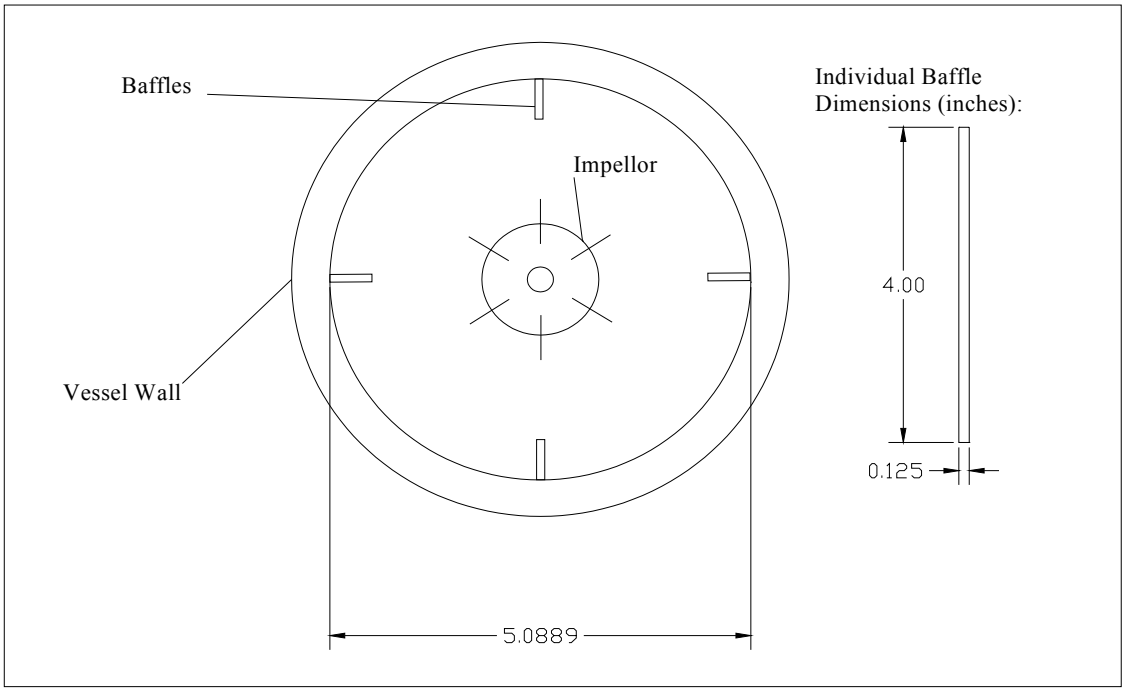

Figure 3.4: Baffle Configuration in Vessel.

Pressurizer:

The pressurizer is made of 316-stainless steel and contains a hollow titanium float, an electronic level sensor, and a mechanical level indicator. The pressurizer is mounted above the pressure vessel and partially filled with liquid so there will not be a free liquid surface inside the vessel. Also, the extra liquid in the pressurizer can be used to automatically compensate for any leaks in the system, maintaining a constant coolant environment within the actual vessel. Argon from a high pressure gas cylinder provides the desired pressure, and a precision gas regulator allows for fine control of this pressure. With the addition of the mixer the function of the pressurizer is especially important because a free surface would cause the coolant to vortex rapidly, leaving the wire bare. At the aforementioned operating heat fluxes, the wire would burnout instantly if left bare even for a moment.

Blow-down System:

The blow-down system is comprised of the blow-down tanks, a drain line, and the valve that isolates the blow-down tank from the pressure vessel. The blow-down tank is a large low pressure, stainless steel tank that catches the superheated coolant at the end of an experiment. The rapid draining of the pressure vessel necessitates a tank that can manage the high temperature coolant. This tank is filled with water and cooling coils to serve that purpose. The drain line connecting this tank to the pressure vessel runs through a custom stainless steel T-junction, which allows the MagneDrive to connect to the vessel and still have the ability to drain the vessel. The drain line has a large valve in it with an extended grip so that it can easily and rapidly be opened at the end of the experiment during the rapid blow-down procedure.

Coolant Sampling and Let-down System:

Lastly, the let-down assembly is designed to obtain coolant samples during an experiment, and to bleed off excess coolant, which usually is necessary prior to a rapid blow-down procedure. There are redundant filters used in case one fails during a let-down procedure. The filter sizes are two, five and nine micrometers, and they are set up so that by switching a few valves a different filter or multiple filters can be used. These small sizes allow just a slow trickle of coolant to drip through the bleed valve so it is easy to control how much coolant is extracted. The two smaller filters drain liquid slowly enough that the pressure is not affected as the precision gas regulator can compensate for the pressure loss. The largest filter will drain quickly enough for the pressure to drop momentarily. Typically, the middle size filter is ideal for draining coolant offering a good compromise between speed and system control. The let-down line in the pressure

vessel is positioned in such a way so that its tip lies right above the test wire. This allows all extra coolant possible to be drained before a rapid blow-down while still keeping the test wire submerged.

3.1.2 Coolant Preparation Systems

The manner in which the coolant is prepared is vital to the reliability of the experiment. Exact concentrations of additives were necessary for maintaining proper pH and replicating the conditions in PWR primary coolant. Two system components that were designed solely for the coolant preparation are the hydrogen saturation tank and the mixing tanks. The mixing tanks are where the coolant begins its preparation. They are identical five gallon stainless steel tanks. Each contains a mixer operated via a top mounted air powered motor. Both tanks are equipped with a heating blanket that surrounds the outside, and mixing tank "A" has a gas sparger on the bottom that bubbles argon through the coolant during mixing. The difference in the tanks can be seen in the system schematic presented in Figure 3.1. The tanks can be evacuated using a vacuum pump or they can be pressurized up to 100 PSIG. The hydrogen saturation tank is a vertically mounted stainless steel tank that brings the coolant up to a saturated level of hydrogen gas concentration. The hydrogen comes from a hydrogen/argon (4%/96%) gas cylinder at a regulated pressure of 300 PSIG.

One additional component used in this process that is used in both coolant preparation and in the test loop is the vacuum pump. The vacuum system can draw a vacuum on any component in the AOA facility. It is most often used to purge a tank of air before coolant is transferred. The tank, whether it is one of the mixing tanks, the

saturation tank, or the high-pressure vessel, will often be evacuated several times, decreasing significantly the concentration of oxygen (the chief component of concern in air) each time. The pump has an associated vacuum gauge, and a typical vacuum is approximately -27 feet of water before use of the tank.

Once the coolant is properly prepared it must be transferred to the test loop for an experiment. There are two high pressure metering pumps that can be used to transfer precise amounts of coolant to the high pressure vessel from the hydrogen saturation tank. They are similar but not identical pumps, and are rated up to 5000 PSIG and a flow rate of approximately 10 mL/min. These pumps can be used at any time during the experiment, but if they were to both fail, there is a backup system that can accomplish the same goal. The coolant is transferred to an intermediate 500 mL tank from the saturation tank via a pressure differential. Then it is isolated and brought to system pressure to transfer into the high pressure vessel. These two transfer mechanisms are used only during the experiment. For the initial coolant transfer before the start of the experiment, the saturation tank feeds directly into the pressure vessel at 300 PSIG.

3.1.3 Data Acquisition and Safety

The AOA test facility was instrumented with numerous sensors to monitor the system during an experiment. Readings from electronic sensors are fed through an analog to digital converter panel into a dedicated computer. A visual basic program was written that can record data at a specified interval, usually every five minutes, throughout the experiment. Parameters that are measured directly are the operating current, level in the pressurizer and saturation tank, the system pressure and temperature, the Teflon

electrode seal temperature, and the pressure in the saturation tank, along with other less critical parameters. The program also calculates the surface heat flux of the wire given a multiplier based on the length of the wire, which is inputted by the user at the start of the experiment.

There are several sensors in the facility used as a back up to the acquisition system described above. The pressurizer level is monitored by a mechanical level indicator that uses magnetic flaps. This sensor does not run the entire length of the pressurizer, but it can give an indication of the liquid level in the pressurizer above the half-way mark. There is also an analog pressure gauge mounted next to the vessel to give a quick indication of system pressure. The Watlow PID controller also gives a visual reading of the vessel temperature and pressure. In addition to having these manual backup sensors, pertinent data readings from the computer are recorded daily in a lab notebook as a backup to the overall acquisition system.

A few safety systems have been added to the facility since its construction. The first is a device to mechanically prevent the electrodes from ejecting in the case of a Teflon/Lava seal failure. This was implemented after such a failure caused an electrode to eject, which is extremely dangerous for anyone who may be in the lab. A thick Lexan shield is located directly in front of the pressure vessel during an experiment for extra protection. Also, there is a narrow-range pressure relief valve to prevent system over-pressurization that would lead to component damage. The float in the pressurizer had to be replaced after being crushed by this type of transient. Finally, an extra valve was installed in the vacuum manifold system that isolates the vacuum gauge from the rest of

the system. This gauge also had to be replaced after it over pressurized, which can happen at relatively low pressures.

3.2 Experimental Procedure

The following will detail the methods by which an experiment was carried out. A typical experiment would last a little over 30 days, during which time the apparatus was monitored carefully and data recorded, however, there were many steps prior to and following an experiment that were equally important in the experimental accuracy of this project. This discussion is therefore divided into preparation of the facility, a typical experiment, and post experiment analysis and maintenance.

3.2.1 Preparation of the Facility

Before the start of an experiment, the facility had to be cleaned from the last run. This involved cleaning the inside of the pressure vessel to remove any substance that would act as a contaminant in the next run. The vessel is cleaned by repeatedly rinsing with distilled water and wiping with paper towels until no more residue is left. Whenever the vessel is opened and not being worked on, a cover is placed over the bottom portion to prevent dust and other contaminants from collecting inside. In addition to the vessel being cleaned, the mixing tanks were also scrubbed before adding the distilled water to them. The other tanks, saturation and blow-down are not cleaned before an experiment. The blow-down tank is the terminal point for the coolant in an experiment, and upon arriving there it no longer has any use. The only concern is when the blow-down tank is too full to accept any more coolant, but it is so large that it does not have to be emptied

regularly. When it does fill up to the point where emptying it is necessary, there is a let down line below the blow-down tank designed for this purpose, where excess waste coolant can be discarded at that point. The saturation tank is permanently sealed and can be evacuated with the vacuum pump so it is not necessary to clean it by hand.

The other major components requiring cleaning are those that interact with the wire. Great care is taken to clean the electrical contacts for the wire. The contact points of the wire holders must be removed of all tarnish and deposits from previous experiments so that arcing is less likely to occur. This is also important to reduce the contact resistance as much as possible so that the heat flux calculation will be accurate for the portion of the wire that is expected to receive the most crud deposition. An arc from the electrodes to any part of the wire will cause intense localized heating and vaporization of the surrounding coolant. This in turn may cause the wire to fail, thereby producing no reliable results from the experiment. The baffles and impeller surfaces are both cleaned. They can be removed for this purpose and reinstalled after they are cleaned.

Once the respective components are cleaned, the coolant preparation begins. First, distilled water is added to mixing tank "A". The amount of distilled water is enough so that there is sufficient coolant for the duration of the experiment to accommodate any leaks and maintain an adequate level in the pressurizer; this amount is typically eight liters. The distilled water can be filtered by transferring it from tank A to tank B. There is a line that has progressively finer filters in it between the two tanks. The transfer process involves filtering it twice by sending the water to tank B, reversing the filters, and then transferring back to tank A. This was done in earlier experiments,

but was later ignored as it provided no real improved water quality. In tank A, the distilled water is deoxygenated by a combination of boiling, mixing, drawing a vacuum on the tank, and bubbling argon through the water using a gas sparger. Simultaneously, the motorized mixer is turning to keep the coolant from becoming stagnant, and expose it equally to the argon gas. In addition, the tank is heated during this process to approximately 200 °F. Degassing continues for nearly eight hours, and the tank is sealed during this process. Periodically a vacuum is drawn on the tank to remove the lighter oxygen gas and lower the pressure in the tank, which vigorously increases boiling.

Meanwhile, the appropriate additives are weighed out, which consist of boric acid crystals, lithium hydroxide, and iron and nickel compounds. The iron and nickel is usually added in nitrate form, and the concentrations of each can vary to give different test conditions. Lithium may be increased or decreased depending on what pH is desired. A pH of 7.1 at temperature of 590 °F requires a Li concentration of 3.1 ppm just to balance out the acidity from the 1500 ppm boron crystals additive. Ultrapure boric acid crystals (99.9995%) are used to eliminate possible contaminants, and the 1500 ppm concentration is reference to typical beginning of cycle conditions of a PWR. These chemicals are then added to the distilled water to produce the coolant used in the upcoming experiment. Particulate matter is not added to the coolant, but instead is placed directly into the vessel. This is accomplished by weighing out the insoluble material, which has always been nickel ferrite ($NiFe_2O_4$) but is not limited to this compound. After the appropriate amount is determined, it is placed into a "bucket," which is just a pipe filter, and the bucket is secured in the vessel by nickel wire. For experiments without the in-vessel mixer, the bucket was hung approximately 2 cm directly above the wire so that

the insoluble material would pass the wire as it fell through the filter. For experiments with the in-vessel mixer, the bucket was wrapped around the inlet pipe to secure it during the experiment. The mixer would then be turned on before the transfer process begins, which is discussed later.

Mixing and degassing continues until the coolant has been in the mixing tank for six to eight hours. From the mixing tank, the coolant is transferred to the hydrogen saturation tank by pressurizing the mixing tank. Before the coolant is transferred however, the saturation tank is evacuated and flushed with the hydrogen/argon mix. This process is repeated a total of three times to virtually eliminate any oxygen in the tank. In between each flushing, the hydrogen/argon gas pressure is vented to atmosphere before applying the vacuum to the saturation tank. This prevents damage to the vacuum pump by over pressurizing it. The excess pressure can be bled off through the same line as the metering valve by just removing the metering valve. It is not necessary to remove the metering valve for draining, but it expedites the process. At the completion of the third flushing, the saturation tank is pressurized to about 30 PSIG and is ready to receive the coolant from the mixing tank. Pressure can be increased in the mixing tank by way of pressurized argon gas through the low pressure cylinder. Typically the pressure in the mixing tank will be 45 PSIG for transfer of the coolant. Transfer from the mixing tank over to the saturation tank usually takes about fifteen minutes. The level in the saturation tank can be read through the dedicated computer, and is given in volts. The volt reading can be converted into liters through the following formula as an approximation (where the reading in volts, V varies as $1 \leq V \leq 2.25$):

$$\text{Level (in Liters)} = 10.43*V - 10.97$$

The transfer process continues until the level reading from the computer is approximately equal to that of the starting amount of coolant, which is usually eight liters. Once the coolant is in the saturation tank, the hydrogen is dissolved into it by the gas entering the bottom and bubbling up to the top. The gas exits through a metering bleed valve which can be used to verify that the hydrogen gas is indeed bubbling through the tank as it should. This process occurs at a pressure of 300 PSIG to ensure the proper hydrogen concentration, and runs continuously for at least 12 hours before the coolant is used in an experiment.

Each experiment used a new test element, which consisted of a 0.0625 inch diameter Zircaloy-4 wire. Each wire had to be prepared in such a way as to maximize the surface area for electrical contact. The last configuration as shown in Figure 3.2 was the most reliable and used for the majority of experiments. The wire was bent into this configuration through a custom built device by hand. The loops at the end were flattened in a large vice. Once in the proper shape, the wires are degreased with acetone, ultrasonically cleaned, and then washed with distilled water. Following this cleaning procedure, the wire is preoxidized by baking it at 675 °F for 12 hours. After being weighed with a high precision Sartorious balance (Model 2434 - accurate to 0.01 mg), the wire is ready to be attached to the electrodes.

3.2.2 Typical Experiment

The wire is placed within the vessel ensuring that it is equally spaced from each electrode. Emphasis must be placed on the wire's orientation and spacing within the vessel to be sure that it is not close enough to anything so that arcing can occur. This

includes the baffles which were orientated as shown in Figure 3.4 to give the maximum distance between them and the wire. The vessel top cover is bolted on by eight large bolts at a torque of 240 ft-lbs for each bolt. The bolts are numbered so the flange fitting is tightened uniformly when the bolts are tightened in order. The amount of torque is scaled up starting at 100 ft-lbs, increasing to 180 ft-lbs, then 240 ft-lbs, and finally 240 ft-lbs again. When the bolts are all tightened, the power cables can be reattached to the electrodes. They are removed at the end of an experiment so that the bolts are more accessible. The thermocouple for the Teflon/Lava seals is also positioned to touch the Teflon plug. Upon completion of these actions, the top of the vessel is prepared for the experiment; the bottom is prepared by reattaching the drain line to the vessel and reconnecting the belt to the magnetic stirrer. When sealed, the vessel and pressurizer are evacuated and flushed repeatedly similar to the process performed with the saturation tank, but this time the fill gas is from the high pressure argon gas cylinder. The system needs to be vented between each evacuation so that the vacuum pump is not over pressurized. This can be done using the valve that isolates the pump from the system and letting the pressurizer and vessel vent to atmospheric pressure before applying the vacuum pump. When the evacuation and purging process is finished, the vessel is filled with argon to a pressure of approximately 200 PSIG, and then the coolant is ready to be transferred from the saturation tank.

The coolant is transferred over to the vessel so that it completely fills the vessel and part of the pressurizer. This is done in a similar manner as the mixing tank to saturation tank transfer. The liquid also passes through the transfer tank during this process, and this liquid can be used as a reservoir for refilling the pressurizer later in the

experiment. The mixer is turned on at the beginning of the transfer process to keep any suspended particles from settling out. The transfer from the saturation tank is continued until the pressurized level sensor first gives a liquid indication. Because of the location of the sensor in the pressurizer this occurs when the pressurizer is about one third full. At this point the transfer process is terminated by closing off the appropriate valves. The heating blanket is activated and the temperature slowly ramps up to the target temperature (usually 590 °F) over several hours. During this process, the level in the pressurizer and the system pressure must both be monitored carefully. To prevent the solution in the tank from boiling, the gas pressure above the free surface of the liquid is maintained well above the saturation pressure for the solution at any given temperature. Secondly, because of liquid expansion during heat-up, the liquid level in the pressurizer has a tendency to rise very quickly near the top of the pressurizer, resulting in a pressure spike which can destroy the titanium float. To avoid this problem, the level is maintained between 60 and 80 percent by using the let-down assembly to release extra liquid. The heating causes the liquid to expand, and when the process is through, approximately 600 mL will have been drained through the let down assembly. The mid-sized filter is used to discard extra coolant while the vessel is heating up. The need to discard this much coolant prevents the pressure from being brought up to full system pressure at the start of the heating process. The pressure can suppress the liquid level reading to well below the target, but when the heating is almost complete this effect is less pronounced and there will not be enough time to let down extra coolant. Once the target temperature is reached and the vessel is in steady state temperature condition, power is applied to the wire by ramping up the current from the power supply. A relatively slow ramp up is necessary to

avoid thermally shocking the wire. The power application starts slowly by raising the current to 40 amps then increasing it in ten amp increments every ten minutes while monitoring the heat flux. The amperage continues to be increased until the desired heat flux is reached, usually between 450 and 500 $^{KBTU}/_{hr\text{-}ft^2}$. Once full power is reached, the data logger is started, and the experiment is now running.

The starting conditions of each experiment ran during the course of this project are summarized in Table 3.1 below. Usually the experiment will run for 30 days, at the end of which a rapid blow down procedure will be used to terminate the experiment. During an experiment, the liquid level is checked daily to ensure an adequate amount remains to compensate for any leaks in the system. Usually, the liquid will have to be replenished at least once during an experiment to maintain at least a 50 percent level in the pressurizer; this is regarded as giving an adequate safety margin. Although uncommon, the level in pressurizer has dropped 40 percent over night as a result of leakage from one or more fittings, and therefore it is important to have an adequate amount of coolant to compensate for these unexpected drops. The liquid level can be increased by one of two ways, the high pressure metering pumps, or via the transfer tank. The metering pumps are a more economical way to transfer liquid, because they do not waste any gas. The main pump is equipped with a speed controller, and both pumps require a piston wash which is enabled through opening the appropriate valve. The pumps take a little longer to get to an adequate liquid level which is about 80 percent full. The transfer tank operates via a pressure differential, which is why it uses up the high pressure argon gas. In addition to closely monitoring the liquid level, the current and voltage to the wire are monitored to see if the resistance increases as the experiment

Table 3.1: Starting conditions of all experiments.

#	ID	Wire Config	Precoated Wire	Heat Flux (kBtu/hr-ft^2)	Days	Coolant Composition (B ppm - Li ppm - Fe ppm - Ni ppm - g of $NiFe_2O_4$)*					Mix
41	0917 1022 04	5	Bare	480	34	1500	5.6	20	10	0.2	Yes
40	0908 0916 04	5	Bare	480	7	1500	5.6	20	10	0.2	Yes
39	0804 0903 04	5	Bare	480	30	1500	3.3	20	10	0.2	Yes
38	0624 0729 04	5	Bare	480	34	1500	3.1			0.2	Yes
37	0513 0617 04	5	Bare	495	34	1500	5.6	20	10		Yes
36	0504 0511 04	5	Bare	490	7	1500	5.6	20	10		Yes
35	0326 0430 04	5	Bare	460	34	1500	5.6	20	10	0.2	Yes
34	0218 0319 04	5	Bare	470	30	1500	5.6	12	6.3		Yes
33	0912 1015 03	5	Bare	450	33	1500	5.6	12	6.3		-
32	0801 0902 03	5	Bare	470	33	1500	5.6	12	6.3		-
31	0527 0630 03	5	Bare	415	34	1500	5.6	20	5		-
30	0328 0414 03	5	Yes	445	17	1500	5.6	20	5		-
29	0313 0324 03	5	Yes	455	11	1500	5.6	20	5		-
28	1219 0128 03	5	Bare	430	40	1500	5.6	12	12.6		-
27	1031 1203 02	5	Bare	445	33	1500	5.6	12	12.6		-
26	0819 0916 02	5	Bare	430	28	1500	5.6	12	12.6		-
25	0628 0726 02	3	Yes	375	28	1500	3.97				-
24	0423 0624 02	5	Bare	400	61	1500	3.97			1.7	-
23	0306 0418 02	5	Bare	500	43	1500	3.47			0.9	-
22	0207 0227 02	5	Bare	500	20	1500	3.47			~1	-
21	0117 0130 02	5	Bare	400	14	1500	3.47	0.2	0.2	&	-
20	1017 1029 01	4	Bare	350	12	1500	3.47	0.2	0.2	&	-
19	1001 1008 01	4	Bare	420	7	1500	3.47	0.2	0.2	&	-
18	0911 0920 01	4	Bare	400	8			0.1	0.1	&	-
17	0822 0829 01	4	Bare	450	7						-
16	0808 0813 01	4	Bare	600	5						-
15	0802 0807 01	3	Bare	350	5						-
14	0731 0731 01	3	Bare	400	<1						-
13	0618 0625 01	3	Bare	400	7						-
12	0530 0611 01	2	Yes	300	12	1500	3.47	0.05	0.05	&	-
11	0504 0514 01	2	Bare	440	10	1500	3.47	0.05	0.05	&	-
10	0419 0501 01	2	Bare	425	12	1500	3.47	0.05	0.05	&	-
9	0328 0409 01	2	Bare	450	12	1500	1.71				-
8	0321 0323 01	2	Yes	440	2	1500	3.47				-
7	0307 0319 01	2	Bare	450	12	1500	3.47				-
6	0221 0305 01	2	Bare	450	12	1500	3.47				-
5	0201 0211 01	2	Bare	400	10	1500	3.47				-
4	0119 0128 01	1	Yes	400	9	1500	3.47				-
3	0104 0115 01	1	Yes	300	11	1500	3.47				-
2	1227 0102 01	1	Bare	300	6	1500	3.47				-
1	1215 1216 00	1	Yes	500	1	1500	3.47				-

& Nickel is in the form of $NiSO_4$ and iron is in the form of $FeCl_3$ for these experiments

progresses. A change in resistance will be a sign that the wire is undergoing some sort of physical change, or temperature increase due to crud deposition.

Once an experiment is ready to be terminated, a rapid blow-down procedure is implemented. This starts with a reduction in the liquid level to a point about 2 cm above the horizontally-oriented Zircaloy-4 wire. Before the let-down begins, the mixer is shut off because of the possibility of vortexing of the coolant, which could expose the wire and consequently burn it out. Since the let-down line inlet is placed within the vessel at the desired liquid level, the let-down assembly will stop draining when that level is reached indicating the vessel is ready for a rapid blow-down. This is accomplished by simultaneously cutting the power to the wire and opening a large drain valve that leads to the blow-down tank. The large operating pressure forces liquid from the vessel exposing the wire so quickly, that any soluble species will be trapped in the wire before they have a chance to dissolve under the no power condition. The vessel cools for several hours under an argon atmosphere, and the wire is now ready for post experiment analysis.

The alternative to the rapid blow-down procedure described above is to do a slow cool-down. This is used to compare the crud of two similar experiments with different methods of ending. The rapid blow-down was intended to capture soluble species, and its effectiveness could be measured by using the slow cool-down in a separate experiment to see how the composition changes. The slow cool-down experiment ends by cutting the power to the wire and turning off the coolant heater. The wire is than immersed in the coolant while it cools down, eventually reaching room temperature. At this point, the coolant is evacuated, and the wire removed from the vessel as usual. Typically, after the

wire has undergone a slow cool-down, the interior of the vessel and the wire itself will both be wet. In this case it is dried before weighed, which is discussed later.

3.2.3 Post Experiment Analysis and Facility Maintenance

After an experiment, the wire is carefully analyzed to examine various properties of the crud. First, the vessel will usually cool for at least two and half hours (sometimes as long as overnight), before the vessel can be safely opened. The wire is carefully removed from the vessel and weighed. Often the crud deposit will be very fragile, and the wire will have to be handled extremely delicately at least until it is weighed. The end of experiment weight is compared to the initial weight to find the mass of crud that accumulated. Sometimes there is a boron crystal that is attached to the wire that will completely negate the weight of the crud by comparison. This is handled by weighing the wire first with the crystal attached and then again after breaking off the crystal. This will give a rough idea of the weight gain of just the crud portion of the wire.

The next data collection step for the post-experiment wire is to analyze the chemical composition of the crud. This is accomplished through Energy Dispersive X-ray (EDX) and Secondary Ion Mass Spectroscopy (SIMS) analysis. Occasionally, a powder x-ray diffraction analysis (XRD) is done when enough crud is present. Laser ablation inductively coupled mass spectrometry (ICP-MS) has also been used, with varying results. Additionally, high definition photos are taken to illustrate the shape and form of the crud; this is done through Scanning Electron Microscope (SEM).

Routine maintenance is also typically performed after an experiment. Several important items had to be attended to periodically, and would usually present themselves

as problems during an experiment. The Teflon/Lava electrode seals have a limited lifetime, the end of which would be determined if they leaked too much during an experiment. These seals are sensitive, so movement of the electrodes during the preparation phase of an experiment could shorten the lifespan of a Teflon/Lava seal. There is a bearing in the MagneDrive unit that had to be replaced which could cause the shaft to rotate unevenly or seize. This bearing is rated at 1000 hours when operated at 2000 RPM; since the mixer was operated at a significantly lower speed, the bearing did not require replacement very often. Finally, the metering pumps could fail and this would require cleaning to get them working again.

CHAPTER 4

RESULTS

The data collected from these experiments span several significantly different testing phases. There are three basic experimentation phases within the lifetime of this facility: optimization, exploratory, and coolant composition. This thesis work was conducted during the most recent phase of this project, which consists of experiment numbers 34 through 41. Earlier experiments are included in this report for the purpose of completeness. All experiments that were run are briefly summarized in Table 4.1, and pertinent experiments from that table are discussed in greater detail in Appendix A. The following will explain each of the phases mentioned above.

Facility optimization was an ongoing process for the first two years of operation and in some respects still is. Often, an experiment failure will bring a new perspective on either the procedure or the actual apparatus components themselves. The earlier chapter on the apparatus and procedures represents the most refined versions of each. The way in which the Zircaloy test element was modified is one example of the optimization process of this project before comparative data was collected. The period of facility optimization yielded its most useful contribution by making later experiments more reliable. However, there are a few experiments from that group that had interesting data, and they will be discussed later.

Two specific optimization procedures that took place have important repercussions for the data collected. One of the earlier goals of this experiment was to

Table 4.1: Result Summary of All Experiments.

#	ID	Duration (Days)	Weight Gain (mg)	Wire Broke?	Other Notes
40	0908 0916 04	7	90	Y	Power transient due to outage
39	0804 0903 04	28	386	-	
38	0624 0729 04	34	6	-	
37	0513 0617 04	34	40	-	
36	0504 0511 04	7	20	-	Leakage & unusual current behavior
35	0326 0430 04	34	435	-	
34	0218 0319 04	30	11	-	
33	0912 1015 03	33	8	-	
32	0801 0902 03	33	-3	Y	No heat flux for one day before blow-down
31	0527 0630 03	34	25	-	
30	0328 0414 03	17	167	Y	No heat flux for 3 days before blow-down
29	0313 0324 03	11	125	Y	No heat flux for 3 days before blow-down
28	1219 0128 03	40	214	-	
27	1031 1203 02	33	-	-	
26	0819 0916 02	28	31	-	
25	0628 0726 02	28	-14	-	Pre-coating came off
24	0423 0624 02	61	7	-	
23	0306 0418 02	43	48	-	
22	0207 0227 02	20	6	-	
21	0117 0130 02	14		-	Hybrid electrode seals first used
20	1017 1029 01	12	-	-	
19	1001 1008 01	7		Y	No heat flux for one day before blow-down
18	0911 0920 01	8		Y	No heat flux for one day before blow-down
17	0822 0829 01	7		Y	Electrode seal failure
16	0808 0813 01	5		Y	No heat flux for 2 days before blow-down
15	0802 0807 01	5		Y	
14	0731 0731 01	<1		Y	Wire broke immediately
13	0618 0625 01	7		Y	Large vessel leakage
12	0530 0611 01	12	18	-	Pre-coating came off
11	0504 0514 01	10	17	-	Slow cool-down
10	0419 0501 01	12	30	-	
9	0328 0409 01	12	43	-	
8	0321 0323 01	2	-	Y	Pre-coating came off
7	0307 0319 01	12	48	-	
6	0221 0305 01	12	32	-	Slow cool-down
5	0201 0211 01	10	50	-	Slow cool-down
4	0119 0128 01	9		Y	Pre-coating came off, 2 days no heat flux
3	0104 0115 01	11	-43	-	Pre-coating came off
2	1227 0102 01	6		-	Failure in rapid blow-down
1	1215 1216 00	1		Y	

produce a crud layer on a pre-coated wire so that the crud growth rate and other important properties could be found as a function of the initial coating thickness and porosity. Unfortunately, this was not possible because the coating was not tenacious enough to withstand the operational heat flux and would invariably flake off. This usually led to an overall weight loss for the wire when weight measurements could be performed, as can be seen in experiments 3 and 25. The initial coatings were made of nickel ferrite and applied by Dominion Engineering of Washington, DC; in some cases, spray pyrolysis was used to apply the coatings in-house. Because the wire configuration was not yet optimal, these wires would often break like their bare counterparts. However, the two that did not break lost all their initial coatings. Sometimes a second coating was on the wires, which had deposited in situ, but it was obviously different than the first; this is illustrated in the case of experiment 12. Even under relatively low heat flux (300 $^{kBtu}/_{hr\text{-}ft^2}$) the pre-coating would still come off. This development changed the course of the project, and the focus was shifted to depositing crud on bare wires in situ.

The second important issue related to facility optimization was the elimination of contaminant based crud (first 20 experiments). The largest source of contamination was the Lava electrode seals, which allowed large amounts of calcium to leach into the coolant and make its way to the wire for deposition. In order to solve this problem, the hybrid Teflon/Lava seals were custom designed and installed on the vessel. The next largest source of contamination was the electrodes themselves. The electrodes were originally made from nickel plated copper rods; they were later replaced by all stainless steel electrodes. The nickel plating apparently corroded off after numerous experiments. The copper then made its way into the coolant and significant amounts showed up in the

crud. The last source of contamination was believed to be the boric acid used for the boron additive. Trace amounts of aluminum, calcium, and silicon were in the standard purity boric acid, so the switch was made to ultra pure boric acid from experiment number 11 on. The elimination of contaminant based crud allows for more realistic crud deposition and therefore leads to better data. It is important to note however, that the crud of later experiments still contains trace amounts of contaminants such as copper, aluminum, calcium, and others, and sometimes inexplicable larger amounts of contaminants such as silver (experiment numbers 37 and 40). The difference being that the majority of the crud no longer consists of contaminants; instead, it consists mostly of iron, nickel, and oxygen.

Next, there were three experiments that were exploratory (unconventional) and do not fit into either of the other two categories, but still produced interesting data. Two experiments (numbers 29 and 30) were run with a pre-coating technique called spray pyrolysis. This is a process where an oxide layer is produced on the wire by simultaneous heating and spraying of a mist containing small amounts of iron and nickel present in the parts per million ranges. Although the goal was to produce a prototypical nickel ferrite layer on the wire, spray pyrolysis would produce a significant deposit of mostly zirconium oxide on the wire, in addition to having the undesired effect of structurally weakening the wire considerably. Both of the experiments ended prematurely because of the wire breaking. Coupled with the fact that the spray pyrolysis process itself was difficult and imprecise, this line of experiments was abandoned. The other unconventional experiment (number 28) was run without hydrogen saturation and

produced a large amount of crud on the wire. However, this is very unrealistic for plant conditions, so more experiments without hydrogen saturation were not run.

The final stage of data from this project, which includes the work performed in this investigation, is the coolant composition experimentation phase. After the facility was optimized as mentioned above, the emphasis was placed on comparing crud composition as coolant additives vary. Soluble nickel and iron were added to the coolant in nitrate form and in relatively large amounts. The excess amount would allow the crud deposition process to accelerate as well as diminish the effects of trace contaminants in the coolant. The iron nitrate has an acidic effect, so an additional 2.5 ppm lithium is added to balance out the pH for a 20 ppm iron nitrate addition (see Appendix B for a complete explanation). High pH experiments were inadvertently run because of an error in the nitrate calculation and then later run at the target pH for comparison. These experiments were 26 through 28 and 32 through 34 respectively. Before using nitrates, the experiment was run with nickel sulfate and iron chloride, but out of concern for the possibility of accelerated corrosion in the high pressure vessel, nitrates were used instead. The nitrate experiments produced many viable data points, specifically experiment numbers 23, 24, 26, 27, and 31 through 41. All of these experiments will be discussed in the data presentation section.

4.1 Preliminary Results

Several important results were found before this thesis work was started. These include creating a porous crud layer, verifying the capture of soluble and boron species through the rapid blow-down technique, and the elimination of contaminant based crud.

The porous crud layer is important because it replicates what has been found in industry crud and the vapor chimneys may be important to the boron deposition process by concentrating borate species. The porous layer is also a verification of the subcooled boiling taking place. In this project, this porous layer was observed in earlier experiments and then verified later in crud of prototypical composition. Specifically, experiments number 10 through 12 all showed a porous layer similar to that of prototypical crud, however, the composition of the crud from these experiments was mostly contaminant based. Later experiments such as numbers 26 and 27 also had a porous crud layer, but with a more prototypical composition. These porous crud layers are illustrated in Figures 4.1 through 4.5.

The next important result of this project that was from initial experiments was the verification of the effectiveness of the rapid blow-down process. This was also a result observed in the experiment series 10 through 12. Evidence of the effectiveness of the rapid blow-down is seen in both the boron concentration and the total weight gain of the crud from each experiment. Experiments 10 and 12 were both ended by rapid blow-down while number 11 was ended by slow cool-down. The weight gain of 12 is skewed because the pre-coating is not included but the comparison of the weight gains of 10 and 11 clearly shows that the slow cool-down experiment has almost half of the total crud of the rapid blow-down experiment. Also, the slow cool-down had less boron by weight percentage than the two rapid blow-down experiments. This comparison can be made without regard for the pre-coating. Both results are presented in Table 4.2.

Table 4.2: Comparison of Boron Concentration and Weight Gain of Experiments 10, 11, and 12.

	Boron (Wt. %)	Crud Weight (mg)
Experiment Number 10	6.68	30
Experiment Number 11	3.90	17
Experiment Number 12	5.75	18

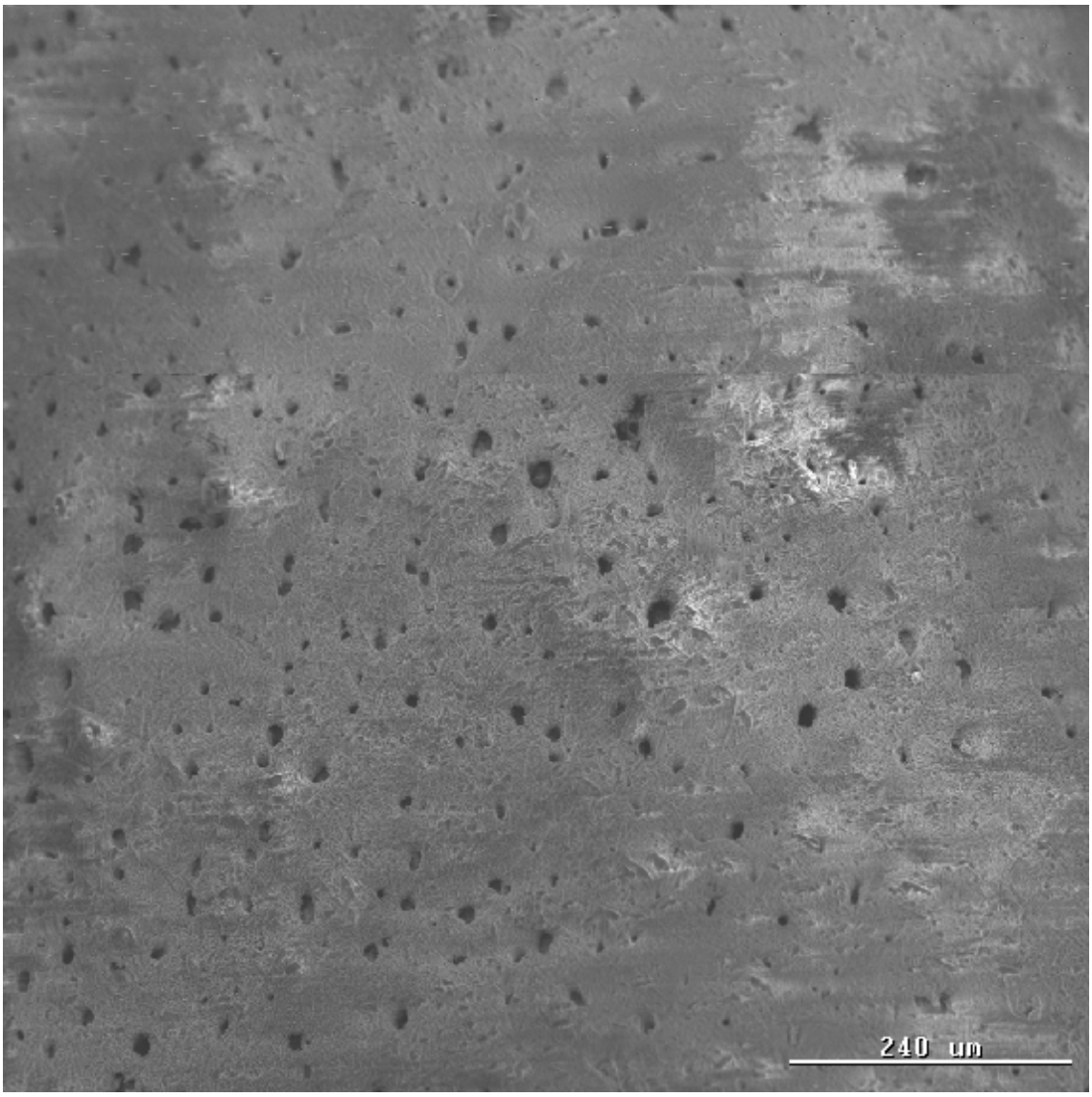

Figure 4.1: SEM Image of Crud on Experiment Number 10 at 100x Magnification.

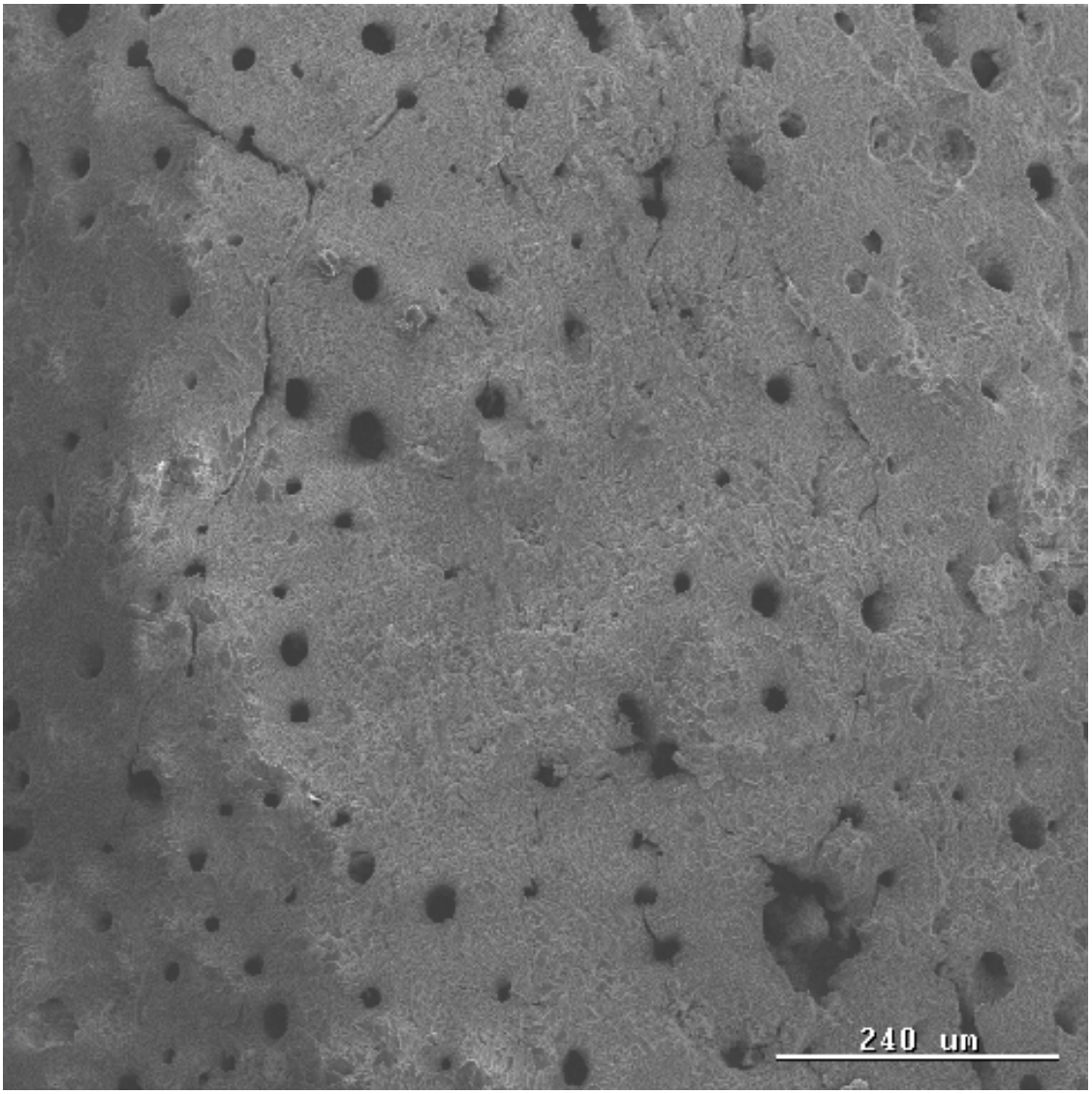

Figure 4.2: SEM Image of Crud on Experiment Number 11 at 100x Magnification.

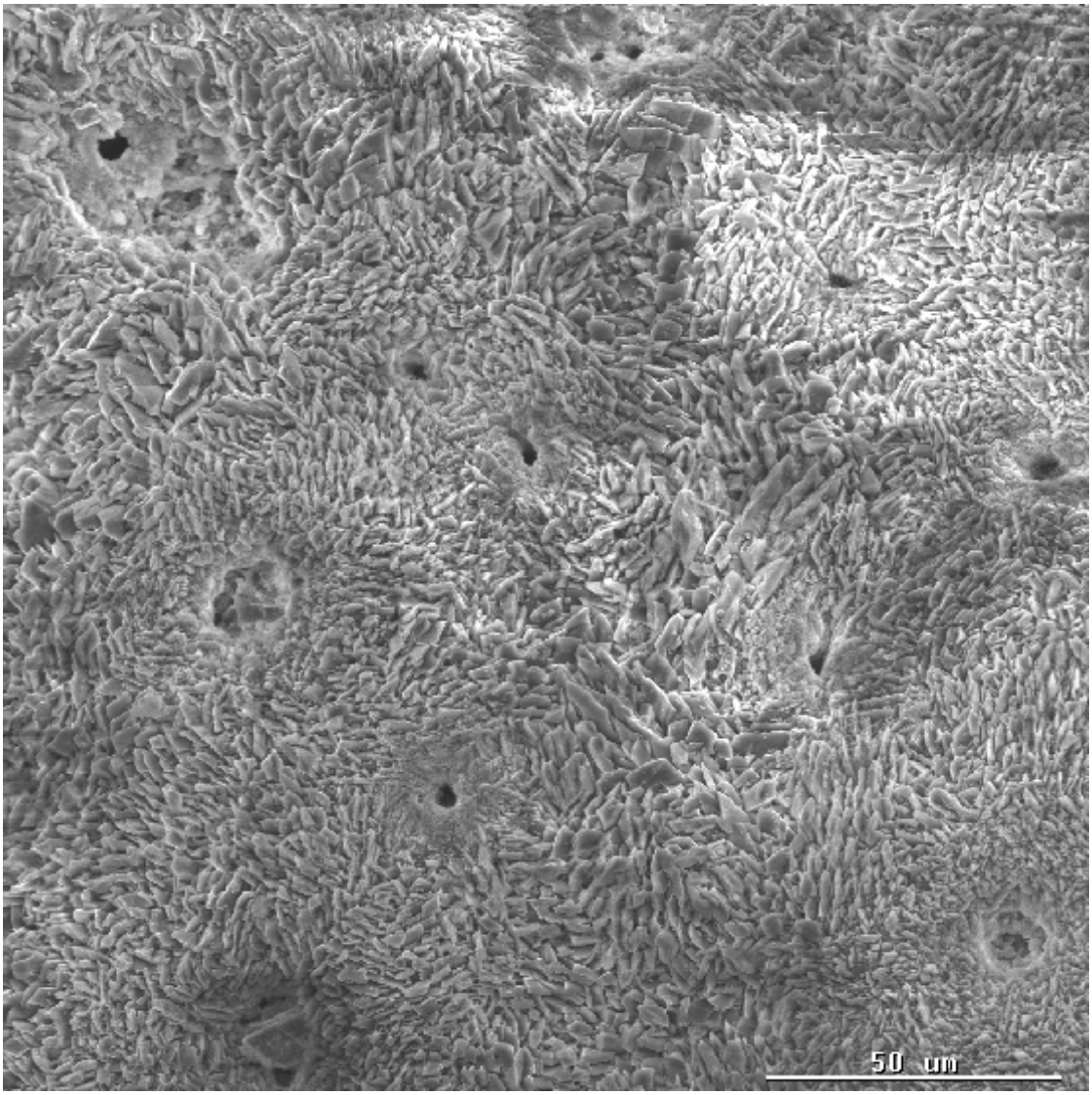

Figure 4.3: SEM Image of Crud on Experiment Number 12 at 500x Magnification.

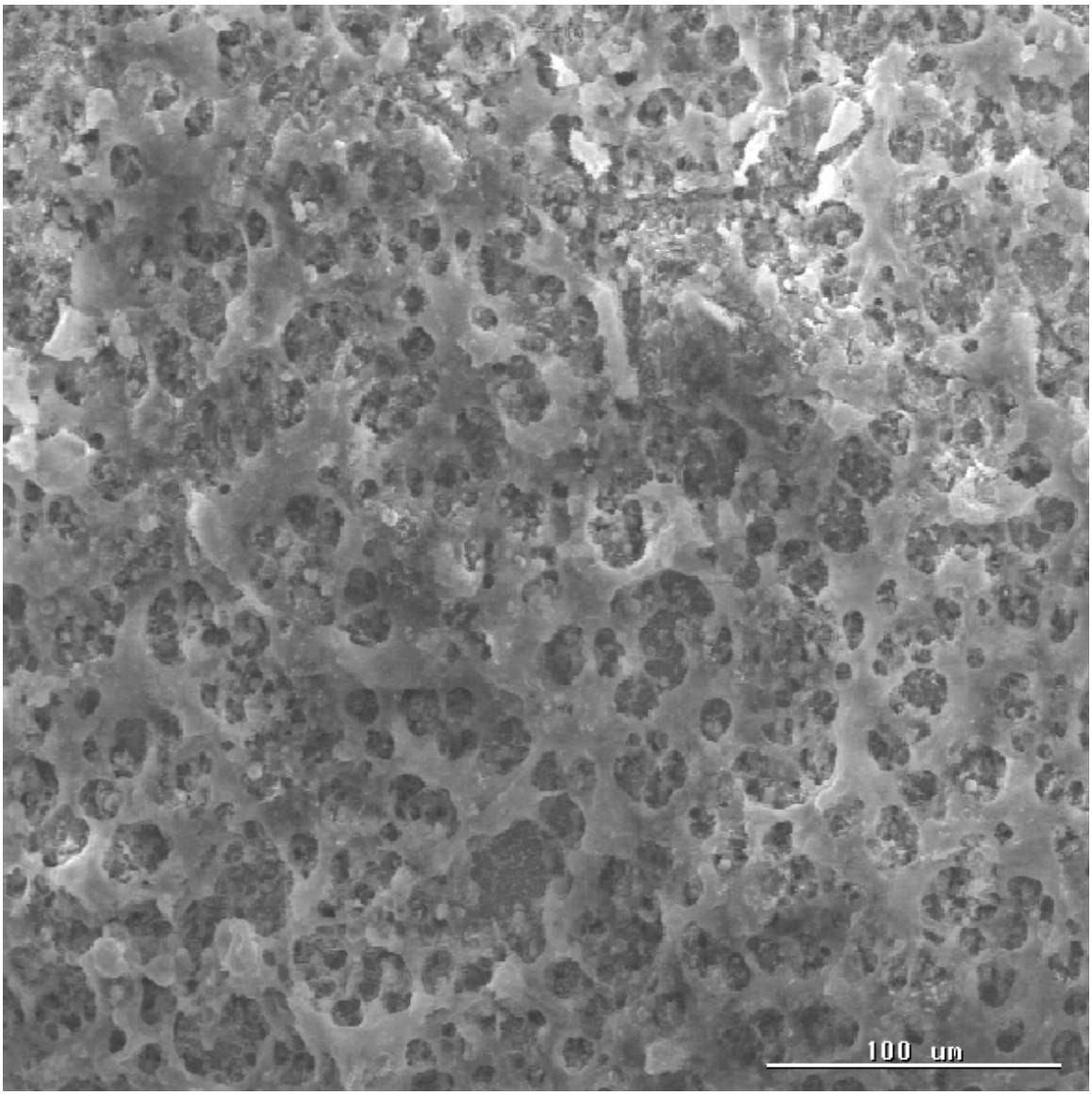

Figure 4.4: SEM Image of Crud on Experiment Number 26 at 250x Magnification.

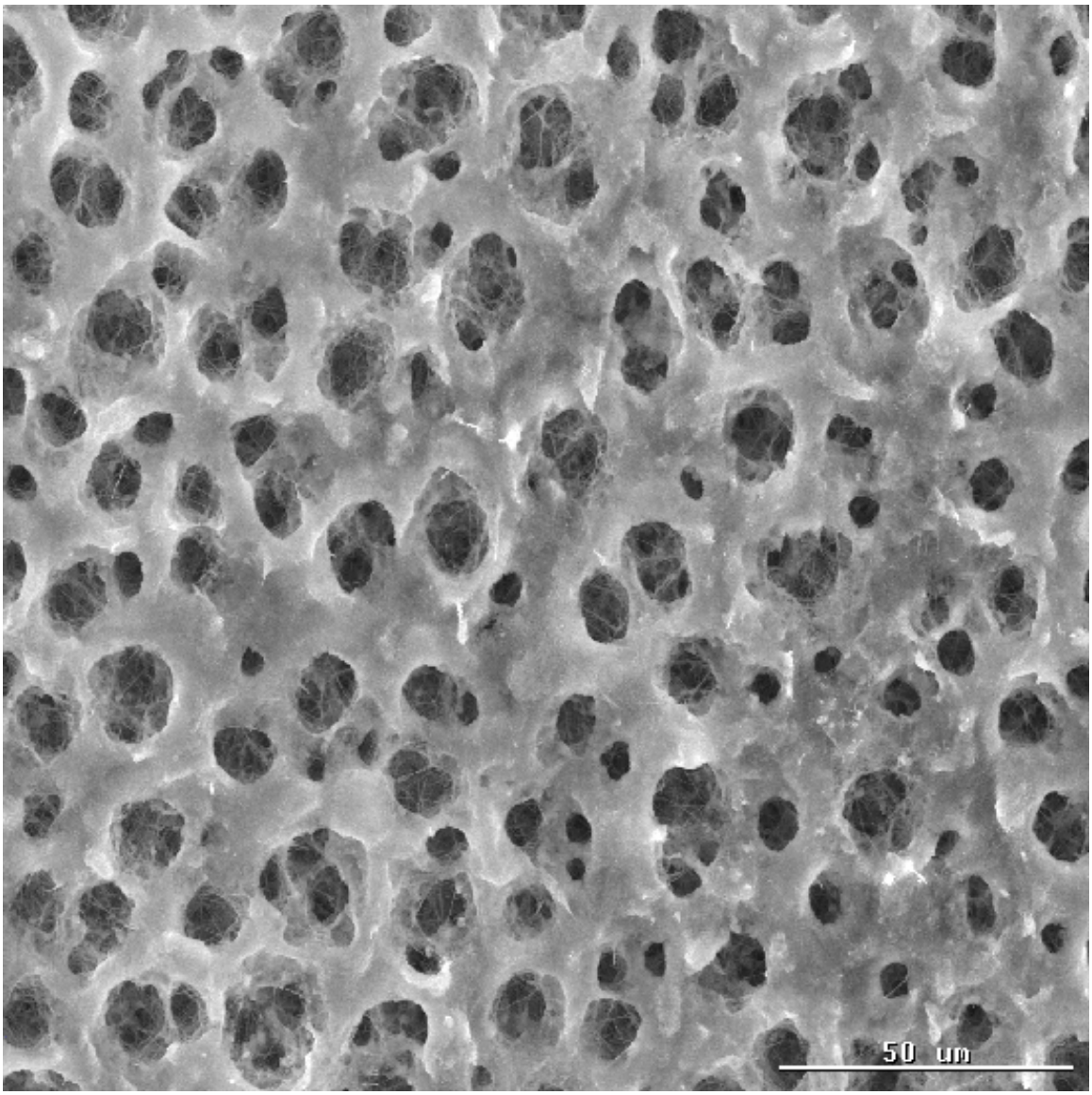

Figure 4.5: SEM Image of Crud on Experiment Number 27 at 500x Magnification.

The final preliminary result is the elimination of contaminant based crud. This is important for the reliability of the crud data collected as mentioned before. The earlier portion of this experiment was successful in elimination of contaminants as a significant percentage of the total crud weight. This is illustrated in Figure 4.6, which compiles the EDX data for all experiments reported in Appendix A.

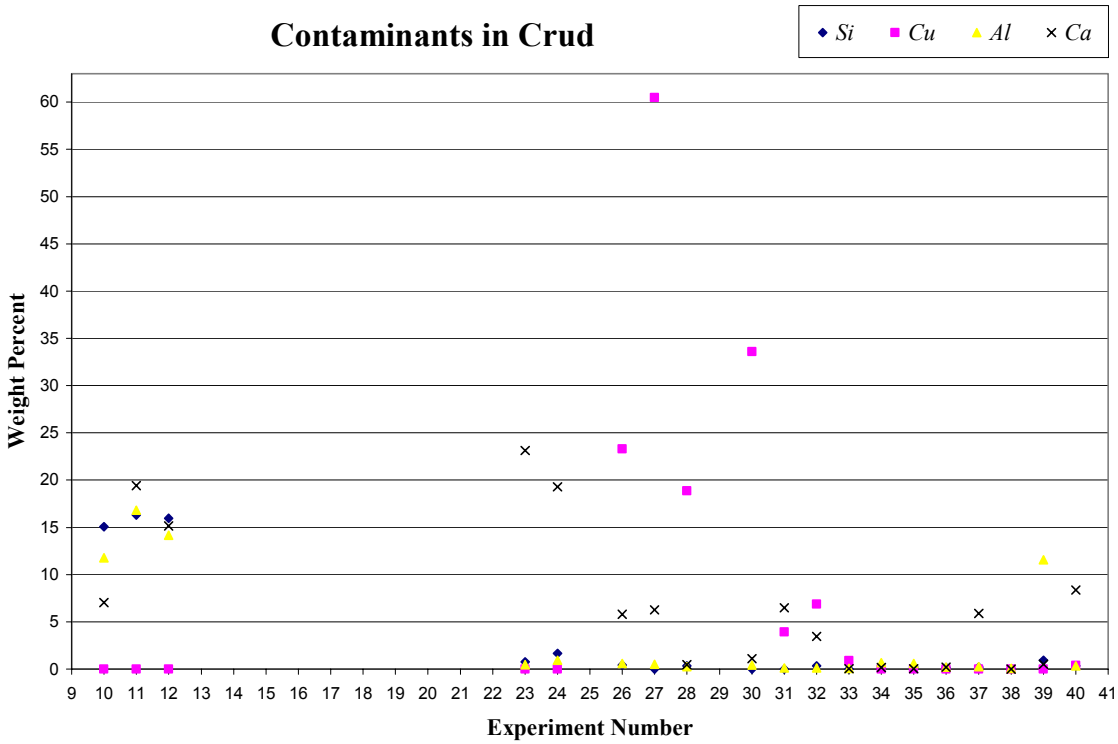

Figure 4.6: Contaminants in Experimental Crud by Experiment Number.

4.2 Thesis Project Results

The thesis portion of this project furthered the research into crud growth and boron deposition within the crud layer. Three results of import to the topic of AOA that have been investigated through this work are the creation of prototypical crud,

identification of boron deposition species, and insight into operating conditions influencing the crud growth and boron deposition processes.

Prototypical crud is important for application of this research to an operating reactor. As mentioned before the presence of contaminants was reduced, and at the same time the nickel and iron deposits in the crud increased as fraction of the whole. This is illustrated in Figure 4.7 below, which has been constructed from the EDX data for each of the experiments summarized in Appendix A. Combined with the fact that the later experiments also have a porous structure, and the crud created during this project does indeed represent prototypical reactor crud. Examples of the porous structure found in later experiments are presented in Figures 4.8 and 4.9.

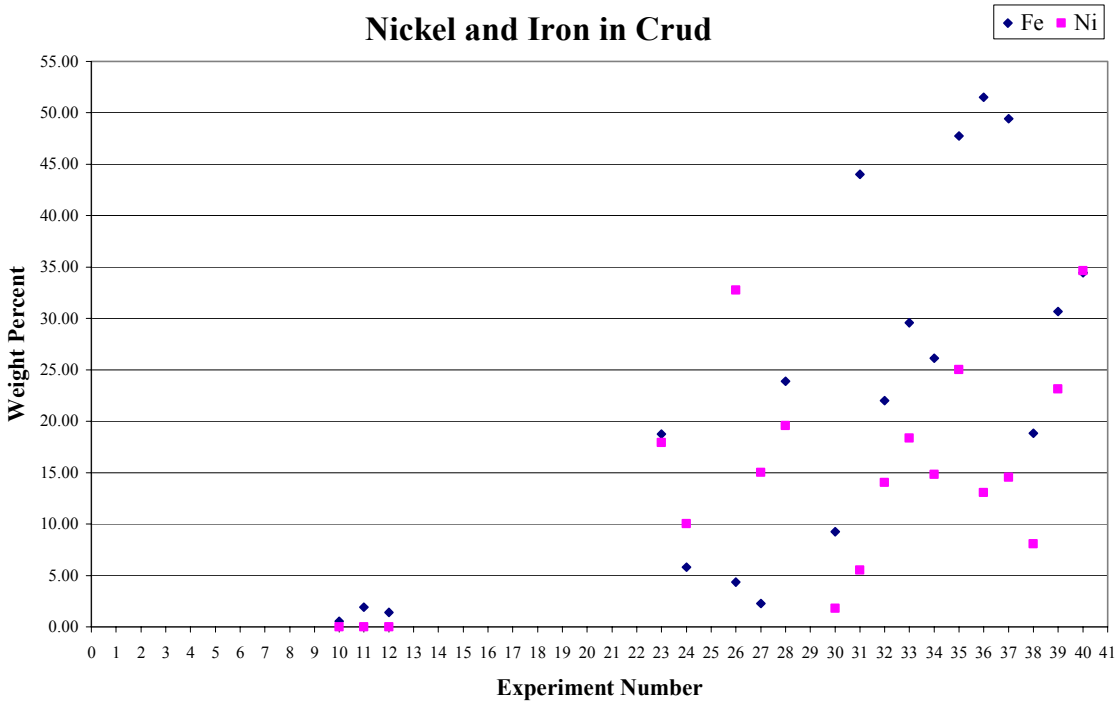

Figure 4.7: Nickel and Iron in Experimental Crud by Experiment Number.

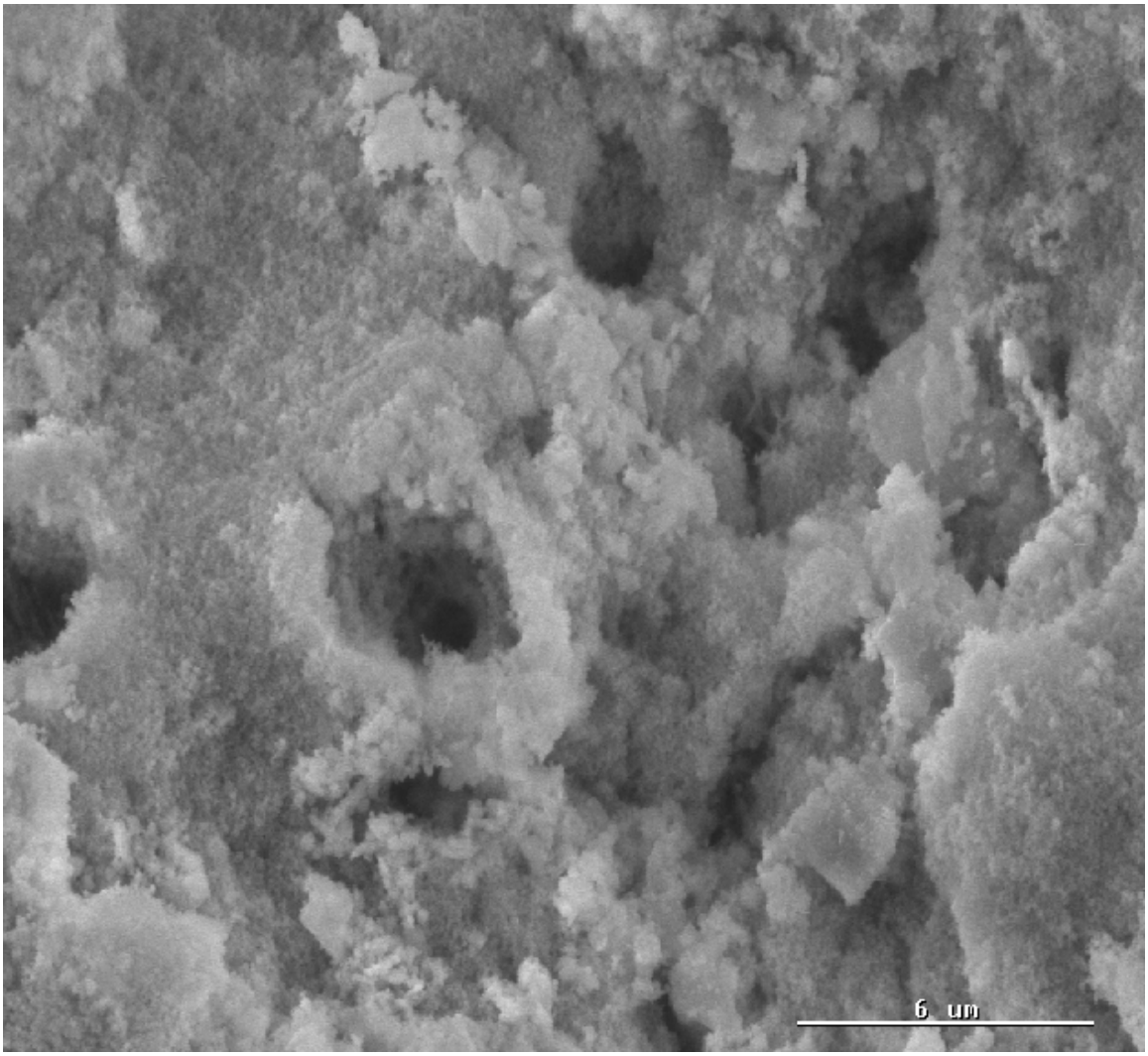

Figure 4.8 Porous Structure in Experiment Number 39 at 4000x Magnification.

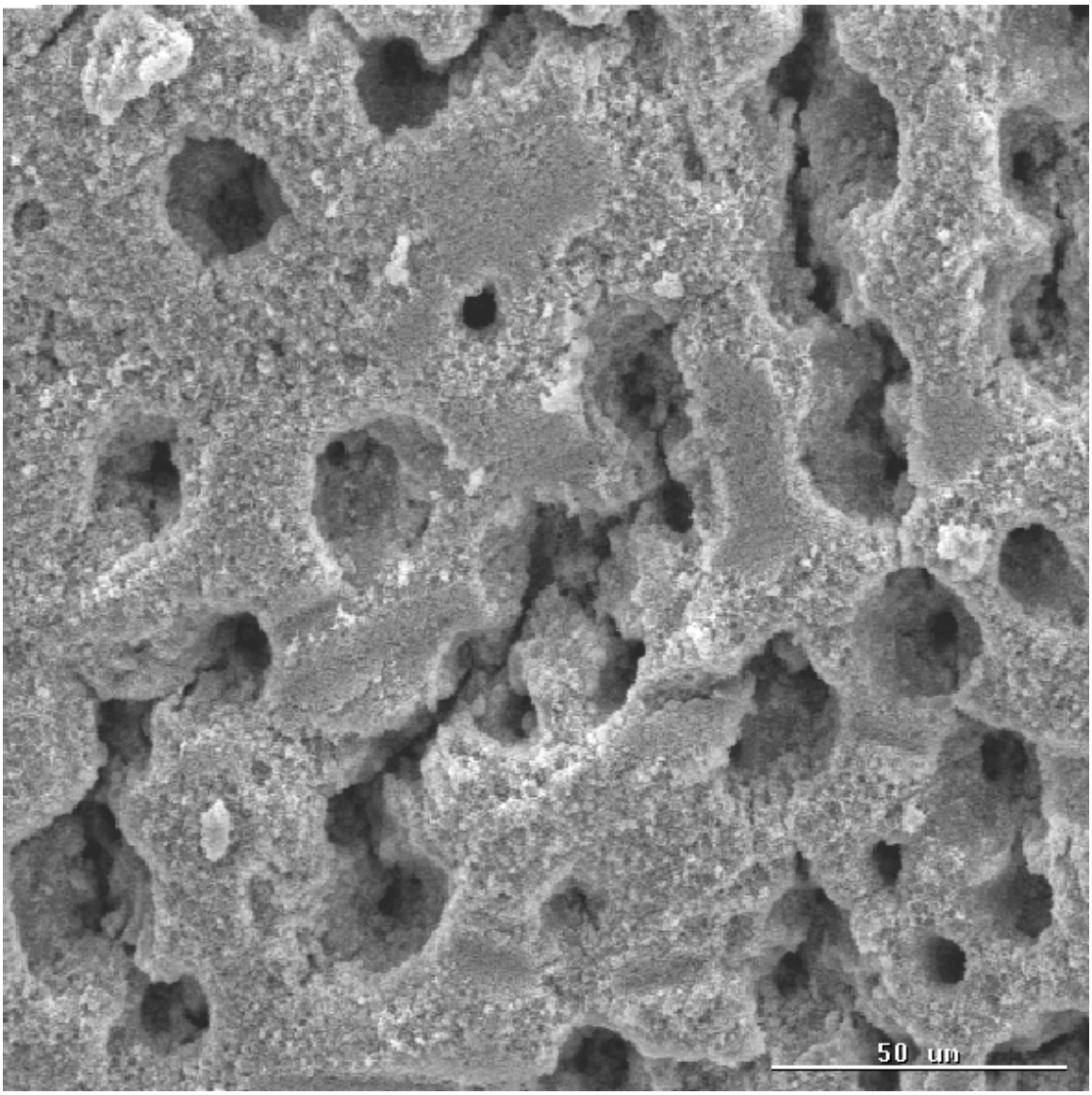

Figure 4.9: Porous Structure in Experiment Number 36 at 500x Magnification.

There is also some variance of the crud within the industry. Specifically, as reported in Chapter 2, plants with different stages of AOA had different nickel-to-iron ratios. The crud from this experiment followed that characterization, not including those wires with a large amount of contamination. Using the fact that more severe AOA plants contain a higher nickel to iron ratio, the crud from this experiment represents that of prototypical substance. Consider the chart below in Figure 4.10. EDX and ICP-MS data are averaged together in this chart. For the two experiments that had separate crystal analysis in the EDX data, these were combined with the bulk to give the overall boron weight percent. Obviously this will slant the data to a higher boron weight percent than is actually present, but this approximation will suffice for comparison purposes. Also the ICP-MS data is given only in weight percent, so the iron to nickel ratio is off but not

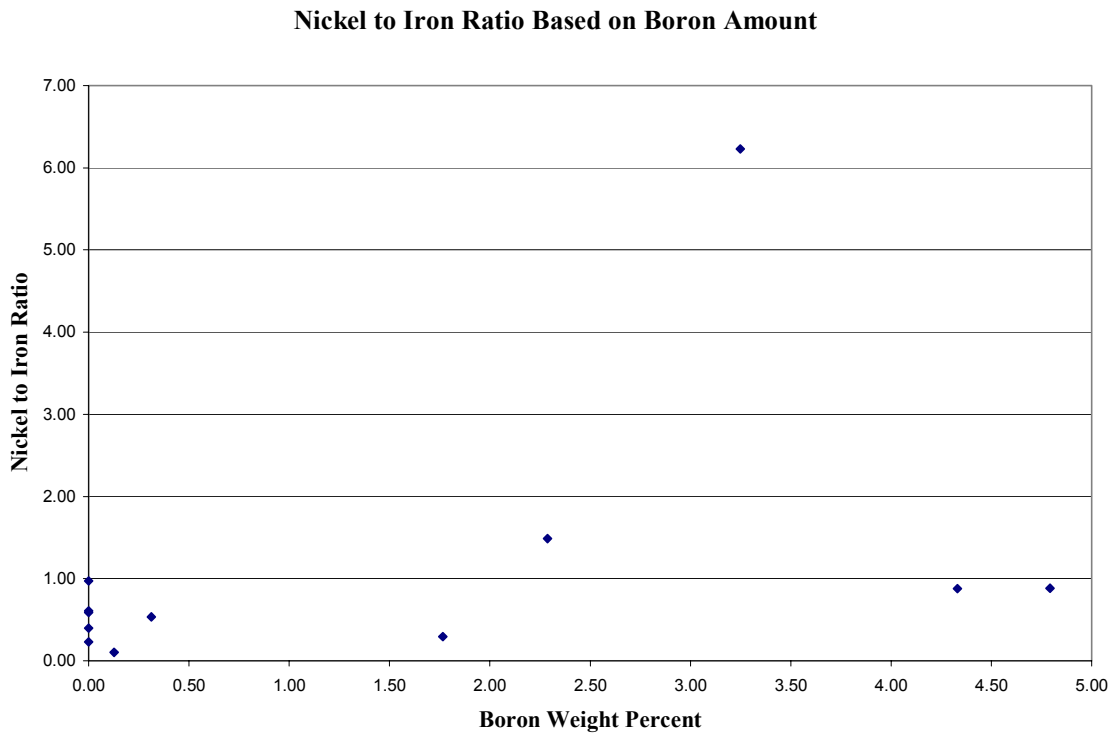

Figure 4.10: Chart of Crud Composition.

significantly. With these considerations in mind, the chart clearly illustrates that crud samples with significantly less than one percent boron deposition all have a nickel to iron ratio around 0.5 or less. The one exception is the crud from experiment 40 that ran under similar conditions (albeit shorter) as the control experiment, but underwent a slow cool-down to end the experiment instead of the rapid blow-down. Here it is expected that the soluble boron species would go back into the coolant as apparently happens in a PWR core. Using this rationalization the crud formed under AOA conditions should (and this case does) have a higher nickel-to-iron ratio and little to no boron. The crud samples with more than one percent boron by weight have more variance in the nickel to iron ratio, but the general trend of increasing is obvious.

The second and most interesting result of this experiment is the discovery of the chemical composition of boron bearing compound deposited within the crud. Experiment number 35 consisted of the ideal conditions for crud growth. Both particulate and soluble matter was combined in the coolant, and the experiment ran with a target pH of 7.1. This led to a crud deposition of 435 mg of mostly nickel and iron species on the Zircaloy-4 test wire, which corresponds to 8300 mg/dm^2. This crud deposit had large crystals scattered throughout as shown in Figure 4.11. These crystals showed a boron concentration averaging 14.5 percent by weight as determined by EDX. The species that these crystals represent was determined by XRD, which also identified a lithium nickel ferrite species as is illustrated in Figure 4.12. The mineral name for the lithium borate species identified by XRD is diomignite ($Li_2B_4O_7$), but it is also referred to as lithium tetraborate. Two high magnification pictures of these crystals are presented in Figures 4.13 and 4.14.

Initially it was suspected that a lithium borate species was precipitating within the crud of PWRs because of the neutron flux behavior (boron effect) and the lithium hideout and return behavior noticed during power transients as shown in Figure 1.2. Indeed, the most plausible explanation for lithium hideout and return within the plant is the precipitation of a lithium borate species. The first such species to be considered was lithium metaborate because of its solubility properties. However, this experiment and another [29] have both repeatedly found a lithium-to-boron ratio much less than one within the simulated crud ruling out lithium metaborate as the likely AOA causing species. In addition, lithium metaborate was never actually observed or direct evidence of it having been in the crud produced. On the other hand, lithium tetraborate has the characteristics required to meet the indirect evidence requirements with the added advantage to have been directly observed in simulated AOA crud. The only unknown with the lithium tetraborate species is the solubility at high temperature, but this can be easily found through a separate experiment.

Lithium tetraborate crystal is a commonly studied piezoelectric crystal. Growth methods have been studied and experimented with in order to grow the crystals more economically. Lithium tetraborate growth studies also center on improving the structural qualities of the crystal. One growth method that suits both of these goals is the hydrothermal growth technique, which is a rather unique property of lithium tetraborate crystals. Hydrothermal growth means growing crystals in an aqueous environment under increased temperature and pressure. That pretty well describes the environment of this project's pressure vessel and of course a PWR. Ideal temperature and pressure conditions for hydrothermal growth are reported in the literature as 482 °F and 1450 PSIA

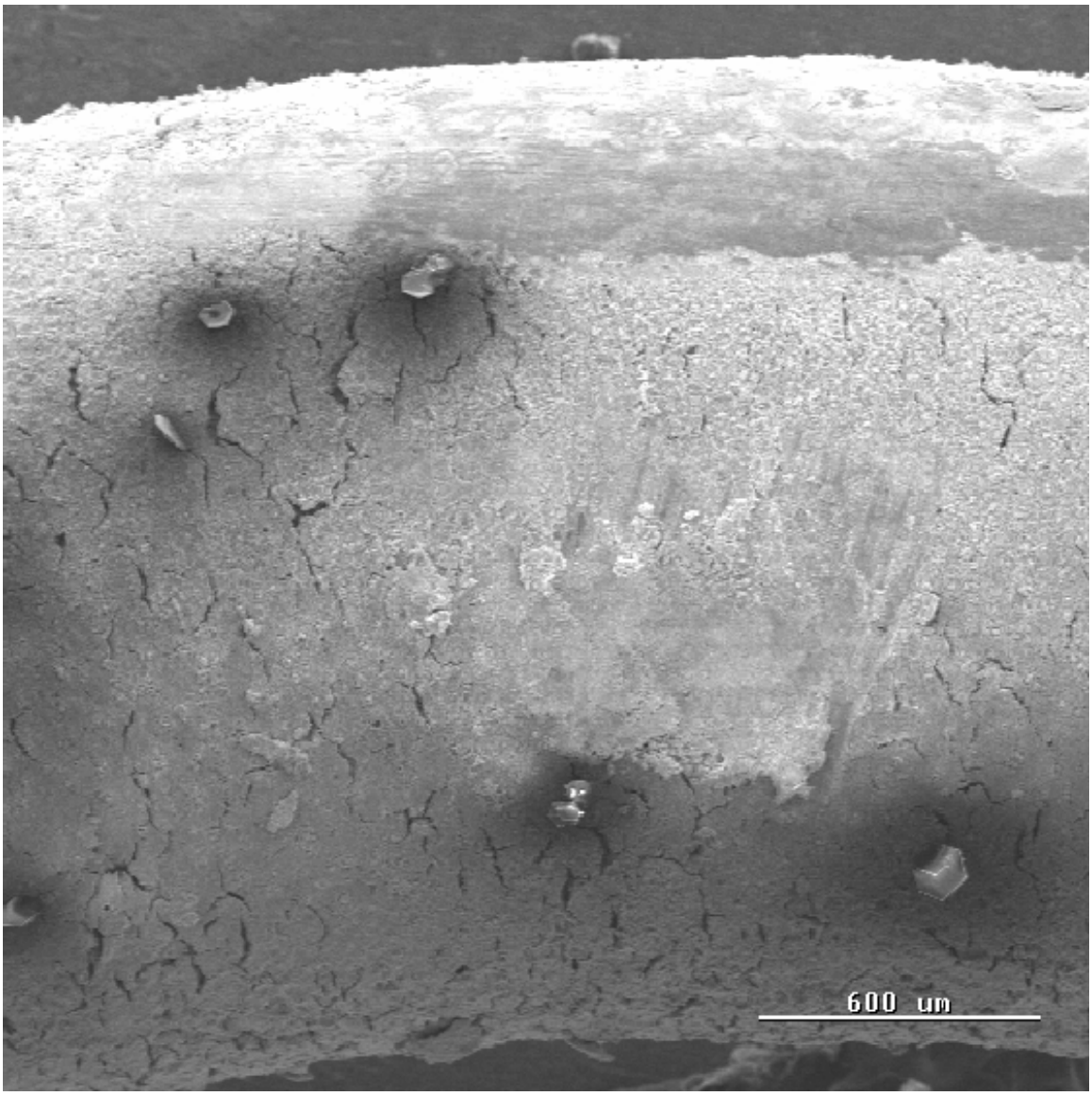

Figure 4.11: SEM Image of Crud on Experiment Number 35 at 40x Magnification.

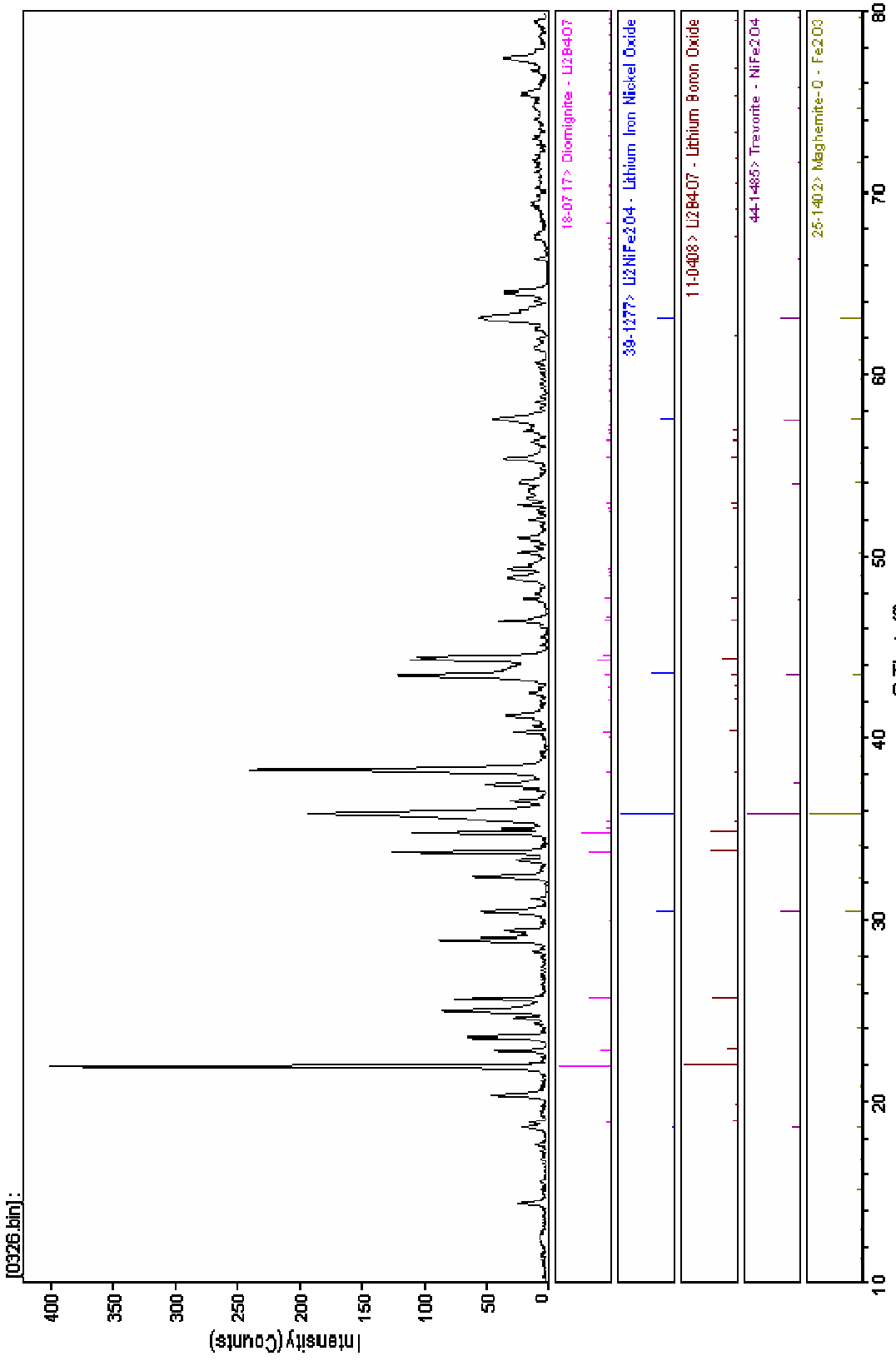

Figure 4.12: XRD Graph of Crud from Experiment Number 35.

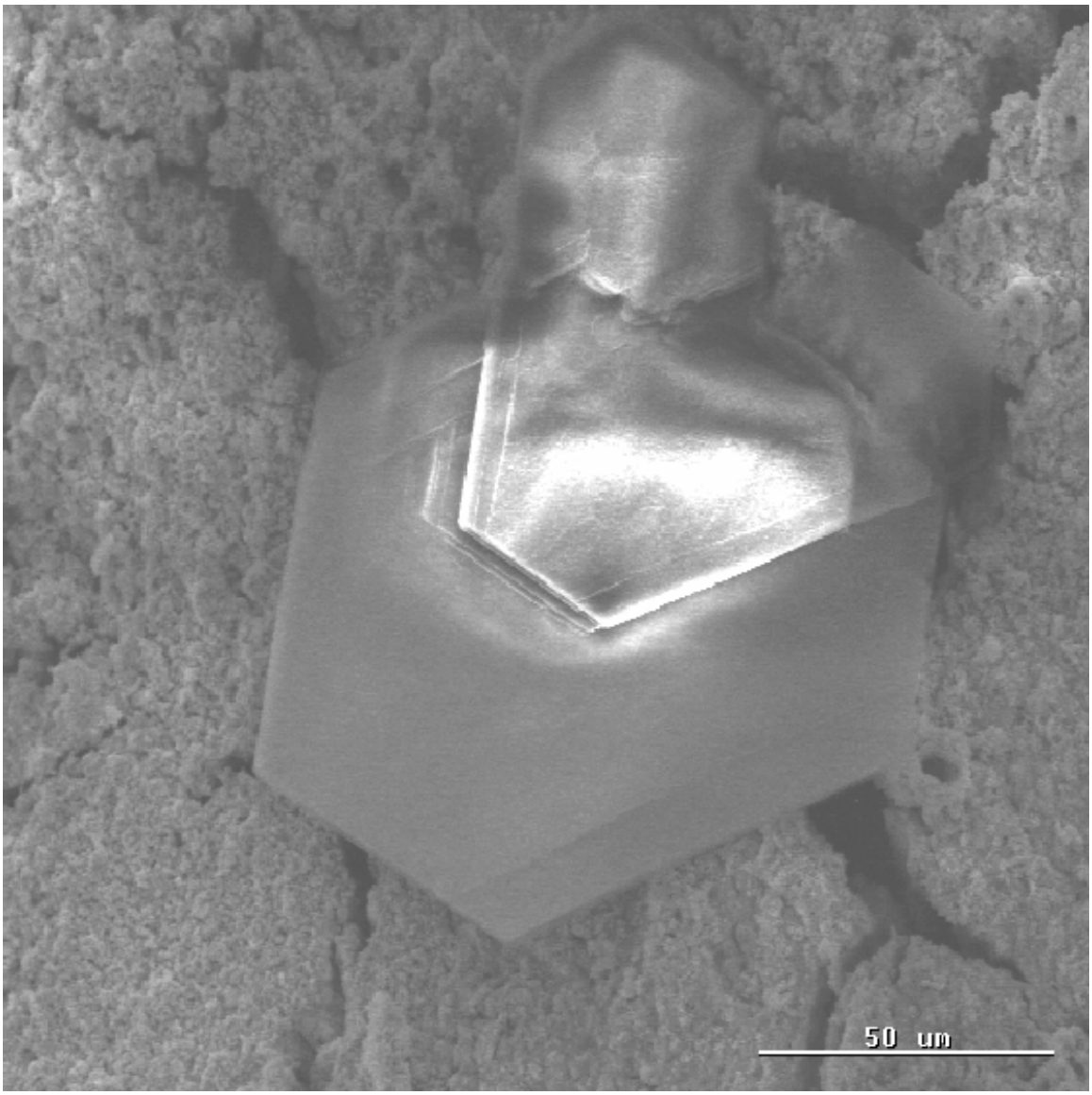

Figure 4.13: SEM Image of Crystal from Experiment Number 35 at 500x Magnification.

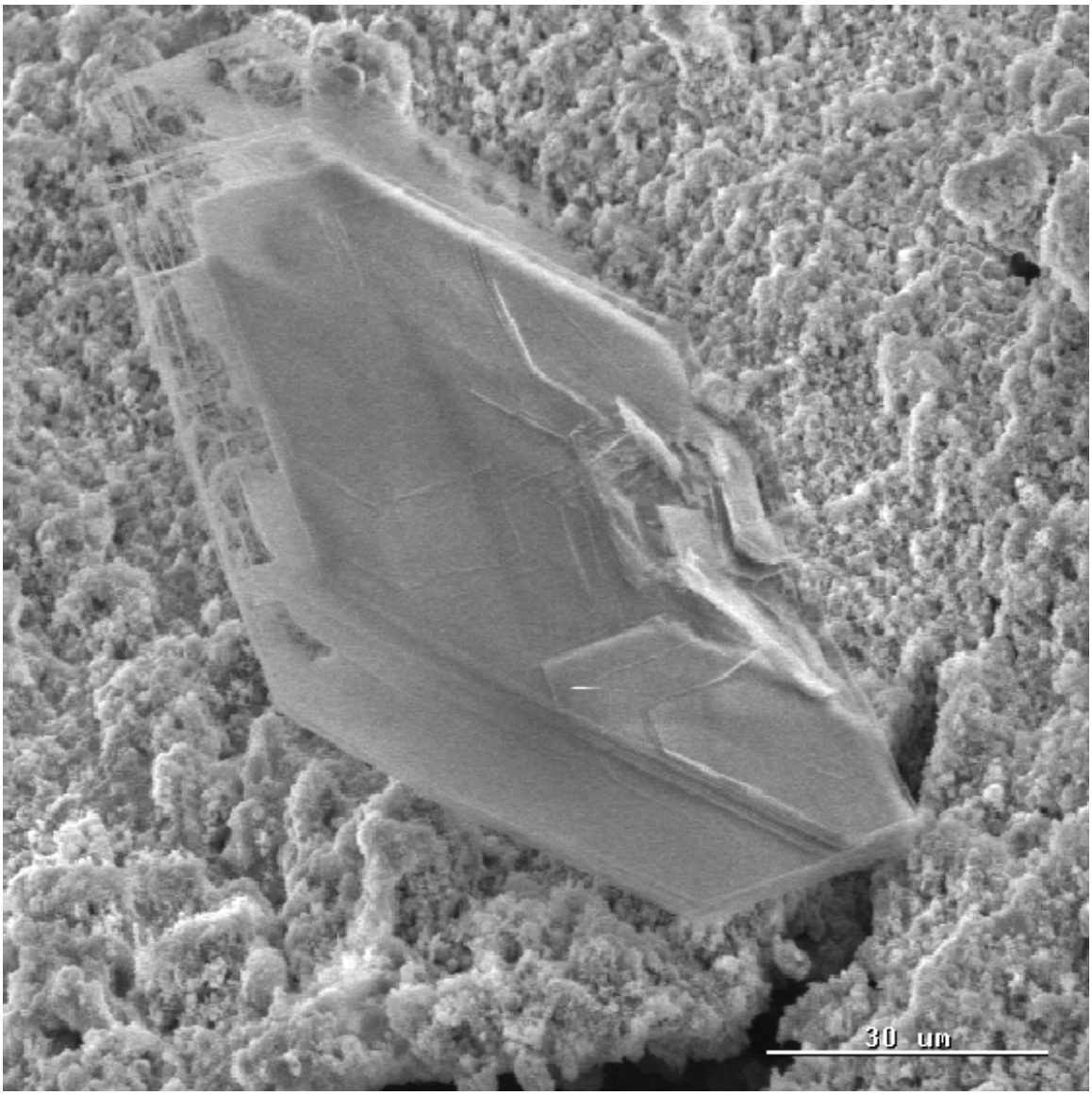

Figure 4.14: SEM Image of Crystal from Experiment Number 35 at 500x Magnification.

respectively [41]. The materials necessary can be as simple as boric acid and lithium hydroxide [42]. This certainly explains how the crystals are able to grow in some of the experiments, and may possibly explain how they grow in PWRs as well.

The final result of this project is the factors which influence crud growth and boron deposition. This project has provided experimental evidence for numerous factors relating to crud growth and boron deposition within the crud. Most of the information has direct application to crud growth as related to these factors: pH of the coolant, impurities in the coolant, length of exposure, heat flux, and coolant turbulence. Two of the factors have implications for boron deposition in the crud, which are porosity and the slow cool-down process versus the rapid blow-down technique.

The pH of the coolant has a significant effect on crud growth. Results found in this experiment confirm what has been suggested for the industry in that a higher pH will result in less crud growth. The one experiment that most prominently displays the high pH effect is number 24. This experiment was exposed for 50 percent longer and had twice the coolant additives yet only a fraction of the crud in experiment number 23 was developed. Although the pH of the iron nitrate experiments is not known with certainty, the pH of these two experiments is known. Other experiments also support the general pH trend, although there is some difficulty in comparing the pre-mixer experiments because of the three unusual runs (numbers 28 through 30). The three high pH experiments of 32 through 34 certainly have less crud than the one comparable low pH experiment, number 31. This comparison is not true if experiment number 26 is considered, but the difference there may be due to the extra nickel content in the earlier experiment. There was one deliberate low pH experiment that showed a very large crud

deposit, which was experiment number 39. This experiment had a very low pH target of 6.6. In fact, since the lower pH had slightly less crud than the control experiment (number 35) a very low pH may start to reverse the crud deposit trend. However, there are more factors that are influencing the deposit, and this experiment ran for five less days than the control.

Next in order or importance on crud deposition are the coolant additives and relative concentrations. Three experiments tested this effect specifically (numbers 35, 37 and 38). A very important point is that crud grows best when both soluble and insoluble coolant additives exist. The control experiment had significantly more crud deposition than the two that lacked either one of the coolant additives. In this respect, it would also seem that soluble matter has a greater effect by itself than particulate matter by comparing experiments 36, 37 and 38. The type and quantity of additives is also important. Earlier experiments that had nickel and iron concentrations in the parts per billion ranges saw little deposit form that was not contaminants. Later, the iron and nickel concentrations were increased 1000 fold, and crud deposition became much more significant. The initial iron to nickel ratio of the additives also affected the crud composition of nickel and iron. Nickel itself seems to be an important enabler of crud deposition as seen in two similar experiments, numbers 33 and 26. The earlier experiment had twice as much nickel and the deposit was almost four fold greater than the latter. Another interesting finding is the effect of zirconium oxide on crud growth. The two experiments with spray pyrolysis (numbers 29 and 30) both had large amounts of crud deposit, which can be explained by one of either two possible effects. First, the zirconium oxide formed on the cladding surface could be enhancing the possibilities of

crud deposition as can be inferred from industry data. Part of the crud composition section of Chapter 2 discussed how a large portion of AOA plants' crud consists of zirconium oxide. The other possibility is that the zirconium oxide layer aided the crud deposition process by acting as particulate matter in the coolant. Since both of these experiments were run without the mixer, the zirconium layer could momentarily flake off or partially detach and then soluble and particulate matter could form a new crud layer together.

The next factor related to crud deposition is rather intuitive. The longer the wire is exposed, the more crud that will deposit if all other factors are equal. This is easily seen in the case of experiment numbers 22 and 23. The operating conditions for these two experiments were virtually identical except the latter was exposed for twice as long. This resulted in eight times the amount of crud depositing on the wire of experiment number 23. It would seem from these two experiments that crud growth follows an exponential growth function. Otherwise, the wire that was exposed for twice as long would only have roughly twice the crud. This simple analysis does not hold true for two other sets of experiments that were the same except for the duration. Although in all cases the longer duration experiment had more crud, these two pairs did not exhibit exponential differences. The first pair (29/30) had fifty percent longer duration for the second wire but only 34 percent more crud. The longer experiment of the second pair had five times the amount exposure yet only twice the net crud amount. However, each of these experiments was under abnormal conditions. The first pair both wires broke which tends to skew the weight measurement unpredictably. One of the second pair of experiments experienced current arcing, which may have caused an increase in the

particulate matter inventory of the coolant. Another explanation is that the crud growth actually plateaus after a certain amount of time for a given set of coolant conditions.

The effect of heat flux is difficult to ascertain from these experiments. The heat flux was intended to be the same for most of the experiments, but the power control rheostat was difficult to precisely adjust. Also, because many of the wires broke, there was reluctance to alter the heat flux in the middle of the experiment after uncontrolled power transients. For unknown reasons, the power would shift, sometimes dramatically, during an experiment and change the original heat flux. Unless the new value was unreasonable, the heat flux was left where it was at to avoid any unnecessary changes. Also because of the sensitivity of the wire to the additional heat, most experiments were run with as high a heat flux as was known not to break the wire. Therefore, most experiments were run with similar heat fluxes. One pair with similar operating conditions actually showed that the higher heat flux experiment had less crud deposit (experiment numbers 31 and 33). This leads to the conclusion that a higher heat flux while initially may aid crud deposition because of increased steaming, as the heat flux rises beyond some critical value its effect on crud deposition reverses. Although this analysis certainly is not supported beyond doubt by the current work, it is a good hypothesis for future study.

The next factor to consider is the effect of coolant turbulence on crud deposition. The project produced the most crud on the wires when operating with the mixer, however other factors were present that prevent drawing a firm conclusion on the effectiveness of coolant turbulence in producing crud deposits. As mentioned before the mixer achieves the coolant turbulence that exists in the reactor, which apparently aides crud deposition.

Intuitively it makes sense that the mixer would aid crud deposition somewhat. It keeps the particulate matter in the coolant from settling. Assuming that crud takes some of its material from soluble impurities in the coolant, the mixer also keeps the soluble matter evenly dispersed after some has deposited in the crud layer. Only one pair of experiments have the same operating conditions save the mixer. Experiment number 34 ran with the mixer and had slightly more crud than the previous experiment that ran without the mixer. As for the very large deposits in experiments 35 and 39, the mixer probably played a role in ensuring a constant supply of coolant additives for deposition as crud.

The two remaining factors, which are the slow cool-down procedure and porosity, will be discussed mainly from the perspective of boron deposition within the crud. The slow cool-down procedure was used twice in these experiments however, many wires broke before the rapid blow-down could be done; also, the rapid blow-down was interrupted for one experiment (number 34). Considering the two that ended with the slow cool-down process, one sheds light on the amount of soluble crud that is actually captured by the rapid blow-down procedure. Experiments 10 and 11 were practically identical, yet number 11 ended with the slow cool-down approach and had 43 percent less crud than the rapid blow-down experiment. The slow cool-down experiment also had less boron by weight as detected by EDX. The boron in these experiments is less significant because the crud was mostly contaminants, but it still shows that soluble boron species were captured with the rapid blow-down technique used in this experiment. The more recent slow cool-down experiment number 40 has prototypical crud yet without boron. As mentioned before, the crud had a higher nickel to iron ratio that would be

characteristic of AOA plants, but the EDX showed no boron and the SEM pictures showed no likely borate crystals.

A unique opportunity to study the effect of porosity on boron deposition was gained by experiment number 27. Here the wire developed two very different crud layers on separate parts of the wires. The porous side showed a higher boron weight percentage than the non-porous side. One caution on this conclusion is that the non-porous side had a different composition than its porous counterpart, which probably affects the boron deposition process. Interestingly, the crystal shown in Figure 4.15 developed on the porous side of the deposit. The porosity itself varied by experiment, and some correlations should be pointed out. The crud seems to become more porous as the initial nickel concentration increases. This is seen in experiments 26 and 27 versus number 31. The first two each had more nickel added with a corresponding more porous structure of the crud. The last had four times as much iron as it did nickel and this led to a less porous structure.

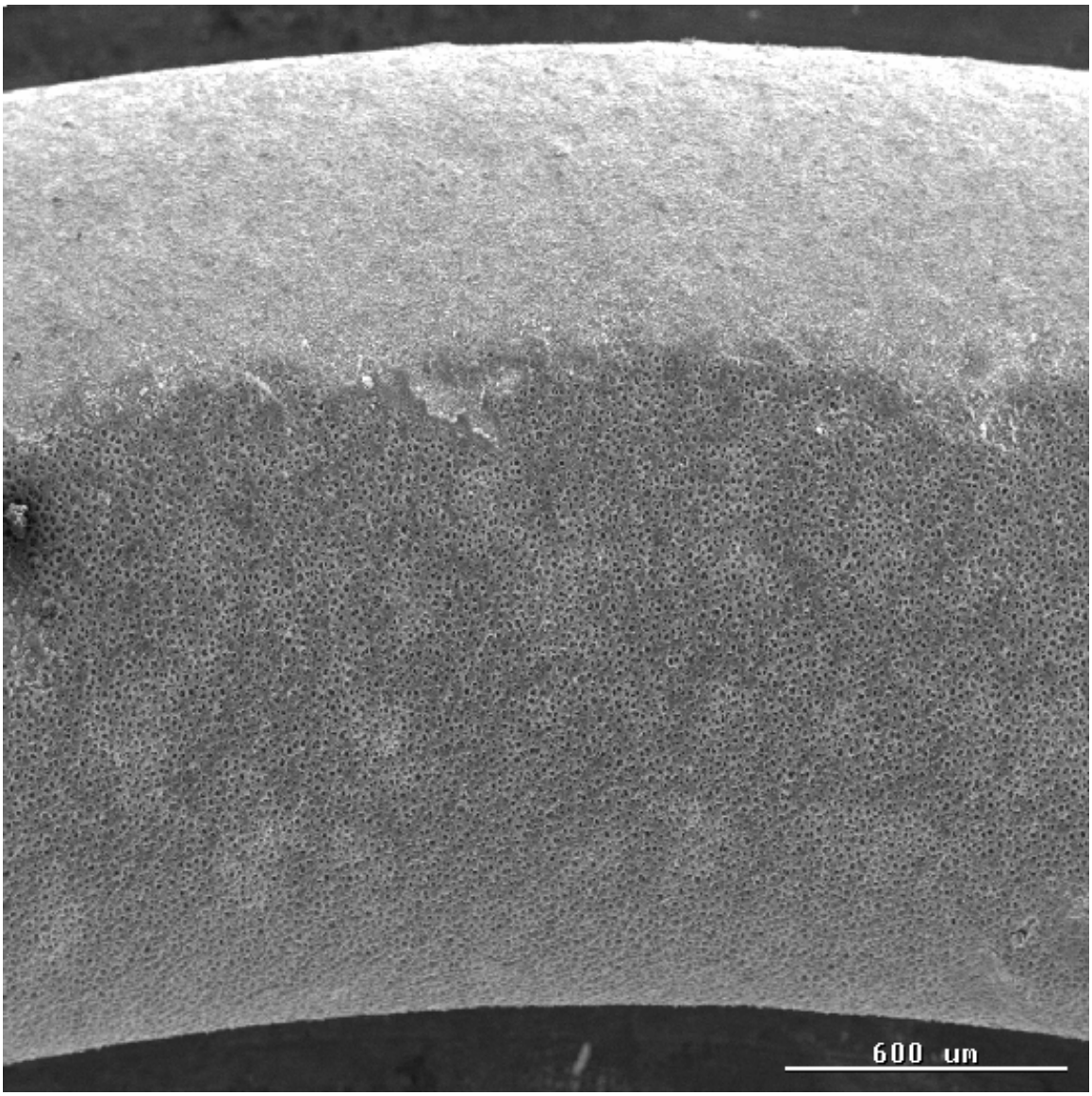

Figure 4.15: SEM Image of Crud on Experiment Number 27 at 40x Magnification. Notice the two distinct regions of porous and non-porous.

CHAPTER 5

CONCLUSIONS AND RECOMMENDATIONS

There are three conclusions from this research: prototypical crud has been created experimentally, boron has been found in high concentration within this crud, and the likely chemical form of boron deposition species has been determined. That the crud created in this project is of prototypical composition has been determined through all data collection techniques. EDX and ICP-MS showed nickel-to-iron ratios that correspond to what has been reported by the industry; XRD showed characteristic species such as nickel ferrite within the crud; and SEM illustrated numerous times the porous structure of the crud. Boron concentration within the crud has been significant for several experiments. The rapid blow-down procedure was fundamental in the capture of boron bearing compounds. Most importantly the boron deposition material has been found to be lithium tetraborate. The precipitation of this compound within the crud is an ideal candidate for the onset of AOA because it explains lithium hideout and return behavior observed in PWR cores exhibiting AOA symptoms, it has been directly observed in prototypical AOA crud, and it is consistent with the low lithium-to-boron ratios reported by earlier results from SIMS analyses.

The recommendations based on the above conclusions are divided into two separate categories. First, the experimental data acquired through this project will be used to make recommendations to the industry on plant operations. The two primary

topics of interest here are pH control and particulate matter inventory. Second, there will be recommendations for future work in the AOA simulation field. This involves testing different scenarios of AOA mitigation and producing more quantitative data with respect to different plant operating conditions.

Strategies for the mitigation of AOA should be focused on the reduction of crud formation. This benefits the plant in more ways than just the reduction or elimination of AOA. The crud that forms on AOA fuel assemblies also has the effect of leading to fuel failures and increased dose rates as mentioned in Chapter 1. In the regard of crud reductions, this experiment served as good confirmation of the industry approach. The largest factor affecting crud growth and therefore the onset of AOA is the pH of the coolant. The experiments in this project show that an elevated pH will keep corrosion products that are in the coolant from depositing on the cladding. The modified chemistry regime discussed in Chapter 2 and illustrated in Figure 2.6 may not result in a high enough pH for the entire cycle, especially at the beginning of long cycles when the boron is as high as 2000 ppm. This may necessitate the use of EBA to allow for higher operating pH throughout the cycle and not just at the end. In addition to monitoring the pH, plant operators can reduce the amount of corrosion product inventory in the plant, thereby removing the source term for AOA crud deposits. One of the methods for removing the particulate inventory for a fuel cycle is already being employed, and that is ultrasonic fuel cleaning. This looks more necessary now that the important interplay between soluble and particulate matter has been illustrated by this project.

Another less preferable scheme to reduce AOA would be focused around the actual boron deposition. One method to accomplish this goal would be to use a different

hydroxide such as potassium hydroxide (KOH) to control the coolant pH. The benefit would be that the borate would no longer be able to deposit in the form of lithium tetraborate or any other lithium borate species for that matter. However, there is no guarantee that a potassium borate would not form in the coolant and precipitate at the same or worse rate. Also, potassium is more likely to be activated in the core while undergoing radiation than lithium, and therefore the switch to KOH would have the undesired side effect of increasing plant dose rates. Also the amount of work that would have to be accomplished for studying the other aspects KOH would have on plant operations such as corrosion effects would need to be seriously considered.

AOA simulation itself is an indeed important part of future plant operations. Crud growth and AOA could be the limiting factors for further optimization and enhancing of old PWR designs. If these plants are to remain economically competitive further upgrades in cycle length and thermal duty may become necessary in the future. AOA and crud growth simulation are the most effective way to measure the effects of core enhancements on these two detrimental consequences. In that respect, the two primary AOA simulation objectives are to test the effects of EBA and KOH on crud growth and boron deposition. The use of EBA would allow for higher operating pH, but it may actually enhance boron deposition [43]. The reference report discussed borates, and states that generally tetrahedral formations of boron are preferred by the smaller isotope of boron ^{10}B. This may have an effect on the formation of lithium tetraborate, and an easy way to test it would be to run a series of experiments with EBA as the boron additive. The other simulation effort necessary is to test whether the potassium hydroxide would lead to the precipitation of potassium borate species within the crud.

Again, this could easily be determined through a series of experiments using unenriched boric acid and KOH as the additive. Other scenarios may present themselves as a possible mitigation effort, and this test facility is well equipped to simulate them and provide insight into the possible consequences.

The future testing could also provide more quantitative data for the industry on how various factors effect AOA. Some of examples of good research into this area would include a series of experiments testing the crud deposition as a function of heat flux, and one as a function of pH. These two appear to the most quantitative approaches to the crud growth and boron deposition. As mentioned earlier, this project was intended to provide quantitative data for the effect of porosity on crud growth and boron deposition, but a method that develops a tenacious crud deposit would have to be developed in order to pursue this line of experimentation.

Further insight into current AOA conditions could also be gained by experiments that approach the problem of crud growth from different qualitative angles. These may include a line of experiments that tests the effects of different particulate matter such as FeO_4, NiO and ZrO_2. These could then be compared to existing data on nickel ferrite. Also a line of experiments that explores the effects of severe power transients could be performed. These would use the control experiment conditions with intentional power transients to the wire. This is common to how PWRs operate, and the effect of a reactor trip on crud would be useful data from this AOA simulation.

APPENDIX A

RAW DATA

Upon removal from the pressure vessel, each test element was first weighed to find the amount of crud mass gain. The next step was to take SEM photographs and a compositional analysis via EDX. The data presented here will be a summary of these three data collection methods. One important note is that the EDX data is taken from small areas of the wire, usually about six different times. Sometimes the crud is uniform and the composition from the scans is relatively constant. Other times this is not the case, and the composition can vary widely. Both cases will be noted when the actual data is presented. When there was enough deposit two other methods (XRD and ICP-MS) were employed to add to the quality of the data already taken. Data from these last two methods are not available for all wires, but they will also be presented here when available. It should be noted that EDX can not detect elements lighter than boron; hence, it could not be used to identify the lithium-boron ratio in the crud. Instead, XRD was used to identify the chemical composition of the borated species deposited in the crud. A brief description of all the analysis techniques used during this experiment is available in Appendix C. Data presented here will be in one of three categories: (1) facility optimization, (2) coolant composition analysis, and (3) unconventional experiments.

A.1 Facility Optimization

A.1.1 Experiment Number 10 (0419 0501 01)

This was the first of a series of experiments to test the effects of soluble iron and nickel additives (in this case $NiSO_4$ and $FeCl_3$). The crud developed was mostly uniform with abnormal structures on parts of the wire. The deposited crud weighed 30 mg, and was mostly aluminum, silicon, and calcium species. The compositional information is shown in Table A.1; however, there was some significant variance in some of the scans. Two scans showed no boron at all, which skewed the average lower than it may actually be. If these two are ignored, the average boron concentration increases to 11.03 atomic percent and 6.68 weight percent. This is more in line with what is found later in a repeat experiment (number 12). The SEM showed the structure of the crud which had small blocky crystals, but more importantly the porous nature of this crud, similar to the chimneys of PWR crud is shown in Figure 4.1. The difference being that the chimneys in the experimental crud are more spaced out (see Figures 2.3 and 2.4 for comparison).

Table A.1: Compositional Information for Experiment Number 10.

0419 0501 01	EDX Data Average Summary									
Element	Fe	Si	O	B	Zr	C	Al	Cr	Cu	Ca
Weight Percent	0.55	15.06	54.75	4.01	-	5.57	11.80	-	-	7.06
Atomic Percent	0.19	10.19	61.89	6.62	-	8.73	8.38	-	-	3.47

A.1.2 Experiment Number 11 (0504 0514 01)

This experiment was the same as the last except for a slow cool-down was performed at the end of the experiment versus the usual rapid blow-down. Unfortunately, this experiment had to run for two less days than desired because of a sudden power drop to the wire on the 8^{th} day. This led to the suspicion that the wire may break if the experiment continued for the full 12 days and therefore it was ended on day 10. The crud

deposit was almost half that of what it was for the previous experiment; a total of 17 mg of crud was deposited on the wire. The EDX scans showed that the composition was very uniform, more so than the last experiment. The boron content was practically the same for all EDX scans, the average of which is shown in Table A.2. The SEM imaging showed a similar structure to the previous experiment, which can be seen in Figure 4.2.

Table A.2: Compositional Information for Experiment Number 11.

0504 0514 01	EDX Data Average Summary									
Element	Fe	Si	O	B	Zr	C	Al	Cr	Cu	Ca
Weight Percent	1.94	16.30	38.94	3.90	-	2.34	16.82	-	-	19.43
Atomic Percent	0.73	12.29	51.50	7.64	-	4.13	13.21	-	-	10.27

A.1.3 Experiment Number 12 (0530 0611 01)

This wire was pre-coated in order to test the effects of a crud layer on further crud growth, but the coating flaked off as mentioned before. Because of the pre-coating and prior experience showing that initial crud layer will flake off, the heat flux was lower for this experiment than the previous two. Other than the lower heat flux and pre-coating, the other experimental conditions were the same as the last two experiments, and a rapid blow-down was performed on the 12^{th} day to end the experiment. The wire remained intact for the entire experiment, and 18 mg of net crud was developed. This weight measurement is skewed by the fact that the original coating flaked off. In other words, enough crud developed on the wire to account for all that flaked off plus the additional 18 mg. The crud from this experiment was of a very uniform composition; the EDX data showed that every scan was very similar, so the averages in Table A.3 are representative of each scan. The SEM images also show very similar structures throughout this crud

layer and to the previous two experiments. An example of this crud is shown in Figure 4.3, although at a slightly more magnified resolution than the previous two SEM images.

Table A.3: Compositional Information for Experiment Number 12.

0530 0611 01	EDX Data Average Summary									
Element	Fe	Si	O	B	Zr	C	Al	Cr	Cu	Ca
Weight Percent	1.41	15.96	43.69	5.75	-	3.68	14.16	-	-	15.16
Atomic Percent	0.51	11.18	53.82	10.50	-	5.97	10.40	-	-	7.50

A.2 Coolant Compositional Analysis

A.2.1 Experiment Number 23 (0306 0418 02)

The importance of this experiment was that it was the first to successfully use particulate matter as part of the coolant composition (successful in that a significant amount of crud was deposited in situ). At this time in the project, the coolant had contained soluble additives in varying concentrations, but insoluble additives were still untested. The experiment directly preceding this one had also added nickel ferrite, but it only had 6 mg of crud deposit while this one had 48 mg. The two experiments were practically identical in starting conditions; except this one had slightly less insoluble nickel ferrite added and ran for 23 days longer. This was the second in a three-experiment series, two of which will be reported in detail. EDX showed no boron as evident in Table A.4. There were a large amount of contaminants, but there was a relatively equal amount of iron and nickel.

Table 4.5: Compositional Information for Experiment Number 23.

0306 0418 02	EDX Data Average Summary									
Element	Fe	Ni	O	B	Zr	C	Al	Cr	Cu	Ca
Weight Percent	18.77	17.94	25.88	-	3.88	-	0.48	-	-	23.13
Atomic Percent	12.38	11.16	48.63	-	1.34	-	0.62	-	-	16.97

A.2.2 Experiment Number 24 (0423 0624 02)

This was a long duration experiment (60 days) with a very uniform and thin coating; only 6 mg of crud was deposited on the wire. This is the third test of the experiments to use only particulate additives, and it ran at a slightly higher pH. Many of the EDX scans had a very large zirconium peak leading to high average zirconium content. This is probably due to the scan picking up mostly just the wire and not zirconium actually present in the crud because of the thin coating. The compositional information obtained by EDX is summarized in Table A.5. The nickel and iron deposits are not indicative of nickel ferrite, but they are both very low compared to the contaminants (calcium in this case) so as to be rather inconclusive.

Table A.5: Compositional Information for Experiment Number 24.

0423 0624 02	EDX Data Average Summary									
Element	Fe	Ni	O	B	Zr	C	Al	Cr	Cu	Ca
Weight Percent	5.82	10.04	37.16	-	16.90	-	0.92	-	-	19.30
Atomic Percent	3.21	4.59	64.44	-	6.23	-	1.01	-	-	12.27

A.2.3 Experiment Number 26 (0819 0916 02)

This experiment was the first to use the nickel and iron soluble additives in the nitrate form. There was an error in the weight calculation of each of these additives, so the pH was inadvertently high. The nickel and iron were inserted in roughly equal amounts (12 ppm each), and the next two experiments (number 27 and 28) were both run under similar conditions. The wire gained 31 mg of weight from the crud deposited. The crud from this experiment was very uniform with a large amount of contaminants (see Table A.6). The nickel deposit is substantial, but the iron is almost insignificant. The

large amount of contaminants precludes any conclusions on the composition, but it is likely not nickel ferrite. The structure was porous, with a candy-like upper layer, which can be seen in the SEM image of Figure 4.4. This was the first experiment to produce a crud layer which was both porous and contained nickel and iron together.

Table A.6: Compositional Information for Experiment Number 26.

0819 0916 02	EDX Data Average Summary									
Element	Fe	Ni	O	B	Zr	C	Al	Cr	Cu	Ca
Weight Percent	4.37	32.74	21.79	-	-	6.82	0.62	-	23.33	5.81
Atomic Percent	2.61	18.83	39.95	-	-	11.44	0.74	-	17.73	4.30

A.2.4 Experiment Number 27 (1031 1203 02)

This experiment also ran at a high pH like the previous one, and was the last one to include the nickel screen. The crud that deposited was significant but unable to be weighed because the wire was fragmented while it was being removed from the vessel, although it remained intact for the duration of the experiment. The crud layer had deposited into two obviously different patterns, half that was porous and the other that was not. The porous half composition more closely resembled prototypical crud in the reactor, while the nonporous half had more contaminants such as copper and calcium. Like the previous experiment, the nickel content is much higher than the iron. The porous half also had more boron as shown by the EDX scans. The compositional data is presented in Table A.7. The visual differences between the two halves can be seen in Figure 4.15. Notice in the figure the crystal on the far left side in the porous region of the crud. This closely resembles crystals found in later experiments, most importantly in experiment number 35. A close up picture of the porous crud is shown in Figure 4.5.

This is meant for comparison to porosity of the industry crud shown in Figures 2.3 and 2.4.

Table A.7: Compositional Information for Experiment Number 27.

1031 1203 02	EDX Data Average of Porous Portion of Wire									
Element	Fe	Ni	O	B	Zr	C	Al	Cr	Cu	Ca
Weight Percent	9.85	65.74	13.45	3.25	-	2.17	0.51	-	2.52	0.47
Atomic Percent	7.07	44.01	27.75	10.56	-	6.41	0.68	-	1.46	0.39
	EDX Data Average Non-Porous Portion of Wire									
Weight Percent	2.28	15.04	23.05	2.45	-	5.20	0.52	-	60.49	6.26
Atomic Percent	1.10	7.10	42.06	5.76	-	13.40	0.53	-	22.55	4.28

A.2.5 Experiment Number 31 (0527 0630 03)

This experiment continued with the iron and nickel nitrate soluble additives, but with a lower nickel concentration and without the weight calculation error; the target pH was 7.1. The result was a 25 mg crud deposit consisting mostly of iron that had a very non-uniform structure. The EDX and ICP-MS data are summarized in Table A.8. The crud did have a little boron concentration found through ICP-MS, although none was seen in the EDX data. EDX and ICP-MS data agree on the order of magnitude difference between the iron and nickel contribution to the crud. ICP-MS showed that this experiment still had a lot of copper contamination, although EDX did not confirm that find.

Table A.8: Compositional Information for Experiment Number 31.

0527 0630 03	EDX Data Average Summary									
Element	Fe	Ni	O	B	Zr	C	Al	Cr	Cu	Ca
Weight Percent	44.03	5.52	20.00	-	6.87	3.87	0.11	6.57	3.93	6.47
Atomic Percent	30.60	3.53	37.20	-	2.67	11.50	0.15	4.62	2.32	5.65
	ICP-MS Data Summary									
Element	Fe	Ni	Li	B	Zr	Mn	Al	Cr	Cu	
Weight Percent	24.01	2.17	0.01	0.25	0.16	0.39	0.07	0.73	42.66	

A.2.6 Experiment Number 32 (0801 0902 03)

This was the first wire to break under configuration five, but it was not the only one. The wire sat in the heated coolant without heat flux for one day before the experiment was terminated. There was very little crud deposit, and the total weight gain was actually a loss of 3 mg. The weight gain may be skewed if fragments of the wire were not weighed because of the wire breaking. The EDX showed a nickel to iron ratio similar to that as might be expected from a nickel ferrite deposit as shown in Table A.9. There was no XRD or ICP-MS because of the small deposit.

Table A.9: Compositional Information for Experiment Number 32.

0801 0902 03	EDX Data Average Summary									
Element	Fe	Ni	O	B	Zr	C	Al	Cr	Cu	Ca
Weight Percent	22.02	14.04	24.78	-	17.14	5.15	0.15	0.17	6.86	3.46
Atomic Percent	14.15	8.65	50.55	-	7.36	7.17	0.18	0.11	5.09	2.81

A.2.7 Experiment Number 33 (0912 1015 03)

This experiment was virtually identical to the last. The total weight gain was a marginal 8 mg of crud, and the EDX and SEM data showed nothing spectacular. This was also run at a higher pH like the last experiment, so a large deposit is not expected

under this condition. The only difference between this experiment and the last is that the nickel to iron ratio is slightly larger but could still be indicative of a nickel ferrite deposit, and there is significantly more zirconium in this deposit than in the last; both of which can be seen in Table A.10. The larger average zirconium concentration is most likely do to the fact that the two area scans that led to the higher average were simply places with little deposit and the wire was actually being scanned.

Table A.10: Compositional Information for Experiment Number 33.

0912 1015 03	EDX Data Average Summary									
Element	Fe	Ni	O	B	Zr	C	Al	Cr	Cu	Ca
Weight Percent	29.57	18.34	16.43	-	25.83	0.48	0.10	1.99	0.91	0.04
Atomic Percent	24.51	14.48	39.61	-	11.95	2.03	0.15	1.39	0.77	0.05

A.2.8 Experiment Number 34 (0218 0319 04)

This is the first experiment to run with the mixer, but besides that, its starting conditions were the same as the previous two. There was slightly more deposit at 11 mg of crud, but this is roughly half of what can be considered to be a meaningful deposit. There was also an interruption in the rapid blow-down because of the valve handle slipping. The power to the wire was suddenly cut, but the valve was not opened until about a minute later because the valve handle had to be reattached. The high pH again yielded a nickel to iron ratio leading to a conclusion that the bulk of the deposit is nickel ferrite as seen in Table A.11. Other than that, the only difference between this and previous experiments was that there was more carbon that deposited in this crud.

Table A.11: Compositional Information for Experiment Number 34.

0218 0319 04	EDX Data Average Summary									
Element	Fe	Ni	O	B	Zr	C	Al	Cr	Cu	Ca
Weight Percent	26.14	14.82	31.84	0.46	19.59	4.88	0.70	0.60	-	0.17
Atomic Percent	13.46	7.26	57.91	1.18	6.52	12.07	0.75	0.33	-	0.13
	ICP-MS Data Summary									
Element	Fe	Ni	Li	B	Zr	Mn	Al	Cr	Cu	
Weight Percent	18.35	9.72	0.05	0.17	0.65	0.29	0.43	0.39	0.68	

A.2.9 Experiment Number 35 (0326 0430 04)

This experiment consisted of the ideal coolant composition that resulted in the most crud growth, and will be referred to as the control experiment. Present in the coolant were 20 ppm Fe and half that of nickel, both in the nitrate form. The boron was at beginning of cycle conditions of 1500 ppm and the lithium was 5.6 ppm to balance out the iron nitrate and boron for a target pH of 7.1. There was also 200 mg of insoluble nickel ferrite inserted in a "dispersal bucket" near the wire, the first time insoluble and soluble were added together. The resulting crud deposit weighed 435 mg and had large borate crystals ($Li_2B_4O_7$) interspersed in the deposit. The compositional information for this deposit is presented in Table A.12, which represents the combined EDX and ICP-MS data. Because some of the crystals were analyzed independently of the bulk deposit, the EDX data is separated for these parts. Also, the EDX and ICP-MS both showed only trace amounts of contaminants. The center of the wire had the most crystals and is shown in Figure 4.11. A zoomed in view of two of the crystals is shown in Figure 4.13 and 4.14. The center of the wire also had a higher nickel to iron ratio of 1.41, which is not indicative of a nickel ferrite crud deposit in this area. The ICP-MS analysis confirmed this as the crud taken for this measurement was from the center of the wire. Four

compounds were identified by the XRD graph shown in Figure 4.12: lithium tetraborate (under two different names), lithium iron nickel oxide, nickel ferrite, and magnetite. An important observation is that none of the main species identified by XRD had contaminant elements in them. As shown in the XRD graph of Figure 4.12, the 22° peak corresponding to the lithium tetraborate is very sharp and pronounced.

Table A.12: Compositional Information for Experiment Number 35.

0326 0430 04	EDX Data Average for Bulk Deposit									
Element	Fe	Ni	O	B	Zr	C	Al	Cr	Cu	Ca
Weight Percent	47.74	25.01	17.61	2.41	-	1.74	0.60	2.47	-	0.05
Atomic Percent	39.97	18.09	27.46	6.06	-	3.41	0.67	2.07	-	0.05
	EDX Data Average for Crystals									
Weight Percent	4.23	2.75	78.24	14.46	-	-	0.09	0.22	-	-
Atomic Percent	1.21	0.74	76.89	21.03	-	-	0.05	0.07	-	-
	ICP-MS Data Summary									
Element	Fe	Ni	Li	B	Zr	Mn	Al	Cr	Cu	
Weight Percent	20.71	41.55	0.10	0.89	0.02	0.48	0.61	1.00	1.10	

A.2.10 Experiment Number 36 (0504 0511 04)

This experiment was run with the exact same conditions as the control experiment (number 35), except for the fact that there was no insoluble nickel ferrite added. Unfortunately, the experiment was ended early because of an unusual behavior in the current and a large amount of leakage. The leakage was the result of some fittings not being properly tightened before the experiment was started, and the current behavior was due to the baffles not being properly oriented. One of the baffles was close enough to the electrode to cause arcing, which damaged the baffle and destroyed the screw that was holding on the wire. Therefore, the current started off unusually high to obtain the proper heat flux, and drifted down as the baffle and screw were eroded from the arcing. This

problem was unexpected, but was avoided in later experiments. In the short time that the experiment ran, the wire accumulated 20 mg of crud deposit. The wire was analyzed by EDX and ICP-MS, the results of both are included in Table A.13. The only abnormality is the higher amount of chromium in the crud, confirmed by EDX and ICP-MS.

Table A.13: Compositional Information for Experiment Number 36.

0504 0511 04	EDX Data Average Summary									
Element	Fe	Ni	O	B	Zr	C	Al	Cr	Cu	Ca
Weight Percent	51.50	13.05	17.91	-	7.22	2.94	0.21	6.57	-	0.22
Atomic Percent	35.65	8.34	39.33	-	2.55	8.35	0.07	4.98	-	0.20
	ICP-MS Data Summary									
Element	Fe	Ni	Li	B	Zr	Mn	Al	Cr	Cu	
Weight Percent	46.01	10.99	0.09	0.05	0.08	0.67	0.07	6.00	0.37	

A.2.11 Experiment Number 37 (0513 0617 04)

This experiment was aimed to correct experiment number 36; the coolant had the same amount of soluble additive as the control experiment but no particulates were added. It was run for the same length of time as the control, 34 days, and the total weight gain of the wire was 40 mg. This is over an order of magnitude less than the amount accumulated when particulate matter was present in the pressure vessel. The EDX and ICP-MS data (Table A.14) agree with the experiment 36 results except for the boron, lithium, chromium, and zirconium. The chromium is lower in this experiment, probably because the baffles provided a source of chromium in the last experiment as they eroded. The zirconium is also lower in this experiment, but this is probably due to the fact that the crud is thicker. The boron and lithium detected by ICP-MS were unusually high for this experiment, even higher than number 35 that had the borate crystals. The SEM images

showed a very non-uniform crud layer, although it looks as though some crud flaked off instead of the layer forming that way. This can be seen in Figure A.1. XRD on this crud did not find any boron bearing species, and this data is presented in Figure A.2.

Table A.14: Compositional Information for Experiment Number 37.

0513 0617 04	EDX Data Average Summary									
Element	Fe	Ni	O	B	Zr	C	Al	Cr	Cu	Ca
Weight Percent	49.45	14.54	20.40	-	0.44	1.86	0.25	0.86	-	5.88
Atomic Percent	32.74	9.35	43.88	-	0.18	5.27	0.34	0.65	-	3.80
	ICP-MS Data Summary									
Element	Fe	Ni	Li	B	Zr	Mn	Al	Cr	Cu	
Weight Percent	46.26	13.30	0.88	2.65	0.85	0.50	0.21	0.72	6.42	

A.2.12 Experiment Number 38 (0624 0729 04)

This experiment replicated the control experiment with the exception of no soluble additives. The boron and lithium added was for a pH of 7.1, and the only additive besides those two was 200 mg of insoluble nickel ferrite. The result was a very small deposit of crud totaling approximately 6 mg. As can be seen from the EDX scans in Table A.15, there was very little crud because of the high zirconium content in the scans. The nickel to iron ratio is close to that of nickel ferrite with just slightly less nickel than would be expected.

Table A.15: Compositional Information for Experiment Number 38.

0624 0729 04	EDX Data Average Summary									
Element	Fe	Ni	O	B	Zr	C	Al	Cr	Cu	Ca
Weight Percent	18.85	8.09	19.11	-	49.34	3.86	0.07	-	-	-
Atomic Percent	11.60	4.69	45.92	-	23.82	13.60	0.09	-	-	-

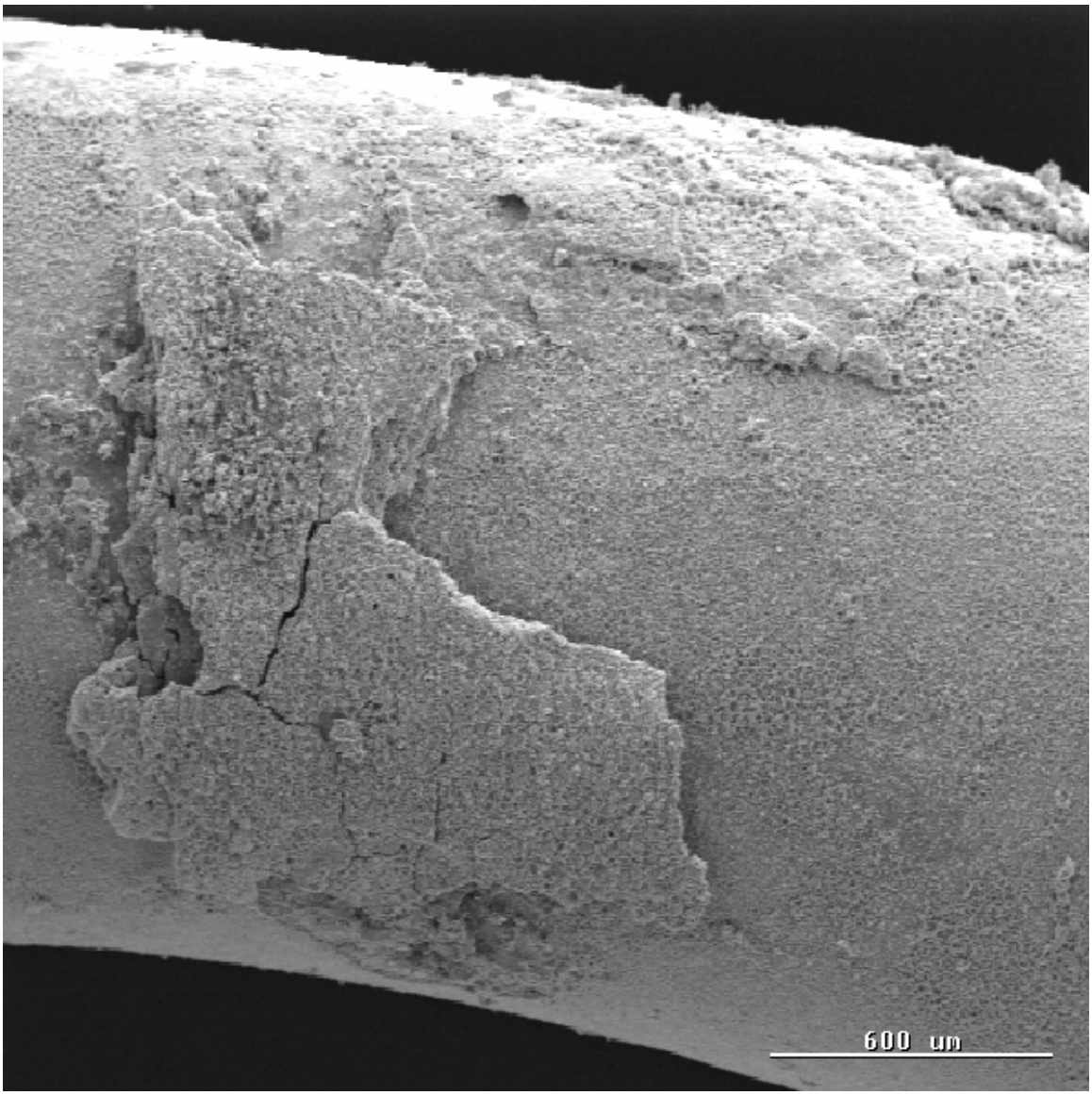

Figure A.1: SEM Image of Crud on Experiment Number 37 at 40x Magnification.

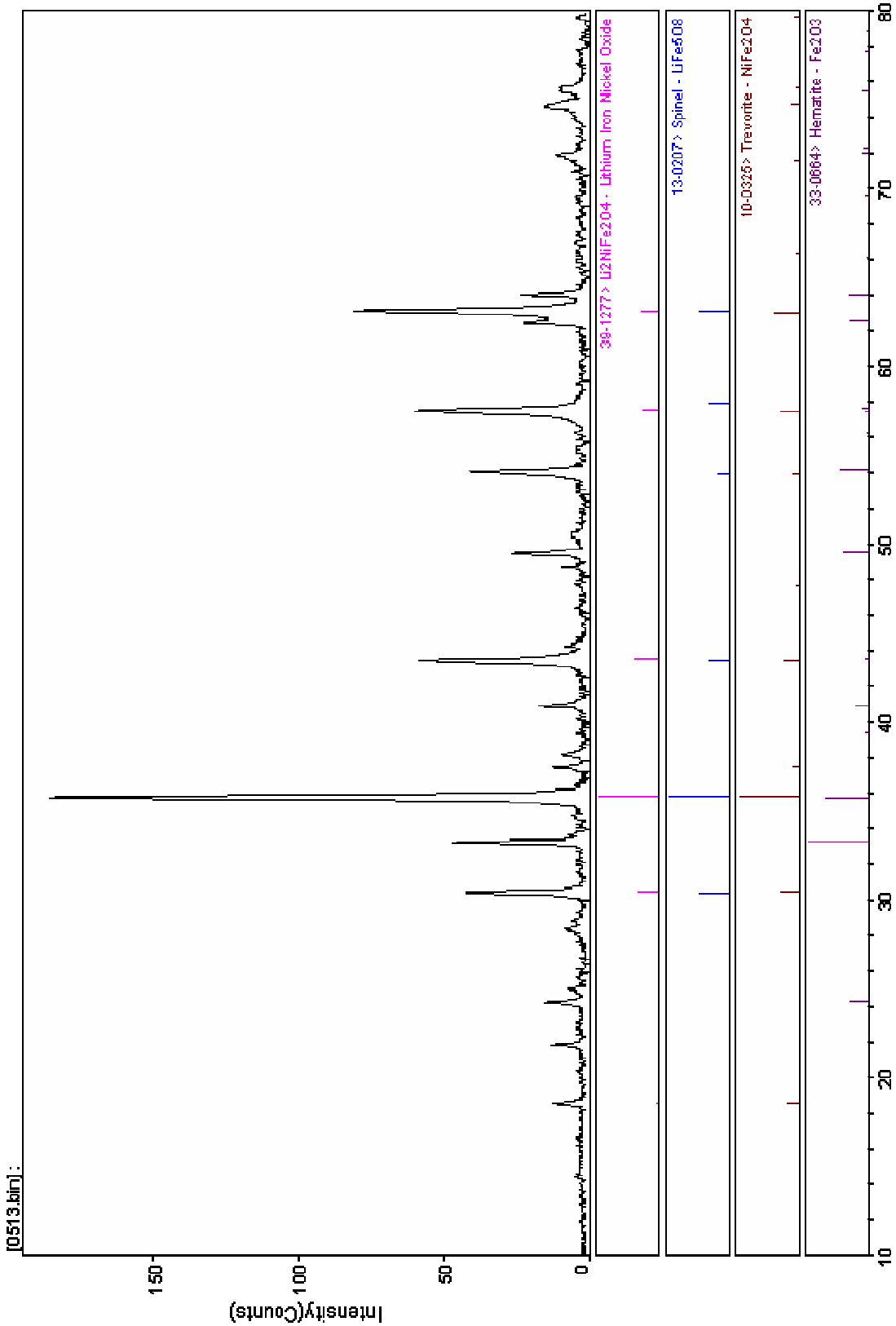

Figure A.2: XRD Graph of Crud from Experiment Number 37.

A.2.13 Experiment Number 39 (0804 0903 04)

This duplicated the control experiment, but with a lower pH. Therefore, only 3.3 ppm of lithium was added to the coolant for a target pH of 6.6, and a very heavy crud deposit of 386 mg was deposited as a result. The EDX results (Table A.16) showed similar crystals to the control experiment (number 35), but they were more numerous and smaller as can be see in Figure A.3. Two other differences between the crystals from the two experiments are that the earlier ones had less nickel and iron in the EDX scan, and the later ones appear darker. The amount of nickel and iron is most likely due to the scan area encompassing more of the surrounding crud versus just scanning the crystal. The darker appearance is not really explainable. The XRD presented in Figure A.4 did not show any boron oxide species, and therefore the crystals were most likely not a large enough portion of the crud to be detected by XRD.

Table A.16: Compositional Information for Experiment Number 39.

0804 0903 04	EDX Data Average for Bulk Deposit									
Element	Fe	Ni	O	B	Zr	C	Al	Cr	Cu	Ca
Weight Percent	30.68	23.16	19.07	-	-	9.56	11.57	0.70	-	0.51
Atomic Percent	18.64	14.36	35.10	-	-	17.75	10.35	0.50	-	0.25
	EDX Data Average for Crystals									
Weight Percent	8.35	18.64	56.87	14.44	-	0.56	0.23	0.17	-	-
Atomic Percent	3.17	7.48	63.20	24.34	-	1.20	0.17	0.08	-	-

A.2.14 Experiment Number 40 (0908 0916 04)

This experiment was intended to duplicate exactly the control experiment (number 35). However, the wire broke unexpectedly on the 7th day. There was a severe power transient because of a black out the facility underwent on day five. The power

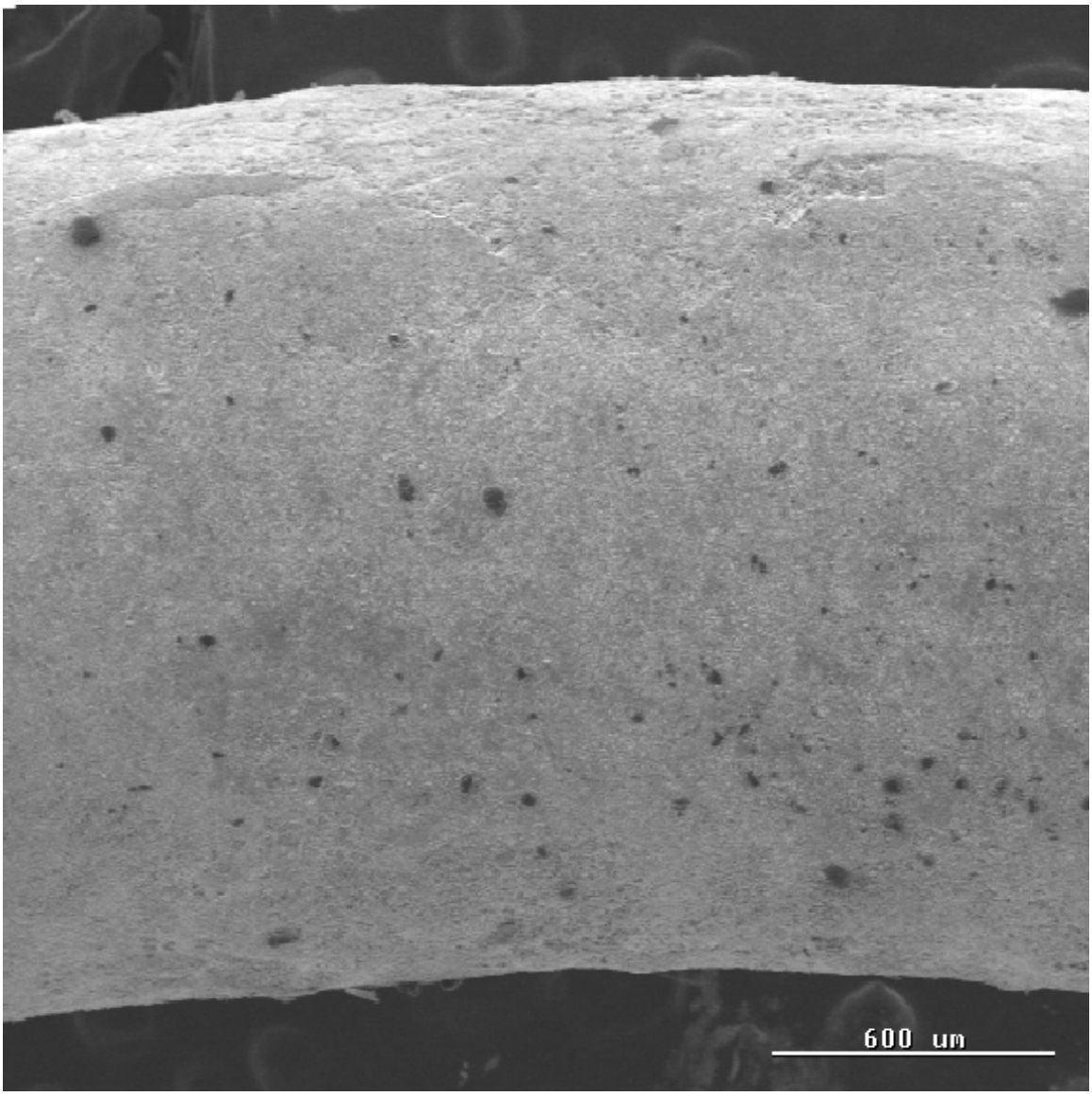

Figure A.3: SEM Image of Crud on Experiment Number 39 at 40x Magnification.

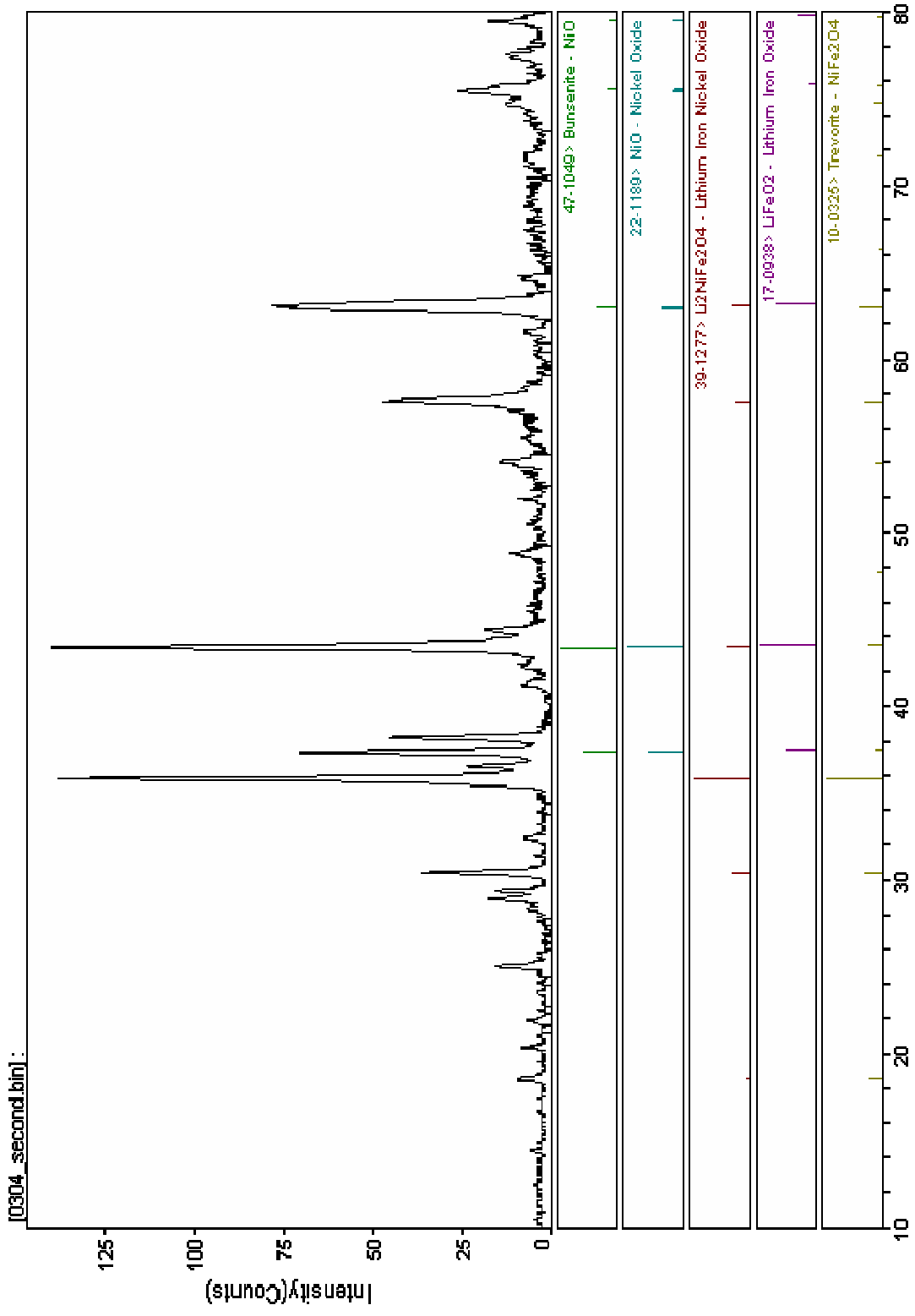

Figure A.4: XRD Graph of Compounds in the Crud of Experiment Number 39.

came back on in six minutes, and the experiment was immediately restarted with the power to the wire being applied slowly. Whether this power outage and recovery caused the wire to break is unknown. The wire still had a fairly thick coating (90 mg) after a slow cool-down procedure was performed to end the experiment. The wire had an interesting composition as reported by EDX as seen in Table A.17. The first observation is that there was no boron discovered even though there was physically enough crud for it to be there. The SEM image clearly shows the lack of crystals as can be seen in Figure A.5. Secondly, there was a large amount of silver contamination, and so the last column in the table is for silver instead of calcium like usual. The silver peaks in EDX are shared with thorium, so the last column could actually represent thorium. The source of this contamination is unknown, but appears to be isolated. The nickel to iron ratio is high which would lead to the conclusion that this crud is representative of moderate to severe AOA crud, but no evidence of boron as mentioned before. If the high silver scans are separated from the others, than the nickel to iron ratio increases for the bulk area average with atomic percent of nickel increasing to 30.04 and that of iron decreasing to 21.84. The silver contaminated areas then represent more of a nickel ferrite deposit with atomic percentages of nickel and iron at 12.16 and 27.62 respectively.

Table A.17: Compositional Information for Experiment Number 40.

0908 0916 04	EDX Data Average for Bulk Deposit									
Element	Fe	Ni	O	B	Zr	C	Al	Cr	Cu	Ag
Weight Percent	34.45	34.64	17.01	-	0.25	1.67	0.34	0.55	0.39	8.35
Atomic Percent	24.01	23.34	40.98	-	0.10	5.39	0.49	0.43	0.27	3.19

A.2.15 Experiment Number 41 (0917 1022 04)

This was the second attempt to duplicate the control experiment. The crud from this experiment weighed 230 mg, which is obviously not as much as the control experiment but still a very significant amount. No boron was found in the EDX scan which can be seen in Table A.18 below. In fact, the composition is very much similar to the bulk crud from experiment number 39 except there are no boron crystals present in the crud. The lack of crystals is illustrated in Figure A.6, which shows a SEM image of the crudded wire. The nickel to iron ratio is certainly lower than previous experiment, and is closer to a nickel ferrite deposit of 0.5 instead of the higher ratios of one to two.

Table A.18: Compositional Information for Experiment Number 41.

0917 1022 04	EDX Data Average for Bulk Deposit									
Element	Fe	Ni	O	B	Zr	C	Al	Cr	Cu	Ca
Weight Percent	35.93	24.03	32.26	-	0.10	3.65	0.69	0.33	-	0.02
Atomic Percent	19.92	12.27	56.60	-	0.03	8.49	0.73	0.19	-	0.01

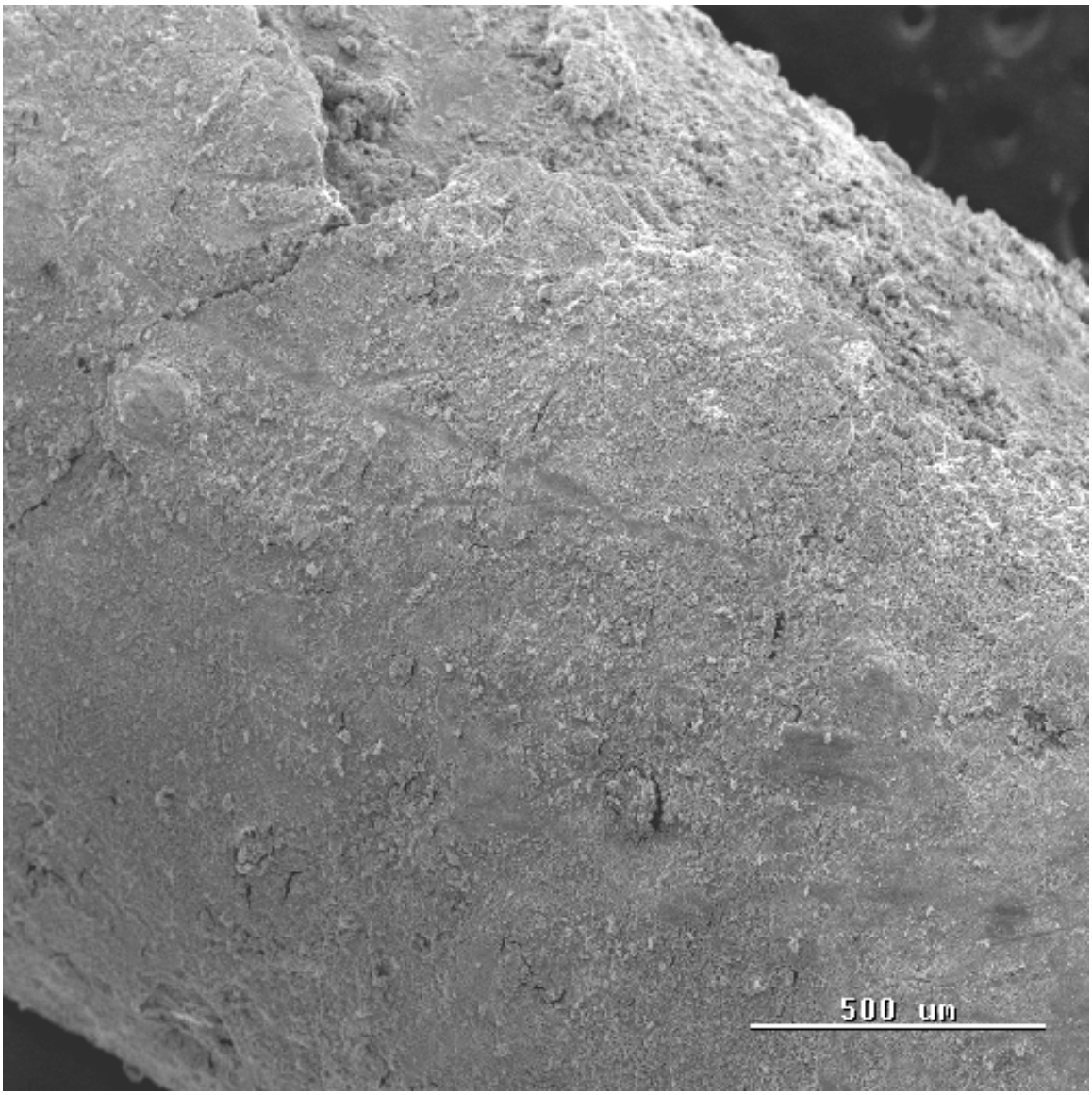

Figure A.5: SEM Image of Crud on Experiment Number 40 at 50x Magnification.

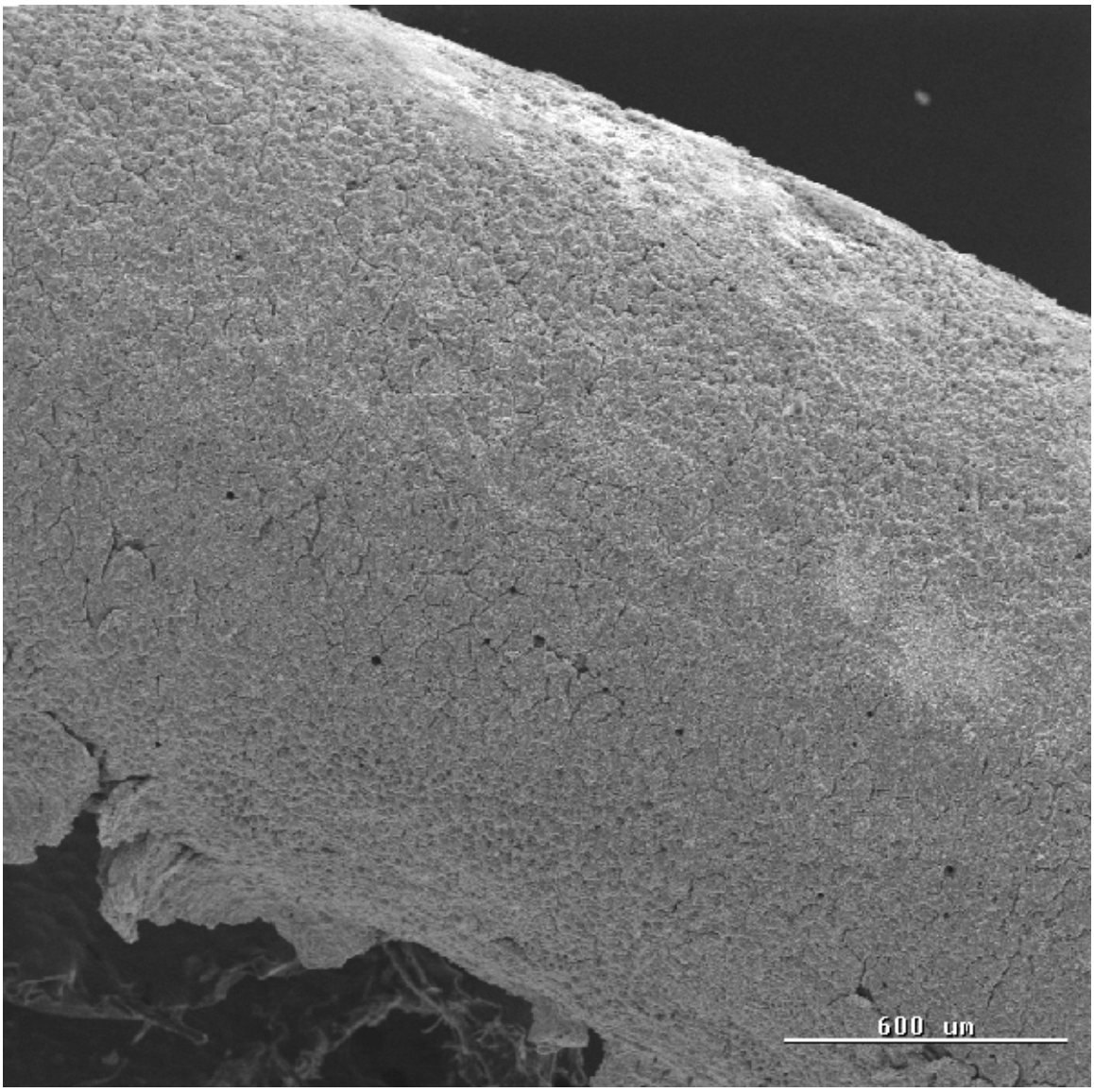

Figure A.6: SEM Image of Crud on Experiment Number 41 at 40x Magnification.

A.3 Unconventional Experiments

A.3.1 Experiment Number 28 (1219 0128 03)

This is the experiment that was run without hydrogen saturation. The experiment ran for 40 days and 214 mg of crud deposited on the wire in that time. The wire remained intact for the duration of the experiment, and the coating was thick, crusty, and rust colored. The EDX data is averaged and summarized in Table A.19. ICP-MS was also done on this wire because of the large amount of deposit, and that is included in Table A.19 for comparison. Some of the elements show good correlation between the two methods, but some are significantly different. ICP-MS gives a better average of the bulk, while EDX gives compositional analysis of certain areas. The non-uniform aspect of the crud is illustrated in Figure A.7. The XRD for this wire showed three compounds all of which contain copper as can be seen in Figure A.8. The crud deposited is not ideal because of the large amount of copper contamination; however, this experiment did show the largest concentration of boron by ICP-MS at roughly 9 percent by weight. According to predictions, this is more than enough to cause AOA.

Table A.19: Compositional Information for Experiment Number 28.

1219 0128 03	EDX Data Average Summary									
Element	Fe	Ni	O	B	Zr	C	Al	Cr	Cu	Ca
Weight Percent	23.90	19.59	17.59	0.59	3.65	3.44	0.27	5.52	18.85	0.46
Atomic Percent	20.28	15.92	37.93	1.91	0.23	9.17	0.36	0.28	12.12	0.33
	ICP-MS Data Summary									
Element	Fe	Ni	Li	B	Zr	Mn	Al	Cr	Cu	
Weight Percent	2.29	2.24	0.31	9.00	0.11	0.09	0.13	0.02	44.52	

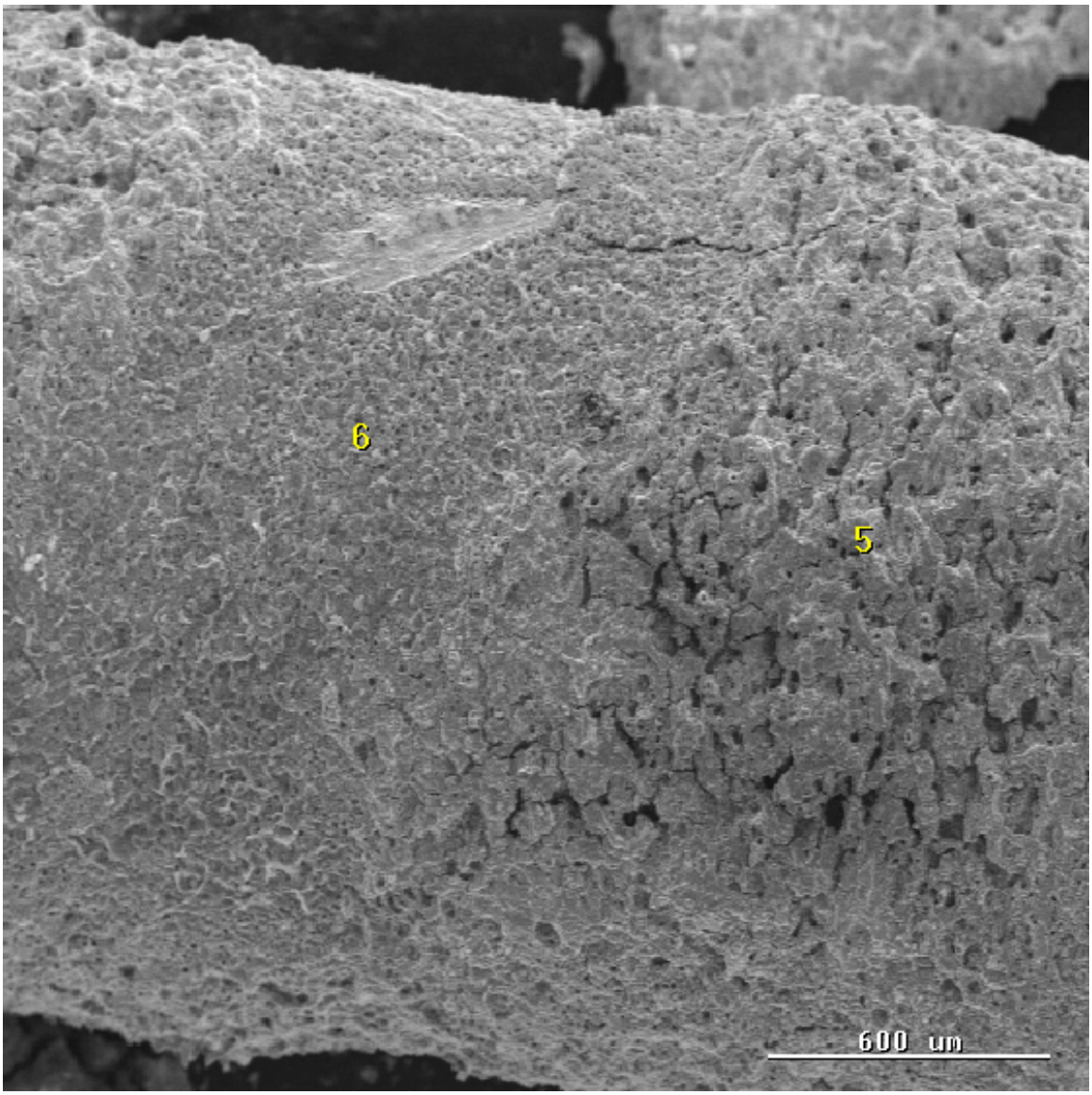

Figure A.7: SEM Image of Crud on Experiment Number 28 at 40x Magnification.

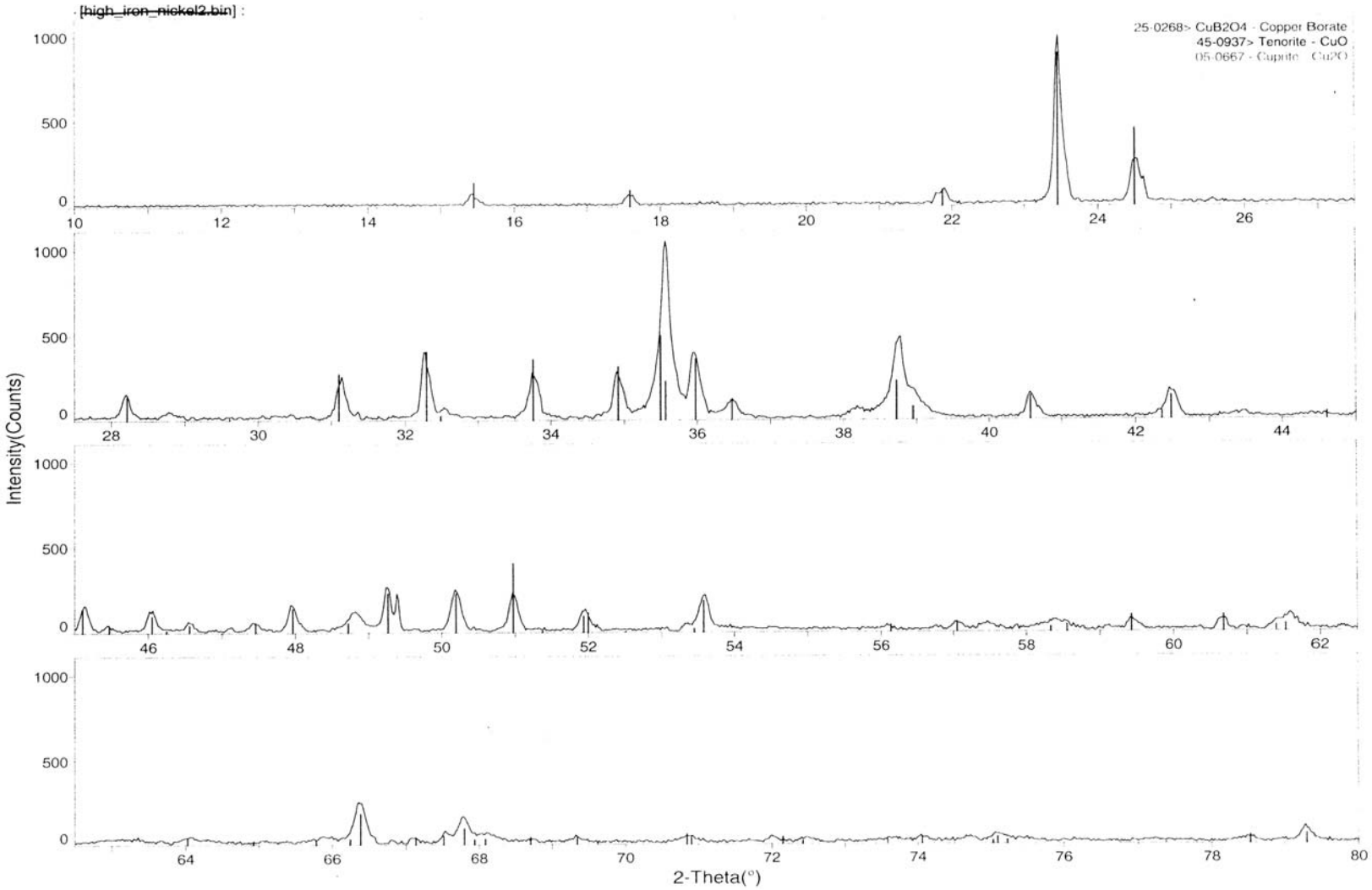

Figure A.8: XRD Graph of Compounds in the Crud of Experiment Number 28.

A.3.2 Experiment Number 29 (0313 0324 03)

This was the first of two experiments that were pre-coated through the spray pyrolysis technique. The coolant contained iron and nickel nitrates for a target pH of 7.1. The wire was only exposed for 11 days because it broke in the middle of the experiment, but the weight gain was large: 125 mg not counting what was added during the spray pyrolysis process. EDX and SEM were not done for this wire, but XRD and ICP-MS were. XRD showed three different species identified in the crud: nickel ferrite, lithium iron oxide and a copper species. The XRD graph is shown in Figure A.9. The ICP-MS data in Table A.20 shows that not much boron was deposited and there was still a problem with copper contamination, although not as bad as the previous experiment. Also interesting to note from the ICP-MS data is that although the wire was totally coated, there was still a large amount of zirconium showing up in the data scan. This is due to the spray pyrolysis process which creates a thick zirconium oxide layer on the wire. This layer than may flake off and reattach later as a crud deposit while the experiment is operating.

Table A.20: Compositional Information for Experiment Number 29.

0313 0324 03	ICP-MS Data Summary									
Element	Fe	Ni	Li	B	Zr	Mn	Al	Cr	Cu	
Weight Percent	7.71	5.29	0.00	0.14	48.30	0.10	0.10	0.26	14.00	

A.3.3 Experiment Number 30 (0328 0414 03)

This was the second spray pyrolysis experiment, with the exact same starting conditions, but the wire lasted longer (17 days) before it broke. This wire had even more crud; a net gain of 167 mg was deposited. All data collection methods were performed

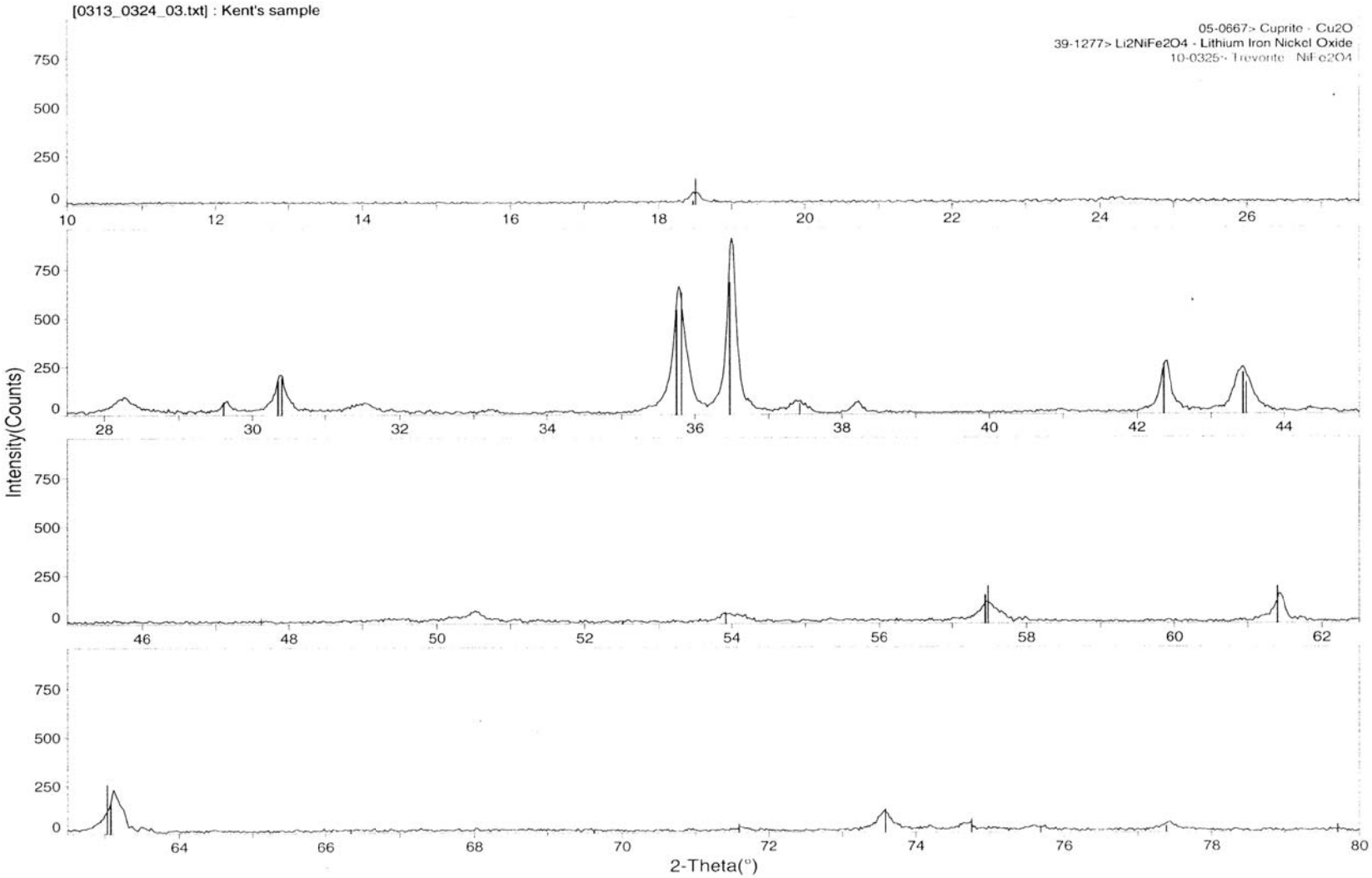

Figure A.9: XRD Graph of Compounds in the Crud of Experiment Number 29.

on this wire and the results were much the same. There was still an insignificant amount of boron deposition, and a large amount of copper contamination. The zirconium deposit was significant, but an order of magnitude less than before. Showing up in the EDX data in Table A.21 is a significant amount of chromium. ICP-MS shows an insignificant amount of chromium and a large increase in copper deposit over the last experiment. The thickness of this deposit is evident from Figure A.10, which shows a SEM image of a relatively uncoated and heavily coated interface in the crud.

Table A.21: Compositional Information for Experiment Number 30.

	EDX Data Average Summary									
Element	Fe	Ni	O	B	Zr	C	Al	Cr	Cu	Ca
Weight Percent	9.24	1.81	17.21	0.75	2.07	1.79	0.44	28.02	33.61	1.10
Atomic Percent	6.59	1.21	38.84	2.85	0.89	5.44	0.61	20.11	20.83	1.00
	ICP-MS Data Summary									
Element	Fe	Ni	Li	B	Zr	Mn	Al	Cr	Cu	
Weight Percent	12.19	13.90	0.01	0.32	5.38	0.24	0.23	0.43	47.19	

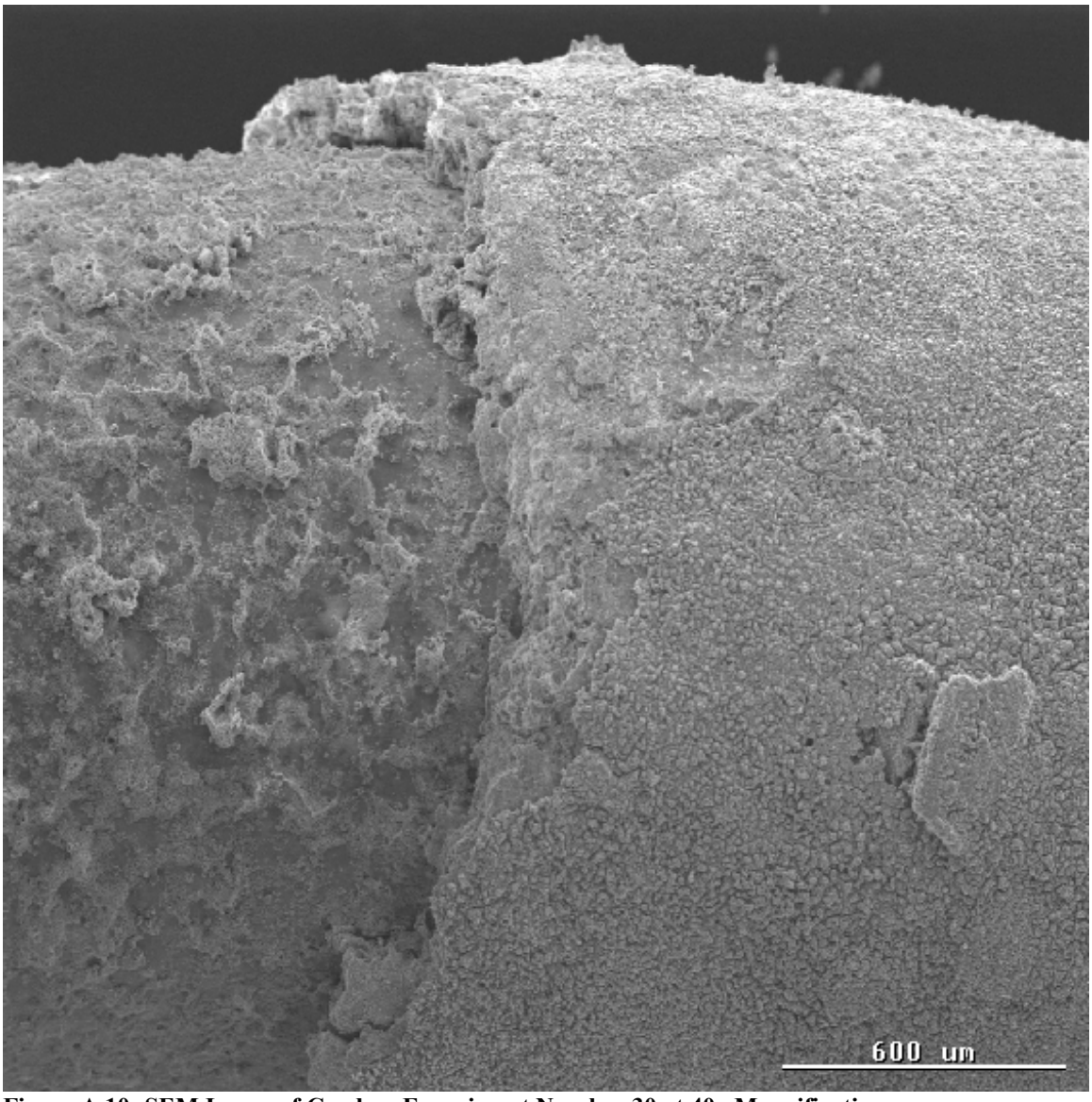

Figure A.10: SEM Image of Crud on Experiment Number 30 at 40x Magnification.

APPENDIX B

DETERMINATION OF pH

Each experiment had a target pH, but the pH is not determined exactly because of the soluble iron nitrate added. For example, most experiments ran with a target pH of 7.1, which would require (for beginning of cycle conditions) 1500 ppm B and 3.1 ppm Li without the iron nitrate additive. This is according to the following Table B.1 below.

Table B.1: pH as a function of B and Li (in ppm) at 310 °C (590 °F).

pHt	6.70	6.80	6.90	7.00	7.10	7.20	7.30	7.40	7.50
B, ppm	Li, ppm								
0	0.10	0.13	0.17	0.21	0.27	0.34	0.43	0.54	0.69
50	0.13	0.17	0.21	0.27	0.34	0.43	0.55	0.69	0.88
100	0.16	0.20	0.26	0.33	0.42	0.53	0.67	0.85	1.07
150	0.19	0.24	0.31	0.39	0.49	0.63	0.79	1.01	1.27
200	0.22	0.28	0.36	0.45	0.57	0.72	0.92	1.17	1.48
250	0.25	0.32	0.41	0.51	0.65	0.83	1.05	1.33	1.69
300	0.28	0.36	0.45	0.58	0.73	0.93	1.18	1.50	1.90
400	0.35	0.44	0.56	0.71	0.90	1.14	1.45	1.84	2.35
500	0.41	0.52	0.66	0.84	1.07	1.36	1.73	2.20	2.81
600	0.48	0.61	0.77	0.98	1.24	1.58	2.02	2.57	3.28
700	0.55	0.70	0.88	1.12	1.43	1.81	2.32	2.95	3.78
800	0.62	0.79	1.00	1.27	1.62	2.06	2.62	3.35	
900	0.69	0.88	1.12	1.42	1.81	2.31	2.94	3.76	
1000	0.77	0.98	1.24	1.58	2.01	2.56	3.27		
1100	0.85	1.07	1.37	1.74	2.22	2.83	3.61		
1200	0.93	1.18	1.50	1.90	2.43	3.10	3.97		
1300	1.01	1.28	1.63	2.08	2.65	3.38			
1400	1.09	1.39	1.76	2.25	2.87	3.67			
1500	1.18	1.50	1.90	2.43	3.10	3.97			
1600	1.26	1.61	2.05	2.62	3.34				
1700	1.36	1.73	2.20	2.81	3.58				
1800	1.45	1.84	2.35	3.00	3.84				
1900	1.55	1.96	2.51	3.20					
2000	1.64	2.09	2.67	3.41					

The pH for experiments without iron nitrate additives is therefore determined almost exactly. Unfortunately the data that made the above table possible, i.e. ionization constants for lithium hydroxide and boric acid, is not available for iron nitrate at such high temperatures. In an effort to account for the iron nitrate additive, the ionization constant for Fe^{3+} at room temperature was used in the following calculation.

The reaction of interest:

B.1. $$MOH_2^{3+} + H_2O \leftrightarrow MOH^{2+} + H_3O^+$$

The ionization constant equation:

B.2. $$K = \frac{[H^+][MOH^{2+}]}{[M^{3+}]} = 7.7 \times 10^{-3} \quad (pKa = -\log(K) = 2.11)$$

To translate the above into pH, the equation below is used:

B.3. $$pH = pKa + \log\frac{[MOH^{2+}]}{[M^{3+}]} = 2.11 + \log\frac{[MOH^{2+}]}{[M^{3+}]} = 7$$

It is desired to have the pH equal to 7 so that the iron nitrate and corresponding lithium have no effect on the rest target pH of the coolant. Equation A.3 can be solved as below:

B.4. $$\log\frac{[MOH^{2+}]}{[M^{3+}]} = 4.89 \text{ or } \frac{[MOH^{2+}]}{[M^{3+}]} = 7.76 \times 10^3$$

The molar equivalent of 20 ppm Fe in the form of iron nitrate is 3.58×10^{-4} M. Using this, equation A.2 can be expressed as:

B.5. $$\frac{x^2}{(3.58 \times 10^{-4} - x)} = 7.7 \times 10^{-3}$$

Where x is the amount of positive ions that require the lithium hydroxide additive. From this expression x is equal to 3.43×10^{-4} and the denominator is therefore 0.15×10^{-4}.

These two values correspond to [MOH^{2+}] which is also [H^{+}] and [M^{3+}] respectively. The corresponding required amount of lithium hydroxide molar concentration can be set equal to 3.58×10^{-4} mol/L. This is converted into 8.57×10^{-3} g/L of LiOH, which can be expressed in terms of Li as 2.5 ppm.

This calculation is crude, and when the ionization constant of Fe^{3+} is reported, a more precise calculation can be performed for the appropriate temperature. However, for purposes of this experiment, the calculation suffices to compensate for the extra acidity of the iron so the target pH is close to what is actually characteristic of the coolant. The amount of iron nitrate is reported consistently for every experiment in Fe ppm. Also, for every experiment that contained iron nitrate, the compensatory amount of lithium added was 2.5 ppm even though some experiments were inadvertently run with less than the 20 ppm Fe that the Li number is based on.

The way the iron is added into the experiment is parts per million by weight of just the iron element. This is also the way the boron, lithium and nickel were added. Originally the intention was to add iron nitrate so that the iron would have a concentration of 20 ppm. This calculation is summarized in Table B.2 below.

Table B.2: Weight Fraction of Iron Nitrate Constituent Elements.

$Fe(NO_3)_3 \cdot 9H_2O$

Amount	Element	At. Wt	Wt Frac.
1	Fe	55.8470	0.1382
3	N	42.0201	0.1040
9	H2	18.1422	0.0449
18	O	287.9892	0.7128
	Total	403.9985	

When the error was made the $\times 9H_2O$ was left off the formula and the weight fraction of the iron went up. This caused less iron nitrate to be added, and therefore less ppm Fe. Later in the project, similar experiments were run for comparison purposes.

APPENDIX C

SURFACE ANALYSIS TECHNIQUES

This project relied heavily on the results of surface analysis techniques, most significantly that of EDX. The discussion here will present the basic principles, advantages, and disadvantages of the three methods used for most of the experiments.

EDX and SEM are used simultaneously. The instrument sends a focused beam of electrons and detects the reflected electrons to produce the SEM image. In addition, the initial electrons will cause the elements of boron through uranium to emit characteristic x-rays for elemental identification. These are also detected, and the intensity of the x-ray peaks can be roughly related to the quantity present in the EDX scan area. The scan area can be as small as 1 micron on each side.

ICP-MS is the next most common method of analyzing the wire. As mentioned above, the EDX method is not sensitive to lithium, and it is important for this project to determine whether or not lithium is present in the crud layer. ICP-MS is sensitive to most elements with the exception of H, C, O, F, and the noble gases. For crud samples that were determined important enough, ICP-MS was run to determine whether the crud contained lithium. An advantage of ICP-MS is that it can detect very small amounts of elements that it is sensitive to. The sample has to be in liquid form, so the crud was scraped from the wire and digested in solvent with internal standards added for quantification purposes. The liquid sample is placed in the machine, turned into an aerosol and then ionized by a plasma gun. The ions are then detected by the mass

spectrometer. The other advantage of ICP-MS is that many samples can be analyzed rapidly.

The final method of analysis used somewhat by this project is XRD. The advantage of this method is that it can detect molecules, but they must be of crystalline structure such as metals or ceramics. The crud is scraped from the wire and left in powder form. An incident beam of x-rays is shot at the powder, and the intensity of the deflection beam is measured at all angles. The results are compared to a standard database that contains the degree and relative intensity for many molecules. The deflection chart can contain several different species as can be seen in the data presented in this report (Figures 4.12 and A.2).

Two other methods that were attempted for this project, but not very successful are AES and SIMS. AES is a nondestructive technique that shoots electrons at a sample and measures characteristic Auger electrons on return. This method is sensitive to lithium and most other elements, but the sample submitted for testing charged too much and was not able to be analyzed. SIMS is a slightly destructive technique that is sensitive to all elements. The technique is semi-quantitative and uses a focused ion beam to sputter the top layer of elements off of the sample. Those elements that are ionized are able to be measured through a mass spectrometer. SIMS was also attempted, but the data returned was with very large errors and not deemed accurate. Alternate methods (ICP-MS) for finding lithium were pursued.

REFERENCES

[1] Nuclear Regulatory Commission. *Official Transcript of Proceedings: Advisory Committee on Reactor Safeguards Reactor Fuels Subcommittee – Open Session*. Rockville, Maryland: Neal R. Gross and Co., INC, September, 2003.

[2] Hoxie-Key, Susan. *An Overview of the Axial Offset Anomaly in High-Duty PWR's.* Presentation given at Georgia Institute of Technology February, 2004.

[3] Electric Power Research Institute. *PWR Axial Offset Anomaly (AOA) Guidelines, Revision 1.* EPRI Report 1003213, October, 2003.

[4] Frattini, P. L., J. Blok, S. Chauffriat, J. Sawicki, and J. Riddle. "Axial offset anomaly: coupling PWR primary chemistry with core design." *Nuclear Energy* 40, no. 2 (April 2001): 123-35.

[5] Roe, J. *NRC Information Notice 97–85: Effects of Crud Buildup and Boron Deposition on Power Distribution and Shutdown Margin.* Washington, D.C. December, 1997.

[6] Song, M. C. K. Lee. "The evaluation of radioactive corrosion product at PWR as change of primary coolant chemistry for longer-term fuel cycle." *Annals of Nuclear Energy 30* (2003): 1231-46.

[7] Konya, M., BK. Bryant, K. Kock, D. Hopkins, G. Hughes, R. Irwin, D. Hurt, C. Riggs, M. Stiller, J. Secker. "Power Distribution Changes Caused by Subcooled Nucleate Boiling at Callaway Nuclear Power Plant." *ASME/JSME Nuclear Engineering Conference – Volume 2*. (1993): 281-87.

[8] Jacobson, S., E. Francillon. "High Burn-up Raises Sticky Issues" *Nuclear Engineering International 41* (November 1996): 23-24.

[9] Miller, R. S. "Steps Toward High Burn-Up in PWRs: a US Perspective." *Nuclear Energy 31* (Feb 1992): 41-47.

[10] Todreas, N. E. and M. S. Kazimi. Nuclear Systems I: Thermal Hydraulic Fundamentals. (1993): Taylor & Francis.

[11] Shi, B., B. Jones, and C. Pan. "Parametric study of boiling heat transfer in porous media." *International Conference on Nuclear Engineering Volume 1*, part A. (1996): 393-402.

[12] Thomazet, J., M. Noe, O. Lavoine. "In-Reactor Corrosion and Crud Deposition Data on Fragema Fuel." *Conference on Light Water Reactor Fuel Performance Held in Orlando, FL 21-24 April 1985*, 3-37 to 3-54.

[13] Wu, W. and B. Jones. "Simulation of bubble dynamics in sub-cooled boiling on fuel clad in PWRs. *Proceedings of 10th International Conference on Nuclear Engineering Held in Arlington, VA 14-18 April 2002,* 867-74.

[14] Jia, W. and V. K. Dhir. "Experimental study of bubble dynamics and concentration variation in the presence of boron in the liquid." *Proceedings of International Mechanical Engineering Congress & Exposition Held in New Orleans, LA 17-22 November 2002,* 179-185.

[15] Actis-Dato, L. O, L. Aldave de Las Heras, M. Betti, E. H. Toscano, F. Miserque, and T. Gouder. "Investigation of Mechanisms of Corrosion Due to Diffusion of Impurities by Direct Current Glow Discharge Mass Spectrometry Depth Profiling." *Journal of Analytical Atomic Spectrometry 15* (2000): 1479-84.

[16] Sandler, Y. H. and R. H. Kunig. "The Solubility of Nickel Ferrite in Aqueous Boric Acid Solution." *Nuclear Science and Technology 77* (1981): 211-18.

[17] Chung, J. Y, and K. J. Lee. "The Solubility of Magnetite and Nickel Ferrite in High Temperature Aqueous Solutions" *High Temperature Science 30* (1990): 51-67.

[18] Kawaguchi, M., K. Ishigure, N. Fugita, and K. Oshima. "Deposition of Model Crud on Boiling Zircaloy Surfaces at High Temperature." *Nuclear Technology 62* (September, 1983): 253-62.

[19] Wood, C. J. "Advances in water chemistry control for BWRs and PWRs." *Nuclear Energy 36* (1997): 355-61.

[20] Jones, R. L. "Some Critical Corrosion Issues and Mitigation Strategies Affecting Light Water Reactors." *Materials Selection & Design* (July, 1996): 63-67.

[21] Polley, M. V., K. Garbett, and M. E. Pick. "A Survey of Coolant pH versus Radiation Fields for Westinghouse PWRs." *Water Chemistry of Nuclear Reactor Systems 7* BNES (1996): 106-08.

[22] Moya, J. S., et al, "Zirconium Oxide Film Formation on Zircaloy by Water Corrosion," *Acta Materialia 48* (2000): 4749-54.

[23] Kido, T. "A Study of Enhanced Uniform Corrosion of Zircaloy-4 Cladding During High Burnup Operation of PWRs" *Sixth International Symposium on Environmental Degradation of Materials in Nuclear Power Systems – Water Reactors,* edited by R. Gold and E. Simonen, (1993): 849-54.

[24] Machet, A., A. Galtayries, P. Marcus, P. Combrade, P. Jolivet, and P. Scott. "XPS study of oxides formed on nickel-base alloys in high-temperature and high-pressure water" *Surface and Interface Analysis 34* (2002): 197-200.

[25] Electric Power Research Institute. *Impact of PWR Primary Chemistry on Corrosion Product Deposition on Fuel Cladding Surfaces.* EPRI Report TR-108783, November, 1997.

[26] Barton, M., M. Conqueror, K. Garbett, M. Mantell, M. Phillips, M. Polley, and W. Westall. "Corrosion product measurements at Sizewell B PWR." *Nuclear Energy 40,* no. 5 (October 2001): 305-17.

[27] Bouaziz, R. "Contribution A L'Étude Des Borates De Lithium Et De Sodium" *Annales de Chime 6* (1961): 345-93.

[28] Electric Power Research Institute. *Rootcause Investigation of Axial Power Offset Anomaly.* EPRI Report TR-108320, June, 1997.

[29] Odelius, H. "Verification of AOA Mechanism." Presentation at Fuel Reliability Program. Studsvik Nuclear Corrosion Laboratory. August, 2004.

[30] Electric Power Research Institute. *Adsorption of Boric Acid on Synthetic Fuel Crud Oxides.* EPRI Report 1003384, November, 2002.

[31] Joe, H. and B. Jones. "Modeling of porous crud layer on effects of diffusion and water radiolysis on anomalous porous crud deposition on fuel pin surfaces in PWRs. *Proceedings of 10th International Conference on Nuclear Engineering Held in Arlington, VA 14-18 April 2002,* 821-27.

[32] Rao, Q and B. Jones. "Study of mechanism of initial crud formation on fuel cladding in subcooled boiling region in PWR." *Proceedings of 10th International Conference on Nuclear Engineering Held in Arlington, VA 14-18 April 2002,* 813-820.

[33] Zhou, D. and B. Jones. "Boron concentration model and effects of boron holdup on axial offset anomaly (AOA) in PWRs." *Proceedings of 10th International Conference on Nuclear Engineering Held in Arlington, VA 14-18 April 2002,* 829-34.

[34] Lukic, Y. and J. Schmidt. "Taming the Crud Problem: a Utility Perspective." *Nuclear Technology 142* (June 2003): 283-93.

[35] Dinov, K. "A Model of Crud Particle/Wall Interaction and Deposition in a Pressurized Water Reactor Primary System." *Nuclear Technology 94* (June 1991): 281-285.

[36] Byers, W. and R. Jacko. "The influence of zinc additions and PWR primary water chemistry on surface films that form on nickel base alloys and stainless steels." *Sixth International Symposium on Environmental Degradation of Materials in Nuclear Power Systems – Water Reactors,* edited by R. Gold and E. Simonen, (1993): 837-44.

[37] Radhakrishnan, S. and B. Jones. "Use of enriched boric acid as chemical shim and effect on B-10 holdup from contributing mechanisms." *Research by U. S. Department of Energy – Sponsored Student,* 355.

[38] Frattini, P.L., Moser, T "The Ultrasonic Key to Clean Fuel." *Nuclear Engineering International 45* (Aug. 2000): 34-5

[39] Kim, K., H. J. Lee, D. W. Kang, and S. Inoue. "Synthesis of Simulated Cruds for Development of Decontaminating Agents." *Nuclear Engineering and Design 223* (2003): 329-37.

[40] Electric Power Research Institute. *Experimental Verification of the Root Cause Mechanism for Axial Offset Anomaly.* EPRI Report 1003212, December, 2002.

[41] Bryappa, K., V. Rajeev, V. J. Hanumesh, A. R. Kulkarni, A. B. Kulkarni. "Crystal Growth and Electrical Properties of $Li_2B_4O_7$." *Journal of Material Research 11* No. 10 (October 1996): 2616-2621.

[42] Kosinski, J. A. "New Piezoelectric Substrates for SAW Devices." *International Journal of High Speed Electronics and Systems 10* No. 4 (2000): 1017-1068.

[43] Smith, R. "Basic Geology and Chemistry of Borate." *Ceramic Engineering and Science Proceedings 22* (2001): 61-74.